

Samuel Jesús Ramos Infante

Design and development of a  
multiscale model for the  
osteoporotic fracture prevention: a  
preclinical tool

Departamento  
Instituto de Investigación en Ingeniería [I3A]

Director/es  
Pérez Ansón, María Angeles

<http://zaguan.unizar.es/collection/Tesis>



Reconocimiento – NoComercial – SinObraDerivada (by-nc-nd): No se permite un uso comercial de la obra original ni la generación de obras derivadas.

© Universidad de Zaragoza  
Servicio de Publicaciones

ISSN 2254-7606



**Universidad**  
Zaragoza

Tesis Doctoral

DESIGN AND DEVELOPMENT OF A MULTISCALE  
MODEL FOR THE OSTEOPOROTIC FRACTURE  
PREVENTION: A PRECLINICAL TOOL

Autor

Samuel Jesús Ramos Infante

Director/es

Pérez Ansón, María Angeles

**UNIVERSIDAD DE ZARAGOZA**

Instituto de Investigación en Ingeniería [I3A]

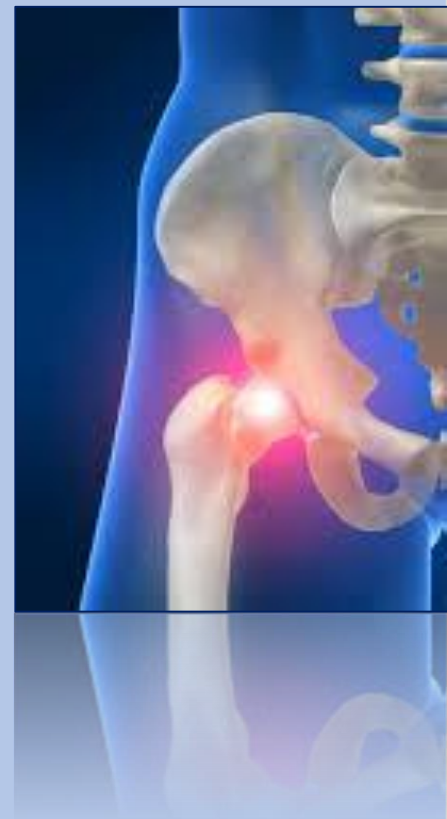
2018



---

# Design and development of a multiscale model for the osteoporotic fracture prevention: a preclinical tool

---



**Samuel Jesús Ramos Infante**

September 2018











# Design and development of a multiscale model for the osteoporotic fracture prevention: a preclinical tool



**Universidad Zaragoza**

Samuel Jesús Ramos Infante

Aragón Institute of Engineering Research (I3A)

University of Zaragoza

Faculty Advisor: María Ángeles Pérez Ansón

A thesis submitted for the degree of  
*Doctor of Philosophy in Biomedical Engineering*

September 2018



A mis padres Luis y Fabiola



# Contents

---

<b>Agradecimientos/Acknowledgements</b>	<b>v</b>
<b>Abstract</b>	<b>vii</b>
<b>Resumen</b>	<b>ix</b>
<b>List of Figures</b>	<b>xi</b>
<b>List of Tables</b>	<b>xiii</b>
<b>Chapter 1. <u>Introduction</u></b> .....	<b>1</b>
<b>1.1 Clinical scenario: Trabecular bone and osteoporosis</b> .....	<b>3</b>
1.1.1 Bone tissue.....	3
1.1.2 Osteoporosis.....	6
<b>1.2 Motivation</b> .....	<b>10</b>
1.2.1 Trabecular bone.....	10
1.2.2 Femoroplasty.....	11
1.2.2.1 Clinical scenario.....	11
1.2.2.2 CPC and PMMA.....	13
1.2.2.3 Surgery planning.....	14
1.2.2.4 Experimental and computational studies.....	15
1.2.2.5 Particle models.....	19
<b>1.3 Objectives</b> .....	<b>20</b>
<b>1.4 Thesis overview</b> .....	<b>21</b>
<b>Chapter 2. <u>In vitro and in silico characterization of open-cell structures of trabecular bone</u></b> .....	<b>23</b>
<b>2.1 Introduction</b> .....	<b>25</b>
<b>2.2 Materials and methods</b> .....	<b>27</b>
2.2.1 <i>In silico</i> characterization.....	29
2.2.2 <i>In vitro</i> characterization.....	32

2.2.3	Statistical analysis.....	32
<b>2.3</b>	<b>Results .....</b>	<b>32</b>
<b>2.4</b>	<b>Discussion.....</b>	<b>34</b>
<b>2.5</b>	<b>Conclusions.....</b>	<b>36</b>
<b>Chapter 3.</b>	<b><u>Discrete particle model for cement infiltration within open-cell structures: prevention of osteoporotic fracture.....</u></b>	<b>39</b>
<b>3.1</b>	<b>Introduction.....</b>	<b>41</b>
<b>3.2</b>	<b>Materials and methods.....</b>	<b>43</b>
3.2.1	Discrete particle model for cement infiltration.....	44
3.2.2	<i>In vitro</i> characterization of augmented open-cell structures.....	45
3.2.3	<i>In silico</i> characterization of augmented open-cell structures.....	47
3.2.4	Statistical analysis.....	49
<b>3.3</b>	<b>Results.....</b>	<b>49</b>
<b>3.4</b>	<b>Discussion.....</b>	<b>53</b>
<b>3.5</b>	<b>Conclusions.....</b>	<b>57</b>
<b>Chapter 4.</b>	<b><u>Development of a rabbit fracture model for evaluation of cement augmentation: an <i>in vivo</i> biomechanical study.....</u></b>	<b>59</b>
<b>4.1</b>	<b>Introduction.....</b>	<b>61</b>
<b>4.2</b>	<b>Materials and methods.....</b>	<b>62</b>
4.2.1	Biomechanical testing.....	62
4.2.2	Statistical analysis.....	63
<b>4.3</b>	<b>Results.....</b>	<b>63</b>
<b>4.4</b>	<b>Discussion.....</b>	<b>65</b>
<b>4.5</b>	<b>Conclusions.....</b>	<b>66</b>
<b>Chapter 5.</b>	<b><u>High- and low-viscosity cement for osteoporotic femoral augmentation: a computational subject-specific approach.....</u></b>	<b>67</b>
<b>5.1</b>	<b>Introduction.....</b>	<b>69</b>

<b>5.2 Materials and methods.....</b>	<b>71</b>
5.2.1 Study sample.....	71
5.2.2 Model development.....	72
5.2.3 Boundary and loading conditions.....	73
5.2.4 Fracture load prediction of nonaugmented subject-specific models.....	73
5.2.5 Local bone augmentation strategy.....	75
<b>5.3 Results.....</b>	<b>76</b>
5.3.1 Local bone augmentation.....	76
5.3.2 Subject-specific fracture load prediction.....	77
<b>5.4 Discussion.....</b>	<b>78</b>
<b>5.5 Conclusions.....</b>	<b>82</b>
<b>Chapter 6. <u>Conclusions, future work and contributions</u>.....</b>	<b>83</b>
<b>6.1 General conclusions.....</b>	<b>85</b>
6.1.1 <i>In vitro</i> and <i>in silico</i> characterization of open-cell structures for trabecular bone.....	85
6.1.2 Discrete particle model for cement infiltration within open-cell structures: prevention of osteoporotic fracture.....	85
6.1.3 Development of a rabbit fracture model for evaluation of cement augmentation: an <i>in vivo</i> biomechanical study.....	86
6.1.4 High- and low-viscosity cement for osteoporotic femoral augmentation: a computational subject-specific approach.....	86
<b>6.2 Future work.....</b>	<b>87</b>
<b>6.3 Contributions.....</b>	<b>88</b>
6.3.1 Articles in peer-review journals.....	88
6.3.2 Presentations in conferences.....	89
<b>Chapter 7. <u>Conclusiones, trabajo futuro y contribuciones</u>.....</b>	<b>91</b>
<b>7.1 Conclusiones generales.....</b>	<b>93</b>
7.1.1 Caracterización <i>in vitro</i> e <i>in silico</i> de estructuras open-cell para hueso trabecular.....	93
7.1.2 Modelo discreto de partículas para infiltración de cemento a través de estructuras open-cell: prevención de la fractura osteoporótica.....	93

7.1.3	Desarrollo de un modelo de fractura en conejo para la evaluación de la cementación femoral: un estudio biomecánico <i>in vivo</i> .....	94
7.1.4	Cemento de alta y baja viscosidad para la cementación del fémur osteoporótico: un acercamiento computacional al paciente específico.....	94
<b>7.2</b>	<b>Trabajo futuro.....</b>	<b>95</b>
<b>7.3</b>	<b>Contribuciones.....</b>	<b>97</b>
7.3.1	Artículos en revistas.....	97
7.3.2	Presentaciones en congresos.....	97
	<b>References.....</b>	<b>99</b>



# Agradecimientos/Acknowledgements

---

En primer lugar, quiero agradecer enormemente a mis padres, Luis y Fabiola, todo su apoyo no sólo durante el transcurso de esta tesis, sino durante toda mi vida. Por estar siempre ahí, por sus esfuerzos, por apoyarme en todas mis decisiones y ofrecerme motivación y afecto en los momentos más complicados. Ellos no sólo me han enseñado el valor de las cosas y el sacrificio que uno tiene que realizar para conseguir sus objetivos, como es la materialización de esta tesis, sino a que ante todo uno tiene que ser persona independientemente de los grados, másteres o doctorados que hayas podido lograr. ¡GRACIAS!

En segundo lugar, quiero agradecer también a mi tutora de tesis y amiga, María Ángeles, todo su apoyo, predisposición y afecto ya no sólo durante el transcurso de la tesis sino desde antes de empezar el Máster. Por todo lo que he aprendido y por su confianza en mí desde el primer momento, y a pesar de nuestros desencuentros en más de una ocasión por diversas causas, estoy convencido que seguiremos en continuo contacto no sólo desde el punto de vista personal sino profesional. ¡Gracias!

También, quiero agradecer la predisposición de todos y cada uno de los miembros del grupo de investigación M2BE a prestar su ayuda en todos aquellos momentos que lo necesitaba. ¡Gracias!

Tampoco me puedo olvidar de Alejandro y Óscar, sin los cuales nunca podría haberme visto inmerso en la rama biomédica y cuyos consejos me ayudaron a tomar la decisión de ir a Zaragoza. ¡Gracias!

Furthermore, it is a pleasure to thank so much Materialise Company for awarding me with the EMEA Second Prize of the Mimics Innovation Awards 2016.

Finally, the authors gratefully acknowledge the support of the Spanish Ministry of Economy and Competitiveness through research project DPI2014-53401-C2-1-R and the European Research Council (ERC) for supporting this work through project ERC-2012-stg306751.



# Abstract

---

Osteoporosis is a major health concern in virtually all developed countries with up to 9 million new osteoporotic fractures expected annually worldwide. It is defined as a systemic skeletal disease characterized by a reduction of mineralized bone and an altered bone microstructure leading to an increased risk of fracture. This risk of fractures is currently estimated based on an assessment of bone mass as measured by dual-energy X-ray absorptiometry (DEXA). However, patient-specific finite element (FE) simulations that include information from multiple scales have the potential to allow more accurate prognosis. This multiscale approach to modelling the mechanics of bone allows a more accurate characterization of bone fracture behaviour. Furthermore, such models can also include the effects of ageing, osteoporosis, drug treatment and even augmentation. Indeed, as trabecular bone is mainly involved in osteoporotic hip fractures, augmentation of osteoporotic femur using Polymethylmetacrylate (PMMA) or cement has been suggested to be an alternative preventive treatment to reduce the risk of fracture.

The main goal of this thesis is the design and development of a multiscale model for the osteoporotic fracture prevention. This model will allow us to know more about the failure mechanisms associated to osteoporosis from the tissue to the organ level in order to assess the femoroplasty feasibility.

Therefore, to achieve this goal, firstly we performed a detailed *in vitro* and *in silico* characterization of open-cell structures, which resemble trabecular bone, to elucidate osteoporosis failure mechanisms from the tissue level. Experimental and image-based computational methods were used to estimate Young's modulus and porosities of different open-cell structures (Sawbones, Malmö, Sweden). The experimental and computational results with different element types (linear and quadratic tetrahedrons and voxel-based meshes) were compared with Sawbones data (Sawbones; Malmö, Sweden) revealing important differences in Young's modulus and porosities. Subsequently, we developed a discrete particle model based on the random-walk theory for simulating cement infiltration within the nonaugmented open-cell structures previously characterized. Model parameters considered the cement viscosity (high and low) and the desired direction of injection (vertical and diagonal). Again *in vitro* and *in silico* characterizations of augmented open-cell structures

validated the computational model and quantified the improved mechanical properties (Young's modulus) of the augmented specimens. These results suggested that the proposed discrete particle model was adequate for use as a generalized augmentation strategy at organ level. Due to the promising results of cements, rabbit femur specimens were *in vivo* augmented to evaluate the safety and feasibility of femoroplasty. Finally, healthy and osteoporotic femur specimens were computationally augmented using the previous strategy to control volume and placement of cement injection. Low-viscosity cement notably increased the fracture load of nonaugmented femur specimens in comparison with high-viscosity cement. Final results suggested that cement can definitely improve the mechanical properties of osteoporotic femur and our model is a powerful candidate for its use as a preclinical tool to allow more accurate prognosis.

**Keywords:** open-cell structures, discrete particle model, multiscale model, finite element simulation, femoroplasty, low- and high-viscosity cement.

# Resumen

---

Se espera que la osteoporosis sea participe de más de 9 millones de nuevas fracturas en todo el mundo en un futuro no muy lejano, ya que es una de las enfermedades con mayor índice de impacto entre la población de los países desarrollados. Se define como una enfermedad sistémica caracterizada por la pérdida de masa ósea y una alteración de su microestructura interna con la consiguiente susceptibilidad a la fractura. Actualmente, la estimación del riesgo de fractura se lleva a cabo mediante tomografía axial computerizada (TAC), Rayos X o densitometrías. Sin embargo, las simulaciones por elementos finitos para un paciente determinado, pueden contener una gran cantidad de información que permitirían unas predicciones más precisas. Una metodología multiescala ayudaría al desarrollo y caracterización de modelos de fractura más robustos que permitirían conocer de una manera más detallada el comportamiento del hueso. Además, dichos modelos podrían incorporar parámetros relacionados con la edad, el grado de osteoporosis o el tratamiento mediante fármacos. De hecho, debido a que el hueso trabecular interviene, en gran medida, en las fracturas de cadera osteoporóticas, un tratamiento preventivo alternativo para reducir el riesgo de fractura osteoporótica consistiría en la inyección de cemento óseo (PMMA) en el fémur osteoporótico.

Por lo tanto, el principal objetivo de esta tesis doctoral es el desarrollo de un modelo multiescala para la prevención de la fractura ósea osteoporótica. Este modelo nos permitirá conocer más acerca de los mecanismos de fallo asociados a la osteoporosis desde el nivel tisular hasta el nivel macroscópico a fin de evaluar la factibilidad de la femoroplastia.

Para alcanzar este objetivo, en primer lugar, se ha llevado a cabo una caracterización *in vitro* e *in silico* de estructuras artificiales de hueso artificial, denominadas open-cell (Sawbones, Malmö, Sweden), con propiedades próximas al hueso sano y osteoporótico, de manera que permita elucidar mecanismos de fractura asociados a la osteoporosis desde el nivel tisular. De esta manera, se han empleado métodos experimentales y computacionales basados en el procesado de imagen con el fin de estimar el módulo elástico y las porosidades de las diferentes estructuras open-cell. Los resultados computacionales y experimentales fueron comparados con los datos aportados por el fabricante. Se apreciaron importantes diferencias no sólo en términos del módulo de Young sino también en las porosidades. Posteriormente, se desarrolló un modelo discreto de partículas basado en la Teoría del

Movimiento Aleatorio para simular la infiltración de cemento a través de las estructuras open-cell, previamente caracterizadas. Los parámetros del modelo incluyeron no sólo la viscosidad del cemento (alta o baja) sino la dirección de inyección (vertical o diagonal). De nuevo, se llevó a cabo una caracterización *in vitro* e *in silico* de las estructuras cementadas, validando el modelo computacional mediante ensayos experimentales. Dichos resultados mostraron que el modelo discreto de partículas era suficientemente robusto para su aplicación en la escala macroscópica. También, se inyectó cemento *in vivo* en fémures de conejo a fin de evaluar la factibilidad de la femoroplastia. Finalmente, se utilizaron fémures sanos y osteoporóticos para la predicción computacional del grado de mejora de las propiedades mecánicas cuando se inyectaba cemento de alta o baja viscosidad. El cemento de baja viscosidad mejoraba notablemente las cargas de fractura con respecto a los fémures no cementados. Los resultados finales mostraron que el cemento óseo mejora definitivamente las propiedades del hueso osteoporótico y la metodología propuesta puede llegar a utilizarse como una herramienta preclínica para un diagnóstico más preciso.

**Palabras clave:** estructuras open-cell, modelo discreto de partículas, modelo multiescala, simulación por elementos finitos, femoroplastia, cemento de alta y baja viscosidad.

## Figure contents

<b>Figure 1:</b> Hierarchical structure of trabecular bone [Hamed et al., 2012].....	4
<b>Figure 2:</b> Electron microscopy images of trabecular bone taken at (a) nanoscale level (10 000x), using transmission electron microscopy (TEM), showing mineralized collagen fibrils, (b) sub-microscale (1000x) showing single lamella, (c) microscale (700x) showing a trabecular strut and (d) mesoscale (20x) showing a porous cellular structure of trabecular bone, using scanning electron microscopy (SEM) [Hamed et al., 2012] .....	4
<b>Figure 3:</b> Schematic diagram showing the mean BMD with SD intervals in women by age and the derivation of Z-scores and T-scores from BMD [Svedbom et al., 2013] .....	8
<b>Figure 4:</b> The distribution of BMD in young healthy women in SD units and threshold values for osteoporosis and low bone mass [Svedbom et al., 2013] .....	8
<b>Figure 5:</b> Distribution of BMD in women of different ages, and the prevalence of osteoporosis (blue). T score below $-2.5$ =osteoporosis [Kanis et al., 1994].....	9
<b>Figure 6:</b> Schematic of an augmentation suggested by simulations (green) and planned path and locations of injection (blue) [Basafa et al., 2015].....	13
Figure 7: Flexural strength differences between CPC and PMMA [Yang et al., 2015].....	13
<b>Figure 8:</b> Curing time differences between CPC and PMMA [Yang et al., 2015].....	14
<b>Figure 9:</b> Injection setup [Basafa et al., 2015].....	15
<b>Figure 10:</b> On the left, specimen #30; in the middle, specimen #20; on the right, specimen #15 .....	28
<b>Figure 11:</b> Workflow for the <i>in vitro</i> and <i>in silico</i> characterization of the open-cell structures of trabecular bone .....	28
<b>Figure 12:</b> Segmentation of CT data for each specimen using FE material assignment module in MIMCS (Materialise NV, Leuven, Belgium).....	29
<b>Figure 13:</b> Three-dimensional reconstruction of the trabeculae using linear tetrahedral (C3D4), quadratic tetrahedral (C3D10) and voxel (C3D8) elements.....	30
<b>Figure 14:</b> FE model reproducing the compression [Hambli, 2013].....	30
<b>Figure 15:</b> On the left, servo-hydraulic material testing machine; on the right, uniaxial compression test .....	32
<b>Figure 16:</b> Comparison among experimental, computational and Sawbones specifications of a) Young's modulus (MPa) and b) porosity. The dashed line represents Sawbones specifications. Bars represented the standard deviation. ....	33

<b>Figure 17:</b> Workflow for the <i>in vitro</i> and <i>in silico</i> characterization of open-cell structures: Nonaugmented vs. augmented with cement .....	43
<b>Figure 18:</b> Probabilities depending on the desired direction of injection .....	45
<b>Figure 19:</b> a) Vertical and b) diagonal injection of two different commercial cements in blocks of approximately 65 x 65 x 40 mm.....	46
<b>Figure 20:</b> Commercial cement injection system (Teknimed S5Kit; Teknimed S.A.S, France) .....	46
<b>Figure 21:</b> Augmented FE model.....	48
<b>Figure 22:</b> Frontal (on the left) and lateral (on the right) view of the cement cloud .....	49
<b>Figure 23:</b> Mean Young's modulus improvement (%) in all the cases tested <i>in vitro</i> and <i>in silico</i> : a) vertical and b) diagonal directions of injection. Bars indicate the standard deviation values (see Table 6).....	51
<b>Figure 24:</b> Qualitative comparison of the cement infiltration patterns within certain open-cell structures in each case simulated .....	51
<b>Figure 25:</b> Setup for mechanical testing .....	62
<b>Figure 26:</b> Fractures occurred a) at the femoral neck in augmented group and b) at the distal region in the nonaugmented group.....	63
<b>Figure 27:</b> Young's Modulus in the nonaugmented and augmented rabbit femur specimens. Bars indicated standard deviation .....	64
<b>Figure 28:</b> Fracture load in the nonaugmented and augmented rabbit femur specimens. Bars indicated standard deviation.....	64
<b>Figure 29:</b> Force-displacement curves for the nonaugmented and augmented rabbit femur specimens .....	64
<b>Figure 30:</b> Boundary and loading conditions of the fall configuration: vertical load on the femoral head toward the floor with the femoral shaft slanted by 30° and internally rotated 15° relative to the floor.....	73
<b>Figure 31:</b> Workflow for the non-linear strain-based FE simulations for the prediction of the fracture risk [Schileo et al. 2008].....	74
<b>Figure 32:</b> Calculated fracture loads for the healthy and osteoporotic bone model for the nonaugmented and augmented states (high- and low-viscosity cement). Bars indicated standard deviation. ....	78
<b>Figure 33:</b> Cement injection cloud (red area) for an augmented osteoporotic femur specimen for a) RATIO 1, b) RATIO 2 and c) RATIO 3 (transversal section).....	78



# Table contents

<b>Table 1:</b> Experimental and computational review of the femoroplasty technique .....	16
<b>Table 2:</b> Open-cell specimen dimensions, densities, volume fractions and Young's modulus .....	28
<b>Table 3:</b> Young's modulus (mean $\pm$ SD) obtained experimentally and through three different finite element analyses.....	34
<b>Table 4:</b> Estimated porosities (mean $\pm$ SD) obtained experimentally and through three different finite element analyses.....	34
<b>Table 5:</b> Open-cell specimens, densities, porosities, mean $\pm$ SD experimental Young's modulus and computational Young's modulus (Chapter 2) .....	47
<b>Table 6:</b> Mean Young's modulus improvement (%) in all the cases tested <i>in vitro</i> and <i>in silico</i> . STD indicates standard deviation. Bold numbers in the p-value column indicate a negative (-1) Pearson correlation coefficient.....	50
<b>Table 7:</b> Sphericity of the cement cloud in all cases tested <i>in vitro</i> and <i>in silico</i> . STD indicates standard deviation.....	52
<b>Table 8:</b> Calculated coefficients for each element.....	76
<b>Table 9:</b> Calculated TV, MD and IF for the healthy and osteoporotic bone models (mean $\pm$ SD).....	76
<b>Table 10:</b> Results of the sensitivity analysis: fracture load improvement (%) (mean $\pm$ SD) ..	77



# Chapter 1

---

## *Introduction*



## 1.1 Clinical scenario: Trabecular bone and osteoporosis

### 1.1.1 Bone tissue

Bone has an important combination of physical properties, showing a very high resistance to traction and compression. At the same time, it presents certain elasticity and the advantage of being relatively light material. At all organization levels, from the macroscopic to the submicroscopic structure of bones, their constitution ensures the maximum resistance with reduced material and lowest weight [Alberich, 2010].

The human skeleton performs some obvious functions: shape and support; attachment of ligaments and muscles; articular leverage in movement; and mechanical protection of vital organs. It also has two vital metabolic functions: haemopoiesis (generation of blood cells), which takes place in red bone marrow, and calcium homeostasis in the blood, which is ensured by controlled dissolution of some mineralized bone matrix during periods of low calcium intake. Primarily, two specialized cell types regulate the maintenance of the mineralized bone tissue: osteoclasts, which destroy the mineralized collagen matrix, and osteoblasts which produce new collagen that is subsequently mineralized into new bone. The modulation of the replication, activation and apoptosis of these two cell populations, and of the mineralization process, produces the net balance of this metabolic process. In healthy conditions, the amount of bone tissue that is reabsorbed is equal to the amount of newly formed bone tissue, and the total bone mass remains unchanged [Cristofolini et al., 2008].

At the macroscopic scale, bone is composed of cortical (compact) bone, forming a hard outer layer, and trabecular (spongy) bone, filling the interior spaces and ends of long bones [Olszta et al., 2007]. In combination with cortical bone, trabecular bone is a major load-bearing biological tissue in human bone. It is involved in bone femur fractures and is the primary site for the insertion of orthopedic implants [Eswaran et al., 2006].

At the submicroscopic scale, bone is a multi-phase composite material consisting of organic phase (32–44% bone volume (BV)), inorganic phase (33–43% BV) and water (15–25% BV). The organic phase is composed of collagen type I (approx. 90%) and non-collagenous proteins (NCPs) (approx. 10%). The inorganic (mineral) phase is made of calcium phosphate, which is similar to hydroxyapatite (HA),  $\text{Ca}_{10}(\text{PO}_4)_6(\text{OH})_2$ . The mineral phase is stiff and strong but brittle, whereas the collagen phase is soft and highly deformable. Water

plays an important role in the bio-mineralization process and serves as a plasticizer, enhancing the toughness of bone. These components are arranged into a complex hierarchical structure, which makes bone stiff, strong, tough and yet lightweight. [Buehler, 2008]. Five levels of hierarchical organization in bone are defined (Figure 1).

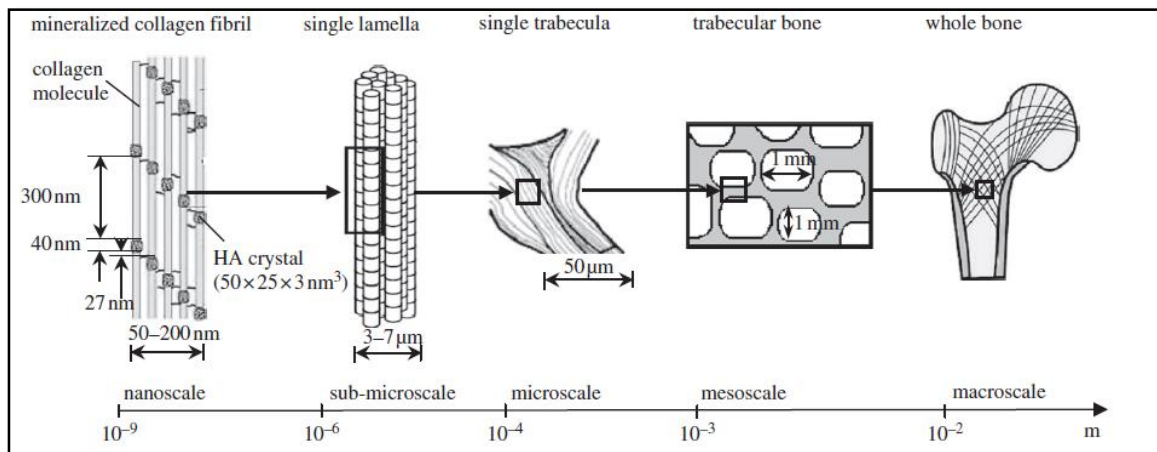


**Figure 1:** Hierarchical structure of trabecular bone [Hamed et al., 2012]

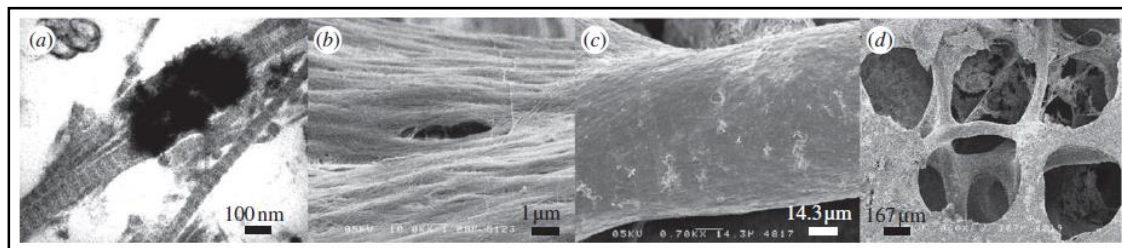


**Figure 2:** Electron microscopy images of trabecular bone taken at (a) nanoscale level (10 000x), using transmission electron microscopy (TEM), showing mineralized collagen fibrils, (b) sub-microscale (1000x) showing single lamella, (c) microscale (700x) showing a trabecular strut and (d) mesoscale (20x) showing a porous cellular structure of trabecular bone, using scanning electron microscopy (SEM) [Hamed et al., 2012]

As we can see in Figure 1, trabecular bone corresponds to mesoscale, ranging from hundred micrometres to several millimetres, or larger, depending on the bone size, consists of a porous network of trabeculae (Figure 2). The pores, typically in the order of 1 mm, are filled with bone marrow, fat and bone cells. In cortical bone, this level represents randomly arranged osteons embedded in an interstitial lamella, with some resorption cavities, all surrounded by a circumferential bone [Hamed et al., 2012].

Bone provides the stability of the organism, harbors hematopoiesis in the bone marrow, opens up regulatory interfaces to other organs and to metabolism, and functions as a reservoir for the delivery of minerals. Bone is efficiently regenerated throughout life and shows a high

capacity of scarless healing. Its strength in terms of fracture resistance results from bone mass, anatomy and microstructure and this is optimally adapted to the power and direction of mechanical forces that occur in everyday life. The sensitivity of the skeleton towards incoming mechanical forces is such that the resulting bone suffices to produce adequate fracture resistance under physiological circumstances. The musculoskeletal unit, consisting of bone, joints, ligaments, tendons and muscle translates forces into bone and orchestrates the principle of “form follows function” [Chen et al., 2010].

Bone formation and resorption are regulated by core signaling pathways for osteoblast/osteocyte differentiation and for osteoclast recruitment, differentiation and activation. Mesenchymal progenitor cells can give rise to e.g. bone, cartilage, fat and tendon.

From its initial formation to growth, maturation and dissolution, apatite crystals interact with the water from the bone matrix. Since crystals do not grow if ions do not diffuse from the milieu, the degree of mineralization does not progress when the water content is too low. Consequently, mineralization is rarely complete and stops at about 90–95% of the expected maximum level. In young bone tissue, the water content is high and ions are constantly exchanged with apatite. Conversely, in old bone tissue, these exchanges decrease considerably.

It is generally agreed that strength of bones depends on the volume of bone matrix and the microarchitectural distribution of this volume, while the degree of mineralization of bone tissue (DMB) is almost never mentioned as a determinant of bone strength. It now has evidence that the DMB strongly influences not only the mechanical resistance of bones but also the bone mineral density (BMD). It exists an heterogeneity in the DMB. This fact is explained by the fact that bone formation which follows bone resorption in the remodeling sequence is a multistep process: following its deposition, the new matrix begins to mineralize after about 5–10 days from the time of deposition. After full completion of the Basic Structural Units (BSUs), a phase of secondary mineralization begins. This process consists of a slow and gradual maturation of the mineral component, including an increase in the amount of crystals and/or an augmentation of crystal size toward their maximum dimensions. This secondary mineralization progressively augments the mineral content in bone matrix. At the end of the primary mineralization, mineral content represents only about 50% of the maximum degree of mineralization obtained at the end of the secondary mineralization phase.

In the particular case in which rapid formation of new bone is mandatory, such as in periods of fracture curation, in skeletal growth in early childhood, or in a particular metabolic

bone disorders, instead of lamellar bone, a provisional distribution of bone is formed, in which the collagen fibers are randomly oriented. Under physiologic conditions, this provisional bone is replaced after some time by lamellar bone, which has better mechanical properties [Baron, 2003; Marks and Hermey, 1996].

After menopause, increased remodeling with a more negative bone balance in the many BMUs removes more bone rapidly from an ever-diminishing and architectural disrupted bone. [Alberich, 2010].

### **1.1.2 Osteoporosis**

Osteoporosis is a major health concern in all developed countries with up to 9 million new osteoporotic fractures expected annually worldwide. Twenty-two million women and 5.5 million men in the European Union (EU) were diagnosed with osteoporosis in 2010. There were 3.5 million new fractures due to osteoporosis occurring that year, and 610,000 of them were fractures in the hip region [Hernlund et al., 2013].

The World Health Organization (WHO) predicts that the incidence of osteoporotic fractures of the hip will triple by 2050 [Hernlund et al., 2013; WHO, 1994]. In the population under 65 years old, the incidence of femoral neck fractures is two to four cases per 10,000 inhabitants. However, the incidence increases in the population above 70 years old, being of 28/10,000 in men and 64/10,000 in women. It is estimated that in 2050 there will occur 6.3 million fractures of the hip due to osteoporosis, a number three times greater than the current one, half of those fractures will happen only in Asia [WHO, 1994].

This situation is very concerning, not just in the health point of view, but also economically, since the treatment of these fractures is a very expensive procedure, combining to antibiotics, analgesics and time of hospitalization, and still the mortality rates are very high. The annual cost in the United States related to the treatment of osteoporotic fractures is US\$ 20 billion, and the contribution of hip fractures in this cost is above 60% [Hernlund et al., 2013; WHO, 1994; Cummings et al., 2002].

About 1.5% of all hospital beds in Europe are occupied by patients being treated for osteoporotic fractures, and the cost for treating these fractures is € 37 billion, being expected to increase 25% by 2025 [Hernlund et al., 2013].



Mortality rate due to the fracture of the proximal femur out of osteoporosis reaches 30% in the first year after surgery. Patients with this type of fracture are at risk of up to 30% to suffer a new fracture in the contralateral hip within two years after the first fracture, and this rate may increase after five years [Lawrence et al., 2010]. In cases of non-simultaneous contralateral hip fracture, the mortality rate can reach 64% in men and 58% in women [Ryg et al., 2009]. With the aging world population, these staggering numbers are projected to double over the next 40 to 50 years with 6 million hip fractures expected to occur worldwide by 2050 [ Kanis, 2007; Kanis et al., 2013; Odén et al., 2013]. The most common osteoporotic fractures comprise vertebral fractures, fractures of the forearm (particularly Colles' fracture), hip fractures, and proximal humerus fractures. [Svedbom et al., 2013]

Osteoporosis is a syndrome of dysadaptation [Jakob et al., 2013] and conceptually defined as a systemic skeletal disease characterized by low bone mass and microarchitectural deterioration of bone tissue, with a consequent increase in bone fragility and susceptibility to fracture. Bone strength reflects the integration of two main features: bone mineral density expressed as grams of mineral per area/volume and bone quality, referring to bone architecture, turnover, damage accumulation, collagen cross-linking, and bone mineralization.

The description of osteoporosis captures the notion that low bone mass is an important component of the risk of fracture, but other abnormalities such as micro-architectural deterioration contribute to skeletal fragility. Ideally, clinical assessment of the skeleton should capture all these determinants of fracture risk, but at present the assessment of bone mass is the only aspect that can be readily measured in clinical practice by dual-energy X-ray absorptiometry (DXA), and forms the cornerstone for the general management of osteoporosis being used for diagnosis, risk prediction, and monitoring of patients on treatment.

The diagnostic criterion for osteoporosis is based on the measurement of BMD. BMD is most often described as a T-score or Z-score, both of which are units of standard deviation (SD). The Z-score describes the number of SDs by which the BMD in an individual differs from the mean value expected for age and sex (Figure 3). The T-score describes the number of SDs by which the BMD in an individual differs from the mean value expected in young healthy individuals.

The operational definition of osteoporosis is based on the T-score for BMD in women and is defined as a value for BMD 2.5 SD or more below the young female adult mean (T-score

less than or equal to  $-2.5$  SD) as shown in Figure 4. This threshold was originally developed for measurements of BMD at the spine, hip, or forearm.

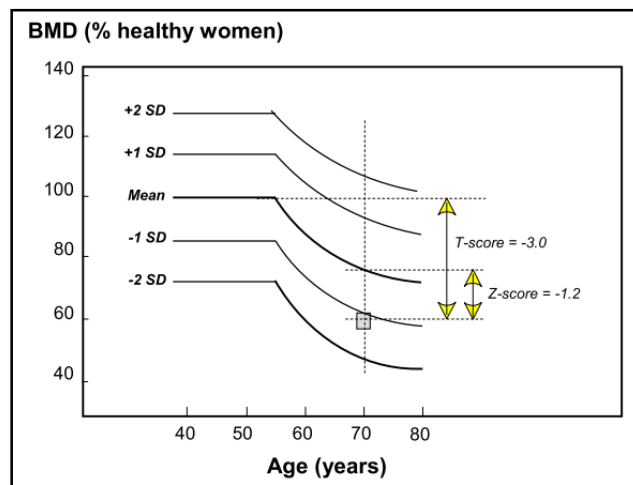


**Figure 3:** Schematic diagram showing the mean BMD with SD intervals in women by age and the derivation of Z-scores and T-scores from BMD [Svedbom et al., 2013]

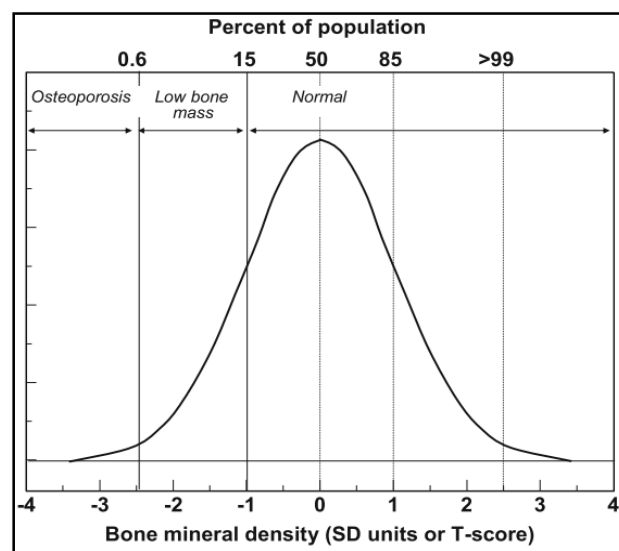


**Figure 4:** The distribution of BMD in young healthy women in SD units and threshold values for osteoporosis and low bone mass [Svedbom et al., 2013]

Furthermore, the proportion of women affected by osteoporosis at any one anatomical site increases greatly with age in much the same way as fracture risk increases with age (Figure 5) [Kanis et al., 1994]. Indeed, the increase in prevalence is roughly exponential and conforms to the known pattern of frequency of many osteoporotic fractures in ageing women. When measurements are made at one site, for example at the hip, then the prevalence of osteoporosis

of the hip in white women aged 50 years or more is about one in six, which is close to the life-time risk of hip fracture [Kanis et al., 2000].

The few studies available [Kanis et al., 2001; De Laet et al., 1998] show that the risk of hip fracture is similar in men and women for any given BMD. Such studies indicate that a similar cutoff value for hip BMD that is used in women can be used in the diagnosis of osteoporosis in men—namely, a value for BMD 2.5 SDs or more below the average for women [Kanis and Glüer, 2000].

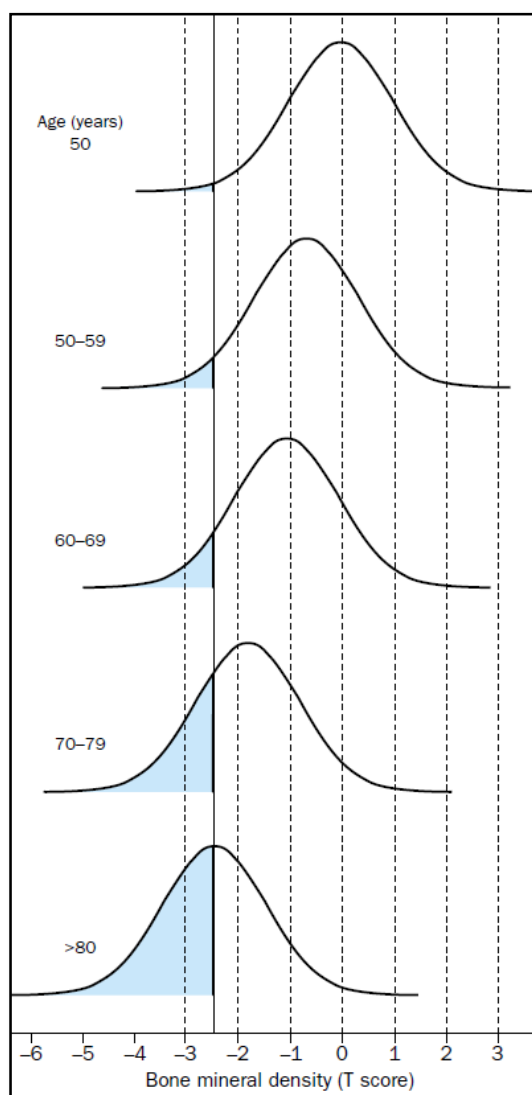


**Figure 5:** Distribution of BMD in women of different ages, and the prevalence of osteoporosis (blue). T score below  $-2.5$ =osteoporosis [Kanis et al., 1994]

More recently, the operational definition of osteoporosis has been refined by WHO with the femoral neck as the standard measurement site and the use of an international reference standard for the calculation of the T-score.

Osteoporosis represents a major non-communicable disease of today and is set to increase markedly in the future. There is underutilisation of the measures available to combat the disease and therefore, there is a need for assessment of best practices in prevention and treatment, since the adoption of these across countries can potentially result in significant reductions in the burden of this disease [Svedbom et al., 2013].

## **1.2 Motivation**

### **1.2.1 Trabecular bone**

The mechanical properties of cancellous bone are a major concern to orthopedic clinicians. Osteoporosis is often regarded as a disease of cancellous bone and the long term success of orthopaedic joint arthroplasty depends on a sound cancellous bone stock [Odgaard, 1997]. Work by biomechanics recognizes the importance of characterizing microarchitecture and bone matrix properties and considering multiple modes of microdamage and failure. Recent pharmacological treatments have increased both bone strength and stiffness by increasing the amount of mineral contained within bone [Wall and Board, 2013].

Cancellous bone constitutes much of the volume of bone which makes up axial skeletal sites, such as the vertebrae of the spine and the proximal femur. The increased vascularity of cancellous bone compared with cortical bone means that it is more prone to drug-, endocrine- and metabolic-related effects and, therefore these skeletal sites are more risk to the osteoporotic condition.

The cancellous bone properties vary greatly as a function of its apparent density. Its elastic compressive modulus at 75% porosity is around 160 MPa, close to the human bone trabecular compressive modulus [Pioletti, 2010]. Cancellous bone is capable at the macroscopic level of large elastic–plastic behaviour, which is due to the microstructural deformations caused by the buckling/bending and rotation of the trabeculae. The other reason is the experimental difficulties in isolating samples of a certain size, design, orientation and of course imposing the necessary loads in a way prescribed in testing methods [Cook and Zioupos, 2009].

Bone is anisotropic, meaning that its properties vary depending on the direction of loading. This is particularly difficult to handle in Finite Element Analysis (FEA) involving cancellous bone as the trabecular struts themselves are running in different directions.

Nevertheless, bone is not an isotropic material and models that assume isotropy are inherently flawed. Moreover, bone is not linearly elastic, but rather viscoelastic. This means that the rate of loading is very important in determining the resulting stress and strain. Bone that is loaded at a higher rate will exhibit stiffer behaviour, whereas, bone loaded more slowly will appear to be less stiff [Burr, 2016].

The assessment and prediction of bone strength has traditionally been related to independent measures aimed at explaining the variation in stiffness and strength. However, it has also been recognized that older persons may lose bone, as expressed by a decrease in bone density, but do not develop fractures because bone mineral density, bone geometry, bone microarchitecture, and bone material properties are all contributing components which determine bone strength [Keller, 1994; Carter and Hayes, 1977].

The limitations of quantitative morphometry in the prediction of bone failure has been demonstrated in previous studies, in which it was shown that strength of trabecular bone specimens depends on the orientation of the applied load [Bevill et al., 2009; Parkinson et al., 2012] and on local variations in the trabecular network [Perilli et al., 2012].

Trabecular bone tissue failure can be considered as consisting of two stages damage and fracture [Taylor, 2003; Wachtel and Keaveny, 1997; O'Brien et al., 2002; Yeh and Keaveny, 2001; Gupta and Zioupos, 2008]:

- **Damage:** is considered to be a loss of mechanical integrity, stiffness or strength but with the material remaining intact, that is, no new surfaces are created.
- **Fracture:** is considered to be the separation of (previously damaged) material producing new surfaces, with the separation in the structure leading to an inability to transfer load between the new surfaces [Harrison et al., 2013].

## 1.2.2 Femoroplasty

### 1.2.2.1 Clinical scenario

Trabecular bone is mainly involved in osteoporotic hip fractures. These are costly and constitute a major health problem worldwide [Lane et al., 2000; Elffors, 1998]. Since the hip fracture is, of all osteoporotic fractures, the one with highest morbidity and mortality and the

highest cost, we need to find associations, or even new methods to prevent with more efficiency this type of fracture [Hernlund et al., 2013; Cummings et al., 2002; Lawrence et al., 2010; Ryg et al., 2009].

Several methods have been applied in order to reduce the risk of fracture of the proximal femoral end due to osteoporosis, such as home care, multidisciplinary treatments, and use of hip protectors, although the most frequent measure is the use of medicines [Hemlund et al., 2013; MacLean et al., 2008].

Care measures for patients with osteoporosis in the EU have had very significant results, with multidisciplinary techniques that are capable of reducing about 80% occurrences of new fractures. However, when we look at the effectiveness of these interventions in preventing new fractures in the hip region, the figure is approximately 40%. This same number is found regarding the use of medicines to prevent hip fractures, besides the undesirable consequences of its use, as significant side effects, adverse effects in long-term use, contraindications and high cost, happening in 50% of the patients [Cummings et al., 2002; MacLean et al., 2008; Chevalley et al., 2007; Kannus et al., 2000].

An alternative preventive intervention is femoral augmentation-also referred to as femoroplasty, which is the process of injecting cement into the proximal femur to prevent osteoporotic hip fractures [Beckmann et al., 2007, 2011; Heini et al., 2004; Sutter et al., 2010a]. Femoroplasty increases the strength and energy to failure of the femur and can be performed minimally-invasively with less hospitalization costs and reduced recovery time [Beckmann et al., 2011; Fliri et al., 2012]. This procedure is still not yet very much used and stimulated by orthopedic society, but most of the studies about this method are *in vitro*, and there it has proven to reduce the risk of hip fractures, and should not be underestimated. Cement augmentation is described in various ways (Figure 6), using several products, but the experimental uses of polymethylmethacrylate (PMMA) and calcium phosphate cement (CPC) have been most frequently studied [Beckmann et al., 2007; Basafa et al., 2015].

However, the side effects associated with femoroplasty may include thermal necrosis, toxicity of the cement, and embolism. Injection of a large amount of cement, which has an exothermic curing process, may lead to osteonecrosis, i.e. death of bone tissue as a result of poor blood supply. Also suboptimal injection can result in bone weakening due to stress concentration, mainly at the cement-bone interface, and render the augmentation unsuccessful

[Basafa and Armand, 2014]. Therefore, it is desirable to use the minimum amount of cement possible to achieve the goals of augmentation.

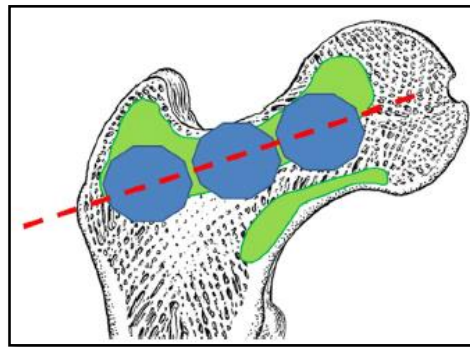


**Figure 6:** Schematic of an augmentation suggested by simulations (green) and planned path and locations of injection (blue) [Basafa et al., 2015]

### 1.2.2.2 CPC and PMMA

The use of cement is nowadays an important aid in the orthopedic field; both in situations in which it is necessary to fix a fracture in patients with severe osteoporosis (“augmentation”) and in cases where it must be ensure greater stability in the system of prosthetic hip, knee and shoulder [Magnan et al., 2013].

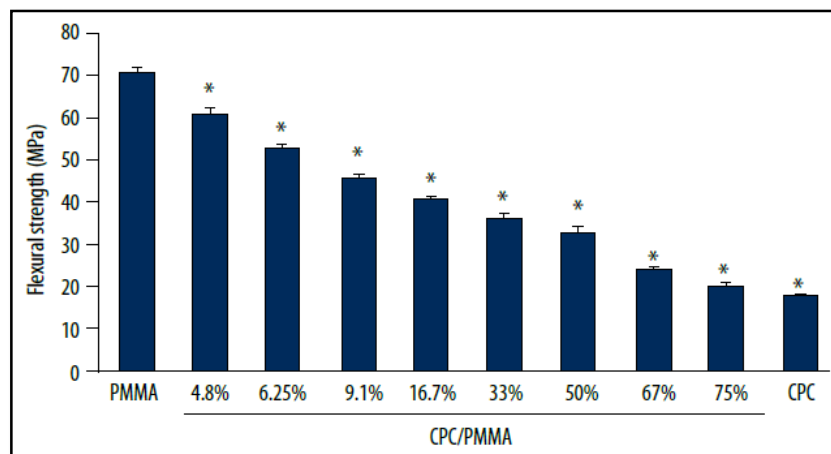


**Figure 7:** Flexural strength differences between CPC and PMMA [Yang et al., 2015]

From the literature, CPC and PMMA are powerful candidates to augment osteoporotic bones, but both the compressive strength and tensile strength have been found to enhance gradually with increasing PMMA concentration and decreasing CPC concentration (Figure 7).

In addition, the curing time has been longer in CPC groups (more than 11 min), but was shorter in PMMA groups (less than 2 min) (Figure 8) [Yang et al., 2015].

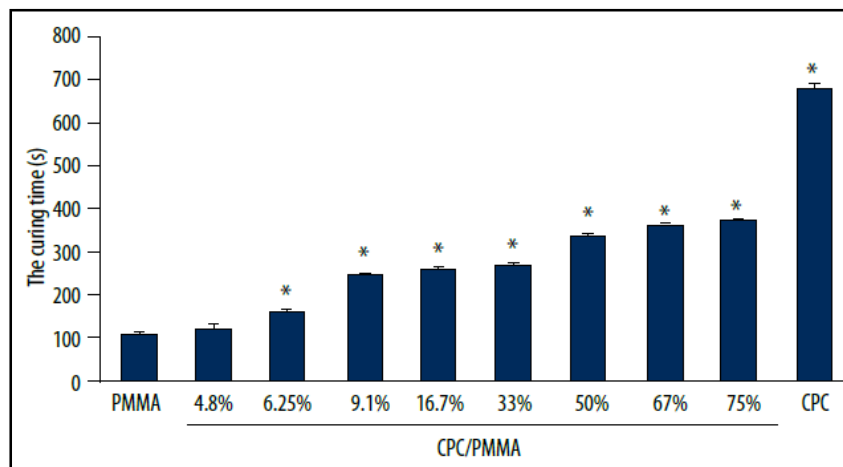


*Figure 8: Curing time differences between CPC and PMMA [Yang et al., 2015]*

In cases of prosthetic infection, joint antibiotic-loaded spacers are used and PMMA has gained favor as a vehicle for the delivery of antibiotics.

The use of antibiotic-loaded cement in joint replacement provides short- to medium-term protection against prosthetic infection. This material exploit their potential biological value allowing the bone integration within the cement structure, favoring the mechanical and biological stability of the cement system [Magnan et al., 2013]. Thus, cements play the most important role for its use in augmentation [Webb and Spencer, 2007].

### ***1.2.2.3 Surgery planning***

Femoral augmentation is a surgical procedure, minimally invasive, performed percutaneously by an incision of about 1 cm in length in the lateral region of the patient's thigh.

Through this incision, a metallic guide is inserted on the lateral cortex of the femur, in direction of the femoral head, through the femoral calcar, region in which the main forces of compression of the proximal femur are concentrated (Figure 9). This wire, introduced with fluoroscopy assistance, serves as a guide for introduction of the other instrumentals, like drills and cannulas. After the introduction of a drill, preparing the intraosseous space to be filled by "bone substitutes", a cannula is inserted through the same incision side, following the path of



metallic wire and drill, by pressurizing with a syringe the prepared space which is refilled by femoral augmentation, replacing the bone portion with compromised quality by other substances and increasing the strength of the proximal femur.

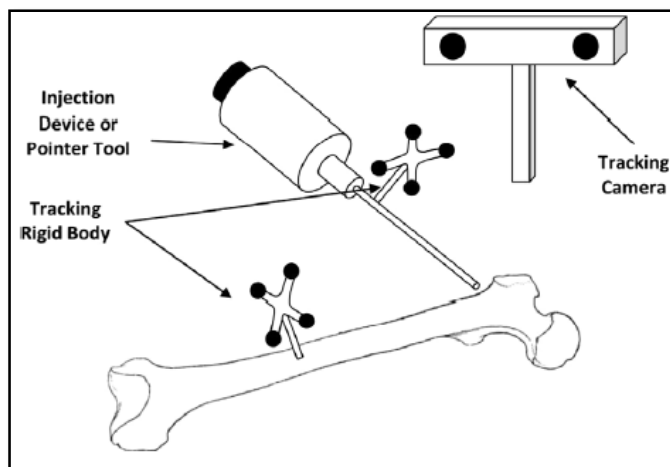


*Figure 9: Injection setup [Basafa et al., 2015]*

The calcium phosphate based cements are ceramic materials, as the PMMA are acrylic materials, both having good biocompatibility due to their chemical composition similar to the bone and bioactivity, promoting osteoconduction. With these characteristics, the use of these materials as filling or bone implants is possible. The cements are materials consisting of a powder and a liquid which, upon mixing, form a paste that hardens spontaneously at room or body temperature [Freitas et al., 2017].

#### ***1.2.2.4 Experimental and computational studies***

All published articles, between the years 2004 and 2018, that were related to the prevention of osteoporotic fractures of the hip (femoral neck and intertrochanteric region) were selected according to the inclusion criteria.

To match the inclusion criteria, only the articles that reported or analyzed exclusively human bone reinforcement with PMMA or CPC, without any focal pathology and whichever methodology that was used as augmentation, were selected.

After the selection of the articles included, we analyzed the specific data: evaluation method, material used in the femoral reinforcement and the obtained results of the procedures (Table 1).

The materials used in all experimental studies were cadaveric femurs with mineral density compatible with osteoporotic bones.

Two of the articles showed unsatisfactory results: it was used PMMA in both of them, the rise of temperature during the curing of the PMMA was indicated as a possibility of thermal injury to the bone tissue and possibly been the cause of the failure. Although one of these studies found an increase of resistance to the possibility of the fracture, using a mean volume of 36 ml [Heini et al., 2004], the other one found no enhancement of mechanical strength, with a mean volume of 15 ml [Sutter et al., 2010b].

According to studies using PMMA, it was proved an improvement in mechanical strength to the occurrence of the fractures. As the thought of the thermal injury occurring to the bone tissue in the indurating process, it was found that the optimization of the amount of volume of PMMA could reduce the rise of temperature and consequently shorten the possibility of a thermal lesion [Sutter et al., 2010b; Beckmann et al., 2011; Fliri et al., 2013; Basafa et al., 2015]. These studies showed the necessity of an increased peak load to the occurrence of a fracture in values up to 33%, using augmentation volumes ranged from 9 to 40 ml. The authors using a lower volume of PMMA intended to decrease the thermal lesion, but, in those cases, they determined an optimization of the augmentation location in the proximal femur. As negative possible outcomes, most of them described the possibility of thermal injury, a more difficult surgery for treatment in case of fracture occurrence and a chance of happening different patterns, more complex or unusual, of fracture due to the local density change.

**Table 1: Experimental and computational review of the femoroplasty technique**

<b>Study</b>	<b>Study type</b>	<b>Material used</b>	<b>Outcomes</b>
<b>Heini et al., 2004</b>	Experimental	PMMA	Volumes of 28-41 ml of cement (mean, 36 ml). The increase of surface temperature at the femoral neck ranged from 18.4° to 29.8°C. For the simulated fall on the hip, the peak fracture load was increased by 82%.
<b>Beckmann et al., 2007</b>	Experimental	CPC	Cement could be injected easily, with a moderate temperature rise. A positive correlation between BMD and fracture load and a significant increase in fracture

			load (+43%) of the augmented femora compared to their native controls, was found. Osteosynthesis was possible.
<b>Strauss et al., 2007</b>	Experimental	CPC	Calcium phosphate cement augmentation of the lag screw defect significantly increased the mean femoral neck failure strength compared to specimens in which the defect was left untreated.
<b>Sutter et al., 2010a</b>	Experimental	PMMA	Femoroplasty significantly increased yield load (22.0%), ultimate load (37.3%), yield energy (79.6%), and ultimate energy (154%) relative to matched controls, but did not significantly change stiffness (-10.9%).
<b>Sutter et al., 2010b</b>	Experimental	PMMA	It was found that femoroplasty with 15 ml of cement did not significantly increase stiffness, yield energy, yield load, ultimate load, or ultimate energy.
<b>Beckmann et al., 2011</b>	Experimental	PMMA	The energy applied until fracture could be significantly increased by two of the four methods by 160 and 164%, respectively. The peak load to failure was significantly increased by three of the methods by 23, 35 and 12%, respectively.
<b>Fliri et al., 2013</b>	Experimental	PMMA	Augmented samples absorbed 124% more energy until fracture compared to their controls. No significant differences were found.
<b>Palumbo et al., 2014</b>	Experimental and computational	PMMA	Percutaneous cementation + internal fixation (PCIF) resulted in the largest failure load though the increase was not significantly greater than the percutaneous cementation (PC) or internal fixation (IF)

---

			groups. Inspection of the PC and PCIF specimens indicated that spanned the superior and inferior cortices of the femoral neck increased failure loads significantly. FEA indicated that IF and PCIF constructs decreased the stress adjacent to the lesion to intact femur levels.
<b>Basafa et al., 2015</b>	Experimental and computational	PMMA	An average of 9.5 (+/-1.7) ml of cement was injected in the augmented set. Augmentation significantly increased the yield load by 33% and maximum load by 30% relative to the nonaugmented controls. Simulations showed that the yield load can be significantly increased by more than 30%, using only 9 ml of cement.
<b>Varga et al., 2017</b>	Computational	PMMA	Augmenting with approximately 12 ml of cement in the newly identified location achieved increases of 11% in stiffness, 64% in yield force, 156% in yield energy and 59% in maximum force, on average, compared to the nonaugmented state. The weaker bones experienced a greater biomechanical benefit from augmentation than stronger bones.
<b>Santana Artiles and Venetsanos, 2017</b>	Computational	PMMA	A new evolutionary optimization method was introduced for the augmentation of osteoporotic bones. The proposed method required much less time to achieve an increase of 115% in the yield load by converging to a cement volume of approximately 12 ml.

---

<b>Santana Artiles and Venetsanos, 2018</b>	Computational	PMMA	This paper numerically investigated the effect of cement porosity on a typical femoroplasty. It was found that, for the same level of cement porosity, the frontal angle has a stronger influence than the transverse angle, with their correlation being highly non-linear.
---	---------------	------	--

Using the CPC, brought a lower temperature rise in both studies, as they exposed as results the increase of mechanical resistance and a reduced possibility of thermal injury to the bone tissue [Strauss et al., 2007; Beckmann et al., 2007].

These studies showed an increase in the peak loading to fracture occurrence in values ranging from 21 to 43%, but the augmentation volumes used of such substance weren't described, but their articles showed a complete filling of the proximal femur, a questionable fact for its application *in vivo*.

#### **1.2.2.5 Particle models**

Some of the presented studies (Table 1) described new approaches to computer-assisted planning of femoroplasty to optimize cement volume and placement [Basafa et al, 2015; Varga et al., 2017; Santana Artiles and Venetsanos, 2017]. A crucial step in the planning process is to determine the optimum volume and filling pattern of the cement so that the best outcome is achieved [Basafa et al., 2013]. A successful planning framework should hence include a module for predicting cement diffusion inside porous cancellous (spongy) bone.

The injection process, which, from a physical point of view, is a fluid-dynamics problem, has been numerically examined using different computational methods [Landgraf et al., 2015]. The simulations are based on the solution of Darcy's law in conjunction with region-specific intrinsic permeability, whereat specific values are directly connected to computer tomography data of the trabecular structure. In order to determine specific relations between trabecular bone morphology and corresponding intrinsic permeability, different approaches on the microstructural scale by computational fluid dynamics (CFD) simulations are reported. Baroud et al. (2006), for instance, used a combination of experimental and analytical methods.

Landgraf et al. (2015) investigated the treatment and the impact of injected cement within an integrated model that included (i) the generation of microstructural computer models based on micro-computed tomography ( $\mu$ CT) images of human cancellous bone, (ii) computational fluid dynamics (CFD) simulations of cement injection into the trabecular structure and (iii) non-linear FE simulations of the subsequent cement curing. Furthermore, numerical simulations of microstructural fluid flow through cancellous bone structure are utilized by using different numerical methods, like the lattice Boltzmann method [Zeiser et al., 2008], the finite volume method [Teo and Teoh, 2012] or smoothed-particle hydrodynamics [Basafa et al., 2013]. Additionally, morphological models have been employed to analyse the microstructural flow of cement [Widmer and Ferguson, 2013].

In the more recent years, particle models have gained popularity for modeling fluid flows [Borau et al., 2014; Basafa et al., 2013]. These models provide a Lagrangian view of the flow, where the simulation (observer) tracks the motion of fluid particles, as opposed to tracking the change of variables inside fixed grid cells in space as in the Eulerian view. Among these models' advantages over grid-based methods are the inherent conservation of mass, no need for creating and maintaining a grid structure and fast computations of equations of motion. Because of their superior simulation speeds, particle models are of utmost interest in the graphics community and they have been used to model fluids and flow of colloids such as sand [Liu et al., 2007; Clavet et al., 2005; Zhu and Brdison, 2005; Steele et al., 2004]. Heuristic approaches are taken in these methods to model the particle-particle and particle-environment interactions that best serve the specific application of interest [Basafa et al., 2013].

### **1.3 Objectives**

Millions of fragility fractures occur directly because of osteoporosis, often at trabecular-dominant bone sites. Indeed, the trabecular bone plays an important role in load transmission and energy absorption in major joints such as the knee, hip, and spine. It is believed that, in addition to the bone volume fraction (the ratio of the volume of bone tissue to the overall bulk volume), the detailed microarchitecture, including trabecular orientation and connectivity, is important in governing the mechanical properties of trabecular bone [Wang et al., 2015]. The structure of artificial open-cell rigid foams resembles that of human cancellous bone. The cell structure is over 95% open and the cell size is 1.5 to 2.5 mm. Furthermore, they are suitable for

a variety of applications that require an open cell structure, such as dynamic testing or cement injection.

As regards cement injection, femoroplasty is a technique to prevent osteoporotic hip fractures by injecting cement, resulting in an increase of the mechanical properties of the trabecular bone.

Therefore, the main goal of this thesis is the design and development of a multiscale model for the osteoporotic fracture prevention. This model will allow us to know more about the failure mechanisms associated to osteoporosis from the tissue to the organ level in order to assess the femoroplasty feasibility. In order to achieve this main goal, secondary objectives are proposed:

- *In vitro* and *in silico* characterization of three types of open-cell structures for trabecular bone.
- Development of a discrete particle model for cement infiltration within open-cell structures.
- *In vitro* and *in silico* characterization of augmented open-cell structures with a quantitative and qualitative assessment of augmentation.
- Development of a local bone augmentation strategy to control cement volume and placement in macroscopic femora.
- *In vitro* biomechanical study for the assessment of cement augmentation in a rabbit fracture model.
- Development of a computational subject-specific approach for osteoporotic femoral augmentation.

#### **1.4 Thesis overview**

This thesis is structured as follows:

This chapter (Chapter 1) is an introduction which describes the main concepts of the clinical scenario of trabecular bone and osteoporosis and its consequences on the bone tissue are detailed. Second, femoroplasty technique is reviewed and specific sequences in femur and, in particular, in trabecular bone are commented. Additionally, the crucial role of the particle

models to simulate cement diffusion inside porous media has been also presented. Finally, we clarify the motivation of this thesis and the objectives of this subject-specific approach.

Chapter 2 shows an *in vitro* and *in silico* characterization of open-cell structures for trabecular bone, in which specific details about experimental data acquisition, image processing, three-dimensional reconstructions and mechanical simulations based in FE method are described.

In Chapter 3 a discrete particle model, based on the random-walk theory [Perez and Prendergast, 2007], for cement infiltration within open-cell structures is proposed in order to simulate augmentation process and to observe *in vitro* and *in silico* mechanical properties improvement in those open-cell structures.

In Chapter 4, we will present a rabbit fracture model for evaluation of the cement augmentation following an *in vivo* and *in vitro* biomechanical study in order to assess the feasibility of the femoroplasty technique in animals.

In chapter 5, we extend the framework shown in Chapter 3 to the human organ level showing a generalized bone augmentation strategy based on previous studies by which we will control cement injection and placement inside macroscopic healthy and osteoporotic femora. Two cement viscosities (high- and low-) will be compared and the final augmented properties will be analysed.

Finally, chapter 6 copes with the main conclusions of this work and also summarizes the possible lines of future work to the final application in clinics.



# Chapter 2

---

## *In vitro and in silico characterization of open-cell structures of trabecular bone*

This chapter is published as:

Samuel Jesús Ramos-Infante and María Ángeles Pérez. *In vitro and in silico* characterization of open-cell structures for trabecular bone. *Computer Methods in Biomechanics and Biomedical Engineering*, Vol. 20 (14), 1562–1570. October (2017).



## 2.1 Introduction

Bone strength reflects the integration of two main features: BMD, expressed as grams of mineral per area/volume, and bone quality, which consists of bone architecture, turnover, damage accumulation, collagen cross-linking, and bone mineralization [Cowin, 1989]. In combination with cortical bone, trabecular bone is a major load-bearing biological tissue in human bone. Trabecular bone is involved in bone femur fractures and is the primary site for the insertion of orthopaedic implants [Eswaran et al., 2006]. Substantial direct and indirect social and economic costs are associated with these fractures, which emphasize the need for the prevention and treatment of osteoporotic disease [Daszkiewicz et al., 2017]. Osteoporosis is now recognized as a major public health problem facing postmenopausal women and ageing individuals irrespective of gender [Stauber et al., 2014]. In fact, osteoporosis is a widespread skeletal disease that is responsible for deleterious fractures [Hadji et al. 2013]. In this context, *in silico* medicine may prove useful [Viceconti, 2015].

Because bone is anisotropic, it is particularly difficult to handle in FEA involving cancellous bone as the trabecular struts themselves run in different directions. The properties of cancellous bone vary greatly as a function of their apparent density. For cancellous bone, the elastic compressive modulus at 75% porosity is approximately around 160 MPa, which is close to the human bone trabecular compressive modulus [Pioletti, 2010].

Many computational models to predict the mechanical properties of trabecular bone have been developed. For instance, the elastic behaviour of trabecular bone was studied using several different approaches, involving analytical and computational techniques. Analytical studies represent trabecular bone as a cellular solid and express its Young's modulus by power law relations in terms of density [Gibson et al., 1982; Gibson, 1985; Gibson and Ashby, 1982, 1999; Gibson et al., 2010; Rajan, 1985]. Although density is a key parameter in determining the properties of trabecular bone, density alone cannot fully capture the mechanical behaviour of bone. Other researchers have defined a fabric tensor, which characterizes the textural or structural anisotropy of trabecular bone, and described the relationships between the elastic constants of trabecular bone and its fabric tensor and density [Kabel et al., 1999; Turner et al., 1990; Zysset, 2003]. Trabecular bone architecture, which is characterized by the thickness, number and separation distance of individual trabecula as well as their three-dimensional connectivity, plays an important role in its response. Thus, high-resolution imaging techniques, that account for actual trabecular bone architecture, such as  $\mu$ CT, were used in combination

with the finite element method (FEM) to predict Young's modulus of trabecular bone [Müller and Rüeegsegger, 1995; Ulrich et al., 1998; Bourne et al., 2004; Harrison et al., 2008; Dobson et al., 2006; Follet et al., 2007; Pahr and Zysset, 2008]. Generally, FE models of bones may be categorized into two groups: micro-finite element ( $\mu$ FE) models, in which the trabecular bone morphology is modelled in detail [Homminga et al. 2004; Verhulp et al., 2006; Fields et al., 2009; Nawathe et al., 2013], and homogenized continuum-level (hFE) models, in which one element covers a larger bone region, which is considered a homogeneous material [Faulkner et al., 1991; Martin et al., 1998; Pistoia et al., 2001; Crawford et al., 2003; Imai et al., 2006; Schileo et al., 2007; Pahr and Zysset, 2009; Pahr et al., 2012]. hFE models have been used for diverse clinical applications such as predicting bone strength [Zysset et al., 2013] and mechanical properties [Van Rietbergen et al., 1995], but meshing [Viceconti et al., 1998; Treece et al., 1999; Ito et al., 2006] and material mapping [Pahr and Zysset, 2009; Taddei et al., 2007] may be challenging. The limitations of quantitative morphometry for the prediction of bone failure have been demonstrated in previous studies, which showed that the strength of trabecular bone specimens depends on the orientation of the applied load [Bevill et al., 2009; Parkinson et al., 2012] and on local variations in the trabecular network [Perilli et al., 2012]. From a geometric or mesh point of view, one can distinguish between voxel-mesh [Crawford et al., 2003; Keyak et al., 1997; Dall'Ara et al., 2013] and smooth mesh geometries (linear tetrahedral and quadratic tetrahedral) [Luisier et al., 2014; Zysset et al., 2015; Jones and Wilcox, 2007; Yosibash et al., 2010]. Although these elements are normally used in full-bone meshes [Pahr and Zysset, 2016], it would be interesting to observe the effects of these element types on the prediction of the mechanical properties of trabecular bone.

Indeed, trabecular bone plays an important role in load transmission and energy absorption at major joints such as the knee, hip, and spine. It is believed that, in addition to the bone volume fraction (the ratio of the volume of bone tissue to the overall bulk volume), the detailed microarchitecture, including trabecular orientation and connectivity, is important in governing the mechanical properties of trabecular bone [Wang et al., 2015]. For this reason, efforts to quantify structural properties have gained prominence, and many different methods have been proposed to further describe the influence of changes in bone microstructure on bone mechanical properties [Hildebrand and Rüeegsegger, 1997; Jinnai et al., 2002; Zysset, 2003; Gomberg et al., 2003]. It is also possible that heterogeneity may locally weaken the trabecular bone structure and ultimately initiate failure. This possibility casts doubt on the reliability of

failure prediction based on average morphometric indices and the appropriate interpretation of the mechanical results from compression testing [Stauber et al., 2014].

The structure of open-cell rigid foams resembles that of human cancellous bone. The foams are produced by a polymerization reaction that takes place simultaneously with the generation of carbon dioxide by the reaction of water and isocyanate. The result is a closed foam structure, which is a cellular solid structure made up of an interconnected network of solid struts or plates that form the edges and faces of cells [Thompson et al., 2003]. The cell structure is over 95% open and the cell size ranges from 1.5 to 2.5 mm. Furthermore, these foams are suitable for a variety of applications that require an open-cell structure, such as dynamic testing or cement injection, prior to clinical purposes. Therefore, this chapter involved *in vitro* and *in silico* characterization of commercial open-cell structures to quantify the influence of voxel-mesh and smooth mesh geometries for the prediction of the mechanical properties of trabecular bone. Our results will reveal new research strategies to prevent osteoporotic fractures. To achieve this goal, Young's modulus was compared between three commercial open-cell structures (Sawbones; Malmö, Sweden) with different porosities to assess the best element type that represents trabecular bone microarchitecture (linear tetrahedral, quadratic tetrahedral or voxel). A 3D reconstruction from  $\mu$ CT images was performed and  $\mu$ FE models were developed using MIMCS (Materialise NV, Leuven, Belgium). Subsequently, the computationally estimated Young's modulus and porosity results were compared with the experimental and commercial Sawbones data.

## 2.2 Materials and methods

Three different open-cell structures were studied (Sawbones; Malmö, Sweden) (Table 2 and Figure 10). Henceforth, we will refer to these as specimen #30 (Sawbones, product no. 1522-525; Malmö, Sweden; Figure 10), specimen #20 (Sawbones, product no. 1522-524; Malmö, Sweden; Figure 10) and specimen #15 (Sawbones, product no. 1522-526-1; Malmö, Sweden; Figure 10). Their densities resembled trabecular bone and varied from 0.24 g/cm<sup>3</sup> to 0.48 g/cm<sup>3</sup> (Table 2). We had 53 cubic specimens (17 of specimen #15, 18 of specimen #20 and 18 of specimen #30) (Figure 10). First, an *in silico* characterization was performed to simulate the experimental compressive test. Then, an *in vitro* characterization was performed (Figure 11).

Both results were compared with Sawbones specifications (Figure 11). The apparent Young's moduli and porosities were assessed.

Table 2: Open-cell specimen dimensions, densities, volume fractions and Young's modulus

Specimen	Number of specimens	Density (g/cc)	Porosity specifications (%)	Young's modulus Sawbones specifications (MPa)	Base (mm)	Height (mm)	Thickness (mm)
#15	17	0.24	85	53	20	40	20
#20	18	0.32	79	105	20	40	20
#30	18	0.48	69	270	20	40	20



Figure 10: On the left, specimen #30; in the middle, specimen #20; on the right, specimen #15

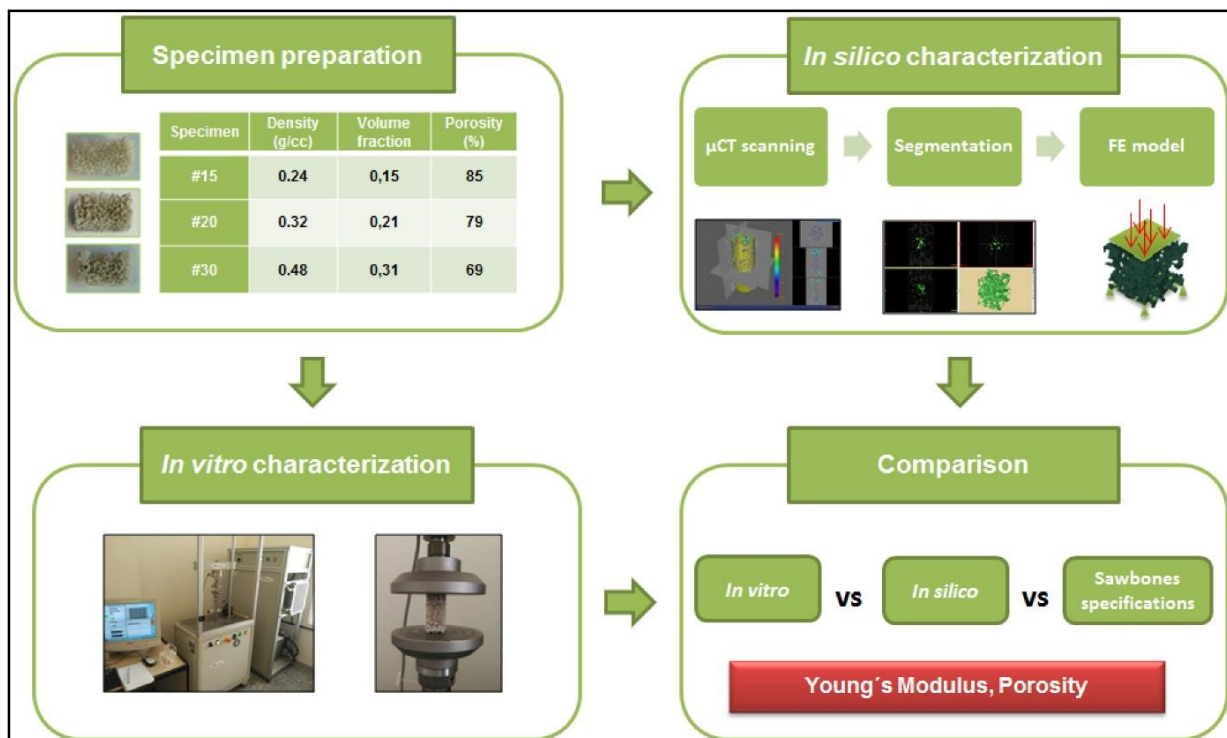
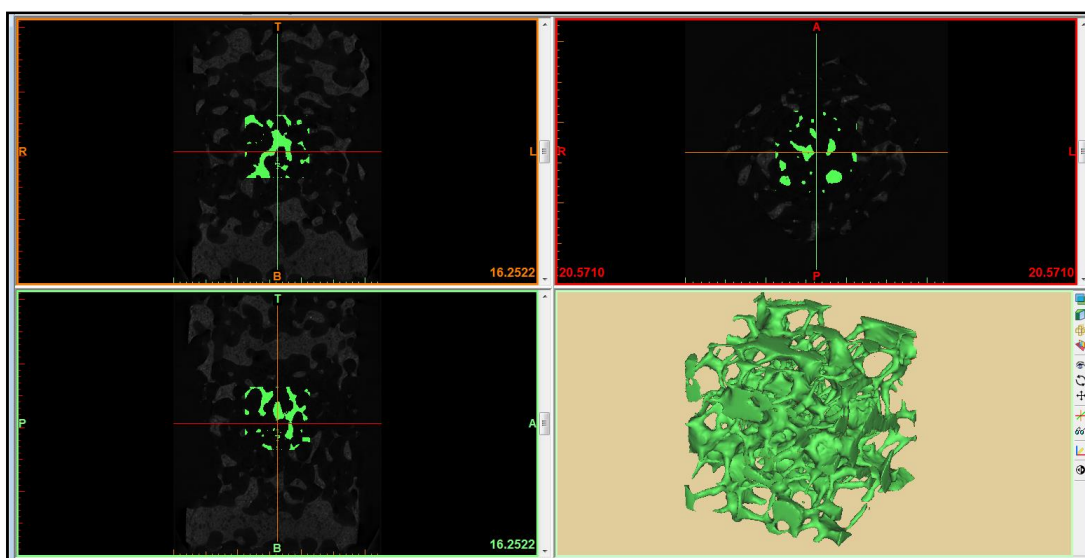


Figure 11: Workflow for the in vitro and in silico characterization of the open-cell structures of trabecular bone

### 2.2.1 *In silico* characterization

First, among the 53 specimens only 18 (6 of each type) were scanned along their height with a microcomputed tomography system prior to the compression tests ( $\mu$ CT50, General Electric; Milwaukee, WI, USA), using a 50- $\mu$ m nominal resolution to assess the architecture of the trabeculae. The scanned images were reconstructed using a semiautomatic reconstruction (MIMICS, Materialise NV; Leuven, Belgium) (Figure 12). All specimens were also digitally cut to exclude bone fragments that might have been generated from the cutting process and to exclude unintentionally cut trabeculae (Figure 12). Therefore, the representative volume element (RVE) dimensions were 10 mm in base, 10 mm in height and 10 mm in thickness (10 $\times$ 10 $\times$ 10 mm).

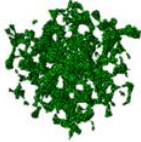
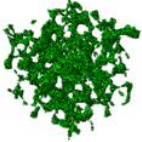
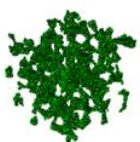
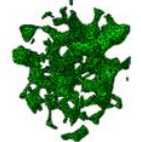
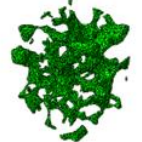
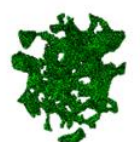
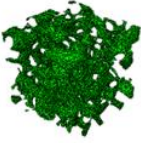
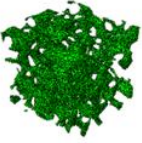
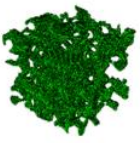
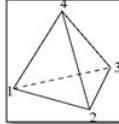
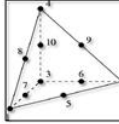
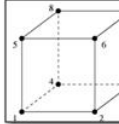


**Figure 12:** Segmentation of CT data for each specimen using FE material assignment module in MIMICS (Materialise NV, Leuven, Belgium)

The threshold  $\mu$ CT images of trabecular bone were converted to  $\mu$ FE models using the 3-Matic tooling module (Materialise NV; Leuven, Belgium) and the Voxel Create Mesh Module supplied by MIMICS (Materialise NV, Leuven, Belgium). After the mesh was constructed, the resulting  $\mu$ FE models were imported into the commercial FE software package ABAQUS v.6.14 (Dassault Systèmes Simulia Corp.; Suresnes, France).

Three mesh types were analysed. First, a voxel mesh based on the original  $\mu$ CT images of trabecular bone (8-node brick element) was constructed. The voxel size was 12  $\mu$ m (Figure 13). Then, a linear tetrahedral mesh (mean element size: 25  $\mu$ m) and a quadratic tetrahedral

mesh (mean element size: 25  $\mu\text{m}$ ) were considered (Figure 13). The final tetrahedral mesh size was defined after mesh convergence analysis.

	<b>C3D4</b>	<b>C3D10</b>	<b>C3D8</b>
<b>#15</b>			
<b>#20</b>			
<b>#30</b>			
<b>Element type</b>			

**Figure 13:** Three-dimensional reconstruction of the trabeculae using linear tetrahedral (C3D4), quadratic tetrahedral (C3D10) and voxel (C3D8) elements

The bulk material was assumed to be linear elastic and isotropic. Therefore, the elements of the FE meshes were assigned a Young's modulus of 3200 MPa ( $E_{tissue}^{FE}$ ). The Poisson's ratio was defined as 0.3. Previous mechanical properties were provided by Sawbones (Sawbones; Malmö, Sweden).

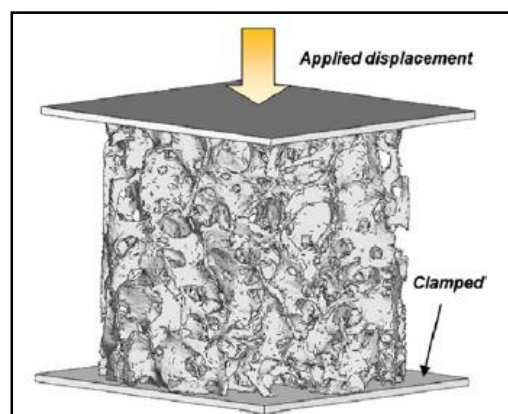


**Figure 14:** FE model reproducing the compression [Hambli, 2013]



The boundary conditions for the  $\mu$ FEM model were based on idealizations of those of a uniaxial compression test [Wang et al., 2015]; a uniaxial displacement (strain of 2%) was applied to the top surface of the cubic bone samples [Wang et al., 2015]. The bottom surface was kept fixed [Van Lenthe et al., 2006], and the sides were calculated as traction-free [Hamed et al., 2012] (Figure 14). In addition, contact between the upper and lower surfaces of the specimen and the plates was modelled using contact elements with a zero friction value to ensure that only compressive forces were transmitted [Hambli, 2013].

Non-linear FE analyses were performed in ABAQUS v6.14 (Dassault Systèmes Simulia Corp.; Suresnes, France) and run in a computational cluster of 224 cores and 576 GB of RAM. After the FE analysis, the apparent Young's modulus (1) was calculated using the following equation:

$$E_{app}^{Voxel} = \frac{\sigma_{app}}{\varepsilon_{app}} = \frac{F/A}{\Delta L/L} \quad (1)$$

in which  $F$  is the force calculated from each FE simulation (N),  $A$  is the apparent specimen cross-section ( $\text{mm}^2$ ),  $\Delta L = 0.2$  mm and  $L$  is the specimen length ( $L = 10$  mm). Once the apparent Young's modulus was calculated, the apparent porosities ( $P_{app}^{Voxel}$ ) were obtained using equation (2), in which  $n$  was determined to be equal to 2 for an open-cell structure [Hamed et al., 2012]:

$$P_{app}^{Voxel} = 1 - \sqrt[n]{\frac{E_{app}^{Voxel}}{E_{tissue}^{FE}}} \quad (2)$$

Furthermore, we could also calculate and compare the above mentioned porosities with the porosity associated with the specimen dimensions:

$$P_{sp} = \left(1 - \frac{V_{app}}{V}\right) \cdot 100 \quad (3)$$

where  $V_{app}$  is obtained from the FE material assignment module in MIMCS (Materialise NV; Leuven, Belgium) and  $V$  is the specimen volume size without pores ( $V \approx 1000$   $\text{mm}^3$ ) obtained after the 3D specimen reconstruction.

### 2.2.2 *In vitro* characterization

Briefly, compression experiments were conducted using a servo-hydraulic material testing machine (Microtest, model EFH; Figure 15). Each specimen was placed between steel plates at room temperature (approx. 23 °C) and loaded in the direction of their axis of symmetry (Figure 15). The quasi-static compression load was measured with a commercial load cell (10 kN) applied at a constant velocity rate of 1 mm/min [Keaveny et al., 1993]. Then, the force-displacement curves were measured for each test, and the Young's modulus was calculated.



Figure 15: On the left, servo-hydraulic material testing machine; on the right, uniaxial compression test

### 2.2.3 Statistical analysis

Significant differences, defined by  $p < 0.05$ , between the *in vitro* and the *in silico* characterizations using paired t-tests were assessed.

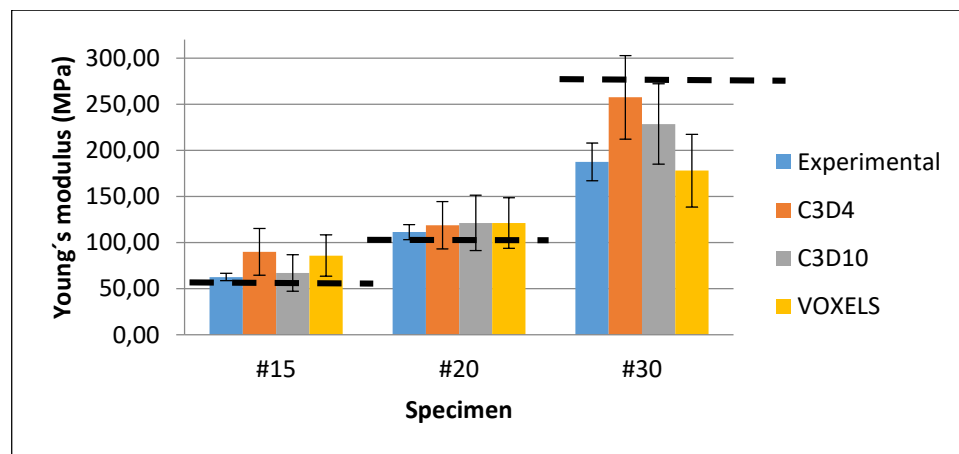
## 2.3 Results

The experimental data clearly showed an increase in Young's modulus with bone volume fraction (Figure 16a). Furthermore, our experimental results for Young's modulus are close to the values provided by Sawbones (Sawbones; Malmö, Sweden) for specimen #15 and #20. In contrast, specimen #30 had a lower Young's modulus (Figure 16a) than the Sawbones specifications.

With regard to the apparent Young's modulus (Table 3), we observed that, depending on the mesh type used to perform the FEA, different values for the apparent Young's modulus could be obtained. For instance, the quadratic tetrahedral elements were more suitable for

representing the real mechanical properties of the specimens that possessed lower volume fractions (Figure 16a) but also overestimated apparent Young's modulus. Statistical analysis verified this observation for specimen #15 ( $p = 0.88$ ). The use of quadratic tetrahedral elements resulted in a reduction in the inherent stiffness of linear tetrahedral elements. In contrast, linear tetrahedral elements were capable of representing the real mechanical properties of specimens with higher volume fractions (Figure 16) but underestimated the apparent Young's modulus. Statistical analysis also verified this observation for specimen #30 ( $p = 0.07$ ). Similarly, we observed that regardless of the mesh type used to perform the FEA, for volume fractions near 0.20 (Figure 16), the Young's modulus results and estimated porosity were similar to the real values ( $p > 0.83$  for all simulated cases). Despite these results, we found that the standard deviations seemed to increase as the volume fraction increased (Table 3).

a)



b)

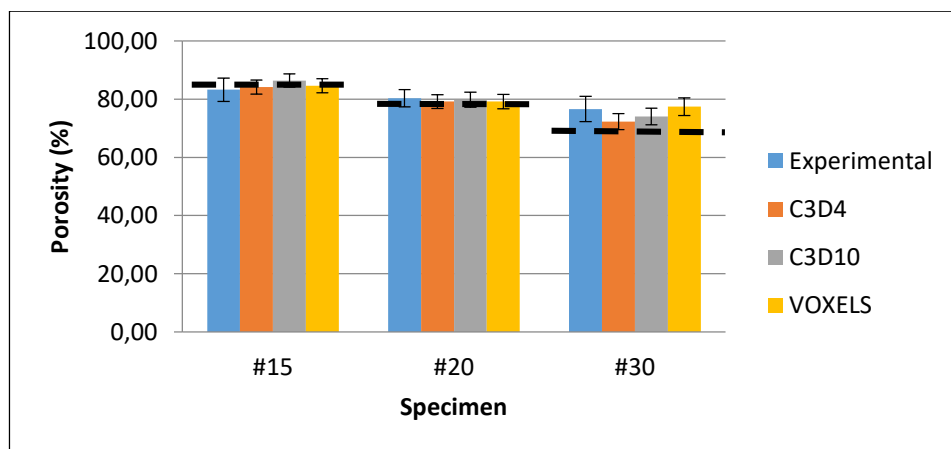


**Figure 16:** Comparison among experimental, computational and Sawbones specifications of a) Young's modulus (MPa) and b) porosity. The dashed line represents Sawbones specifications. Bars represented the standard deviation.

With regard to estimated porosities (Table 4), large correlations between the estimated and real porosities were observed regardless of mesh type (Figure 16). In addition, the mean porosities and standard deviations seemed to increase as the volume fraction increased (specimen #30). Nevertheless, the porosity results showed that linear tetrahedral elements were more suitable for representing the actual porosity of specimen #30.

**Table 3: Young's modulus (mean  $\pm$  SD) obtained experimentally and through three different finite element analyses**

Specimen	Dimensions (mm)	$A_{app}$ (mm <sup>2</sup> )	$E_{experimental}$ (MPa)	$E_{app}^{lin tet}$ (MPa)	$E_{app}^{quad tet}$ (MPa)	$E_{app}^{Voxel}$ (MPa)
#15	10×10×10	15.39±3.20	62.74±4.14	89.93± 5.45	67.15±19.82	85.89±22.33
#20	10×10×10	23.36±2.53	111.35±8.24	118.67±25.70	121.38±30.17	121.16±27.36
#30	10×10×10	26.18±2.70	187.47±20.53	257.57±45.29	228.58±43.55	178.05±39.44

**Table 4: Estimated porosities (mean  $\pm$  SD) obtained experimentally and through three different finite element analyses**

Specimen	Dimensions (mm)	$P_{sp}$ (%)	$P_{app}^{lin tet}$ (%)	$P_{app}^{quad tet}$ (%)	$P_{app}^{Voxel}$ (%)
#15	10×10×10	83.21±3.98	84.15±2.44	86.38±2.21	84.55±2.44
#20	10×10×10	80.31±2.96	79.15±2.38	79.75±2.59	79.15±2.48
#30	10×10×10	76.59±4.34	72.30±2.75	74.02±2.81	77.38±2.99

## 2.4 Discussion

Anderson et al. [2007] outlined the major steps required to build a conceptual model that is a simplification of the actual conditions of interest and to then build a physical model (laboratory experiment) and a mathematical FE model from the conceptual model. After testing and simulation, the results are compared, the uncertainties are analysed, and a statistical statement is formulated that determines whether the simulation model fits the experiment. Therefore, in this chapter, an *in vitro* and *in silico* characterization of open-cell structures of trabecular bone was performed.

Daszkiewicz et al. [2017] obtained a broad range of bone volume fraction (BV/TV) for the healthy femur of  $0.242 \pm 0.060$ . Therefore, to accurately predict the mechanical properties of both healthy and osteoporotic cancellous bone, we used three different specimens of open-cell structures (Sawbones; Malmö, Sweden) (Table 2) of the same size but different densities.

We obtained experimental and computational results through compression tests and  $\mu$ FE analyses, respectively, of previous open-cell structures. A major strength of this study was the use of specimens with large variations in their microarchitecture and bone volume fraction for the experimental validation so that an accurate prediction of the mechanical properties of the artificial cancellous bone was achieved.

The gold standard for determining bone competence is an assessment of its mechanical properties in a functional mechanical test that determines the resultant stress and strain [Burr, 2016]. First, experimental tests have been proposed to assess specimens. The experimental data clearly show an increase in Young's modulus with the bone volume fraction. Furthermore, our experimental results for Young's modulus are on the higher side but are on the lower side of the values provided by Sawbones (Sawbones; Malmö, Sweden) depending on the volume fraction. Hamed et al. [2012] showed that machining bone samples may cause significant surface defects that may result in a reduction in the mechanical properties of the specimen, that is, a reduction in Young's modulus (specimen #30). In fact, our initial specimens ( $20 \times 20 \times 40$  mm) were cut from a larger specimen with a volume of  $180 \times 130 \times 40$  mm. Additionally, Dendorfer et al. [2008] showed that the accumulation of trabecular tissue damage and fracture affects the induced force-displacement curve of the whole specimen. Furthermore, Hambli [2013] observed that in some cases, Young's modulus increases significantly because the progressive contact of the trabeculae generates compaction of the specimen microstructure (specimen #15). In fact, the loading rate plays an important role due to the stiffer behaviour bone exhibits when it is loaded at a higher rate, whereas bone that is loaded more slowly will appear to be less stiff [Burr, 2016]. Despite these limitations, our experimental results are in agreement with the mechanical properties provided by Sawbones (Sawbones; Malmö, Sweden).

Second,  $\mu$ FE models were used and continue to be an important simulation tool. These models help interpret the results of mechanical tests and can reduce *in vitro* testing. However, we should take into account the numerical errors and uncertainties that occur with these methods [Ladd and Kinney, 1998; Hamed et al., 2012]. Therefore, in this paper, the effects of element type and element size and the effects of different specimen volume fractions were

investigated. The results showed that the element type had some effects on the predicted yield behaviour. Due to the better bending behaviour for quadratic elements in specimen #15, the predicted Young's modulus were considerably lower than those obtained using linear elements [Verhulp et al., 2007]. In contrast, specimens #20 and #30 showed better correlations for Young's modulus prediction with linear tetrahedral elements. A poor correlation was predicted using the voxel FE mesh for specimen #30. This result could be due to the substantial lack of connections during voxel meshing [Ulrich et al., 1998]. Nevertheless, some simplifications in our model have been assumed, so further analysis is needed.

In the present chapter, we found that the variance in volume fraction in a single specimen can be relatively large [Stauber et al., 2014] due to the cutting process during specimen manufacture. Therefore, the first challenge is how to set a threshold value for  $\mu$ CT images to accurately capture bone architecture and porosity. FE predictions of the Young's modulus were already reported to be strongly affected by the threshold used for the segmentation of CT data to create the FE mesh [Hara et al., 2002] and are extremely sensitive to errors due to the power relationship between the volume fraction and mechanical properties [Chevalier et al., 2007]. A finer resolution would better capture the trabecular bone architecture and lead to more accurate FE predictions. Another assumption is related to the constitutive behaviour of trabecular bone tissue. In this case, the non-linear nature of trabecular bone tissue has been simplified. This process can lead to errors due to modelling hypotheses and experimental errors in the compression test procedures [Keaveny et al., 1997], and in some cases, can lead to surprisingly low values for Young's modulus [Hou et al., 1998; Ladd et al., 1998]. Finally, to avoid large computation time that can arise for more complex analyses, some authors [Lu et al., 2015; Bayraktar and Keaveny, 2004; Jaasma et al., 2002; Niebur et al., 2000] have instead used smaller sub-regions, but this approximation was already said to result in errors as large as 9.5% in predictions of apparent stiffness [Bayraktar et al., 2004].

## **2.5 Conclusions**

To summarize, our results indicate differences among the element type used for the FEA (linear tetrahedral vs quadratic tetrahedral vs voxel mesh). For instance, it could be concluded that quadratic tetrahedral elements were more suitable for representing the actual mechanical properties of specimens with lower volume fractions (high porous structures); that is, osteoporotic cancellous bone failure was able to be predicted using quadratic tetrahedral

elements. In contrast, linear tetrahedral elements were capable of representing the real mechanical properties of specimens with higher volume fractions (low porous structures). Similarly, we observed that regardless of the mesh type used to perform the FEA, both Young's modulus and estimated porosity were similar to the values in actual cases when the volume fractions were near 0.20. The use of linear and quadratic tetrahedral elements has not only allowed us to predict the mechanical properties of trabecular bone, but also led to a considerable reduction in computational costs.

A detailed *in vitro* and *in silico* characterization of open-cell structures was performed in this chapter. Thus, our results will contribute to new strategies for osteoporotic fracture prevention that should be tested *in vitro* and supported by computational models.





# Chapter 3

---

## *Discrete particle model for cement infiltration within open-cell structures: prevention of osteoporotic fracture*

This chapter is published as:

Samuel Jesús Ramos-Infante, Amadeo Ten-Esteve, Ángel Alberich-Bayarri and María Ángeles Pérez. Discrete particle model for cement infiltration within open-cell structures: Prevention of osteoporotic fracture. PloS ONE, Vol. 13 (6), e0199035. June (2018).



### 3.1 Introduction

Osteoporosis is a skeletal disease characterized by low bone mineral density (BMD) and micro-architectural deterioration of bone tissue, leading to increased bone fragility and risk of fracture [Who, 2003]. Osteoporotic proximal femur fractures are associated with high morbidity and dramatically reduce a patient's quality of life [Hopley et al., 2010]. Although these events account for less than 20% of all osteoporotic fractures, they represent the majority of fracture-related health care expenditure and mortality in men and women over the age of 50 years [Ström et al., 2011].

Current preventive measures include lifestyle interventions, fall prevention and hip protectors [Cianferotti et al., 2015; Santesso et al., 2014; Zimmerman et al., 2010]. A variety of drugs have been tested but are limited in efficacy due to long delays in restoring bone strength, high costs, and side-effects such as an increased risk of cancer [Kanis et al., 2013; Ferrari et al., 2016; Pike et al., 2010].

Because morbidity associated with such fractures has a significant socioeconomic cost [Santana Artiles and Venetsanos, 2017], various treatments have been proposed to increase bone mass and decrease fracture incidence. One such treatment is the mechanical reinforcement of functionally relevant osteoporotic bones such as the femur [Beckmann et al., 2007]. Femoroplasty is the process of injecting polymethylmethacrylate (PMMA) hereafter referred to as cement, into the proximal femur to prevent osteoporotic hip fracture [Beckmann et al., 2011; Heini et al., 2004; Sutter et al., 2010a]. Femoroplasty increases the strength and energy to failure of the femur and can be performed in a minimally-invasively manner with lower hospitalization costs and reduced recovery time [Beckmann et al., 2011; Fliri et al., 2012]. The reinforcement is achieved via percutaneous cement injection to prevent progressive deformity or collapse and to alleviate disabling pain [Heini et al., 2001]. Initially, the injected material takes the form of a viscous dough, and a few minutes after injection into the bone, the dough polymerizes and solidifies.

A vast number of published studies [Beckmann et al., 2011; Heini et al., 2001, 2004; Feng et al., 2014; Steenhoven et al., 2012; Jensen et al., 1997; Tohmeh et al., 1999; Zoarski et al., 2002] have concluded that after augmentation using cement, osteoporotic femurs may become significantly stronger, offering a reduced risk of fracture [Heini et al., 2004; Sutter et al., 2010a; Aquarius et al., 2014]. First-generation femoroplasty approaches resulted in significant improvements in both fracture load and energy compared with those on the

nonaugmented contralateral side [Beckmann et al., 2007; Heini et al., 2004; Sutter et al., 2010a]. However, an elevated risk of biological impairment was recognized due to heat, toxicity, pressure, leakage or blockage of the blood support associated with the large cement volume. Therefore, in second-generation femoroplasty studies, the amount of cement was decreased [Beckmann et al., 2011; Fliri et al., 2012; Springroum et al., 2014; Sutter et al., 2010b]. Additionally, suboptimal injection can result in bone weakening due to stress concentration, primarily at the cement-bone interface, rendering the augmentation unsuccessful [Basafa and Armand, 2014].

Another study revealed that the location of the cement cloud influences the biomechanical outcome [Beckmann et al., 2011]. However, further investigations are currently seeking to identify the ideal augmentation strategy [Varga et al., 2017]. Customized treatments require special planning and controlled injection techniques that are not widely available. The goal can be stated as an optimization problem, the solution of which is sought through the application of a robust optimization procedure. Until now, notably few papers have been published in this direction. A variation of the well-known bidirectional evolutionary structural optimization (BESO) method [Querin et al., 2000] was applied to find the minimum volume of cement needed to increase the predicted yield load of the specimens [Basafa and Armand, 2014] and to optimize the cement pattern for femoroplasty [Basafa et al., 2015]. Additionally, computational fluid dynamics (CFD) simulations of cement injection into the trabecular structure have been performed to investigate the treatment and impact of injected cement [Landgraf et al., 2015]. In addition, a deterministic method based on sequential quadratic programming (SQP) was completed to evaluate the influence of certain parameters on the cement distribution [Santana Artiles and Venetsanos, 2017]. Although new evolutionary optimization methods for the augmentation of osteoporotic bones have been developed, none have been validated with experimental studies [Santana Artiles and Venetsanos, 2017; Basafa and Armand, 2014; Varga et al., 2017; Basafa et al., 2015; Landgraf et al., 2015]. With respect to experimental validation, the method of smoothed particle hydrodynamics (SPH) has been utilized to model the flow of cement inside porous media with the incorporation of different viscosities [Basafa and Armand, 2013]. Although certain studies qualitatively compared three-dimensional results with those obtained in experiments, only the cement cloud [Basafa and Armand, 2013] and bone infiltration [Widmer and Ferguson, 2011] inside trabecular bone were studied. Therefore, mechanical property improvements were not assessed computationally or experimentally. According to the literature, the best augmentation strategy is currently

unknown [Basafa et al., 2015]. Due to high computational costs, particle models have gained popularity for modelling fluid flows [Borau et al., 2014]. Therefore, the main goal of this chapter is the development of a discrete particle model for cement infiltration.

We performed an *in vitro* and *in silico* characterization of augmented open-cell structures to assess qualitative and quantitative results. The infiltration of two commercial cement types with different viscosities (high- and low-viscosity) within open-cell structures (Sawbones; Malmö, Sweden) of three different porosities was analysed. To validate the proposed model, *in vitro* experiments were performed, and the results were compared with *in silico* FE simulations. We demonstrate that cement injection increases the mechanical properties (Young's modulus) of open-cell structures resembling different trabecular bone structures. Furthermore, cement viscosity affects the mechanical performance of the augmented open-cell structures. The main novelties of this chapter are the proposed *in vitro* experiments used to validate the *in silico* approach and the employment of two cement viscosities and three open-cell structures with different porosity fractions (Chapter 2).

### 3.2 Materials and methods

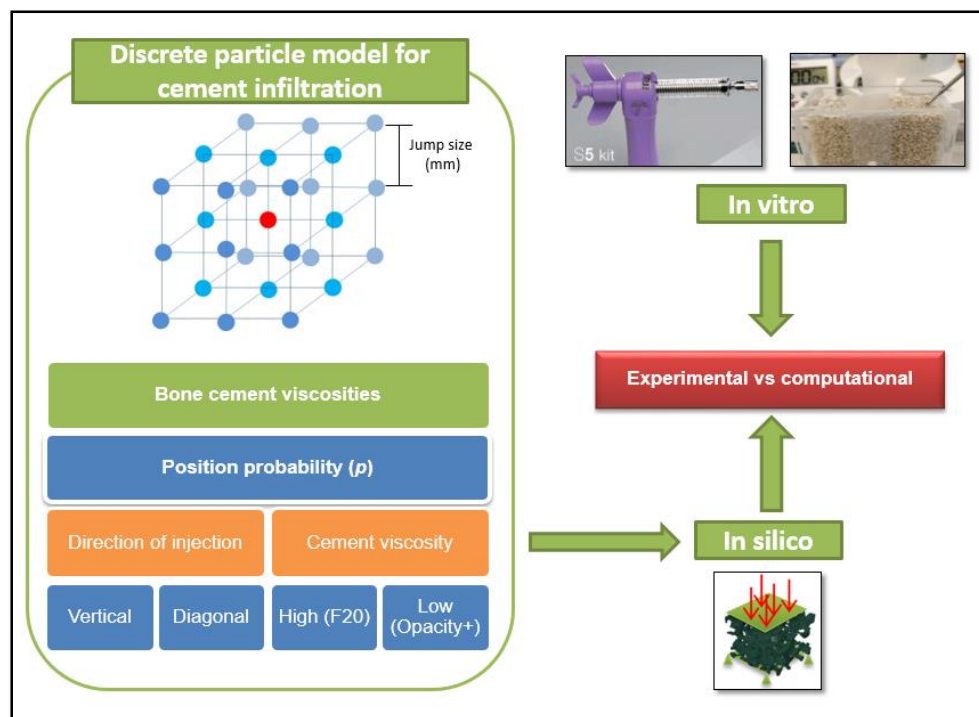


**Figure 17:** Workflow for the *in vitro* and *in silico* characterization of open-cell structures: Nonaugmented vs. augmented with cement

A discrete particle model for cement infiltration based on the random-walk theory [Pérez and Prendergast, 2007] is presented in this section (Figure 17), and *in vitro* and *in silico* characterizations of augmented open-cell structures are described (Figure 17).

*In vitro* and *in silico* characterizations of nonaugmented open-cell structures were performed in chapter 2.

### **3.2.1 Discrete particle model for cement infiltration**

The complexity of *in vitro* testing led to the planning and computational simulation of cement infiltration through a porous medium resembling the trabecular bone structure. An approach for modelling the cement infiltration based on the random-walk theory [Pérez and Prendergast, 2007] was proposed. This phenomenological model allowed us to control selected parameters (viscosity and direction of injection) that are important in planning the femoroplasty technique. Initially, a cement particle is assumed to be surrounded by 26 locations that could be occupied by a particle (Figure 17 and Figure 18). The cement particle distance depends on the voxel size (Section 3.2.3). Cement particles are not allowed to remain in their initial position. Therefore, a cement particle is moved to another controlled location. We opted for an anisotropic diffusion, i.e., cement particles can occupy neighbouring positions with different probabilities  $p$  depending on the desired direction of injection (Figure 18). We considered two directions of injection: vertical and diagonal. In each case, the neighbouring cement particle positions are evaluated, and depending on the available states, the corresponding value of  $p$  is computed to fulfil  $\sum_{i=1}^{n1} p_1 + \sum_{i=1}^{n2} p_2 + \sum_{i=1}^{n3} p_3 + \sum_{i=1}^{n4} p_4 = 1$  (Figure 18). For the vertical direction of injection, a strongly preferred upright direction was assumed as  $p_1=15p_2=50p_3=90p_4$ , and in this case,  $p$  can be calculated as  $\frac{150}{269}$ . For the diagonal direction of injection, the oblique direction is the preferred direction, which was assumed as  $p_1=5p_2=20p_3=90p_4$  with  $p$  equal to  $\frac{90}{163}$ . Additionally, the model incorporated “contact inhibition” by searching for vacant positions when a cement particle moves, depending on the available positions. The model considers that the positions representing the bone trabeculae cannot be occupied by cement particles. At the end of the injection, the availability of the final position is verified. If that position is not free (bone or cement particle position), another neighbouring location is randomly chosen. The cement viscosity was considered in our model as the jump size that a particle could undergo in each iteration (Figure 17). Basically, this jump

size represents the shear rate for a constant shear stress. Therefore, the jump size that a particle could undergo in each iteration increased as the cement viscosity decreased. For high-viscosity cement, the jump size was assumed as one voxel, whereas for low-viscosity, the jump size was equal to five voxels. This parameter takes into account in a phenomenological manner, the different diffusive capacity due to cement viscosity. Notably, a cement particle finds more free positions as the infiltration increases, i.e., as the cement viscosity decreases.

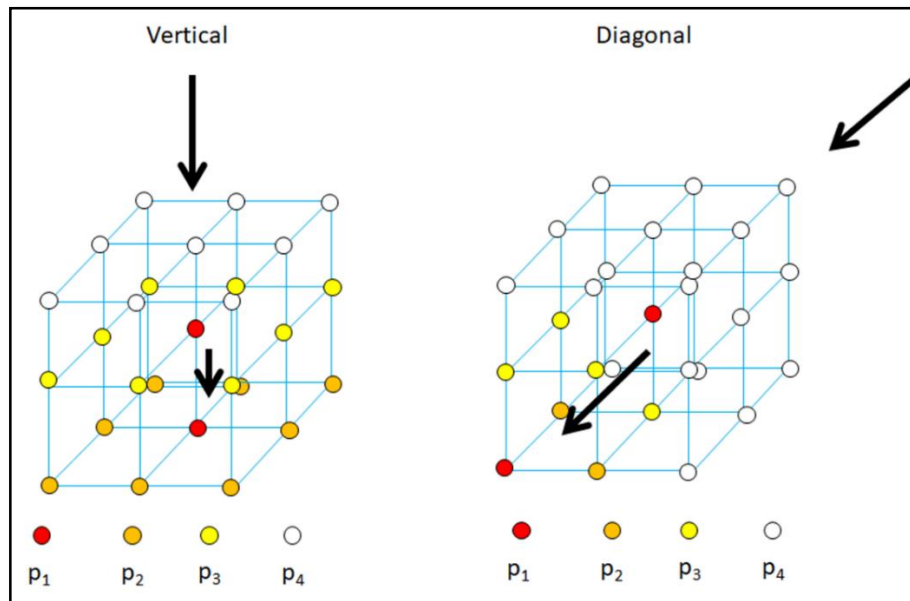


Figure 18: Probabilities depending on the desired direction of injection

The number of cement particles injected ( $N_{\text{injected particles}}$ ) depends on the cement volume injected ( $V_{\text{cement}}$ ) and the cement particle volume ( $V_{\text{cement particle}}$ ), which is directly related to the voxel volume (Section 3.2.3) as  $V_{\text{cement}} = N_{\text{injected particles}} * V_{\text{cement particle}}$ .

### 3.2.2 *In vitro* characterization of augmented open-cell structures

The augmentation of three open-cell structures (Sawbones; Malmö, Sweden) was studied with three different densities similar to that of trabecular bone (Table 5). Hereafter, we refer to these items as specimen #15 (Sawbones; product no. 1522-526-1; Malmö, Sweden), specimen #20 (Sawbones; product no. 1522±524; Malmö, Sweden) and specimen #30 (Sawbones; product no. 1522±525; Malmö, Sweden). The *in vitro* characterization of nonaugmented open-cell structures was previously conducted (Chapter 2) (Table 5). Twelve open-cell structures (#15, #20, #30) were cut into blocks of approximately 65 x 65 x 40 mm. Each block was enclosed in a Plexiglass shell of 5 mm thickness, as the cortical shell (Figure

19). Two different commercial cements were injected, i.e., F20 (Teknimed, Toulouse, France) and Opacity+ cement (Teknimed). F20 is a high-viscosity cement for vertebroplasty that is extremely visible and safe to use due to its high concentration of radio-opaque agent, whereas Opacity+ is a low-viscosity cement for vertebroplasty, whose high concentration of zirconium oxide allows to monitor the flow of cement using a scanner or image intensifier. Both cements are available as an ampoule of sterile liquid and a sterile powder pouch (powder polymer and liquid monomer).

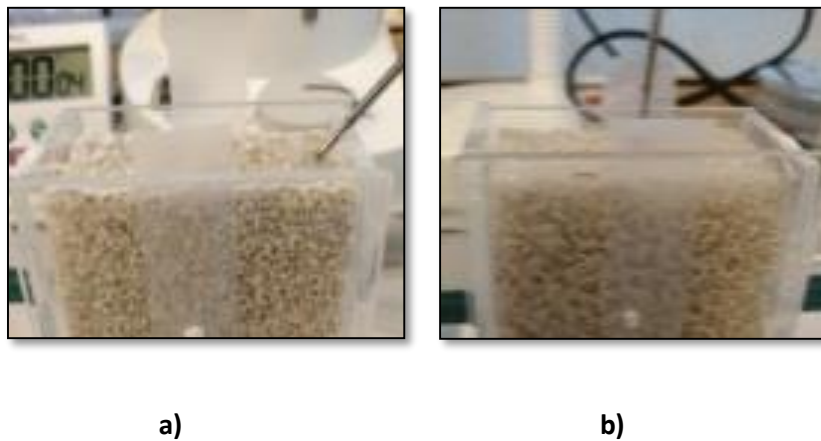


**Figure 19:** a) Vertical and b) diagonal injection of two different commercial cements in blocks of approximately 65 x 65 x 40 mm

A commercial cement injection system (Teknimed S5Kit; Teknimed S.A.S, France) was used in the cement augmentation procedure (Figure 20). The corresponding cement instructions for mixing were followed.



**Figure 20:** Commercial cement injection system (Teknimed S5Kit; Teknimed S.A.S, France)

Four millilitres of cement was injected into each specimen through a drilled hole 3 mm in diameter on the top face (vertical direction) (Figure 19a), but the effect of injection in a diagonal direction was also analysed through a 3 mm hole on the corner top face (Figure 19b). Two open-cell structures of each density were analysed in each direction (vertical and diagonal)



with the two cement types (Figure 19). The injection procedure was repeated for all the prepared specimens. After 24 h of cement curing, compression mechanical tests were performed using a servo-hydraulic material testing machine (Microtest; model EFH, Spain). Each specimen was placed between steel plates at room temperature (approx. 23 °C) and loaded in the direction of the axis of symmetry. The quasi-static compression load was measured with a commercial load cell (10 kN) applied at a constant velocity rate of 1 mm/min. From the force-displacement curve, Young's modulus of each specimen was estimated, and the increase in mechanical properties was calculated.

**Table 5: Open-cell specimens, densities, porosities, mean  $\pm$  SD experimental Young's modulus and computational Young's modulus (Chapter 2)**

Specimen	Number of specimens	Density (g/cc)	Porosity	Experimental E (MPa)	Computational E (MPa)
			specifications (%)		
#15	4	0.24	85	62.74 $\pm$ 4.14	85.89 $\pm$ 22.33
#20	4	0.32	79	111.35 $\pm$ 8.24	121.16 $\pm$ 27.36
#30	4	0.48	69	187.47 $\pm$ 20.53	178.05 $\pm$ 39.44

### 3.2.3 *In silico* characterization of augmented open-cell structures

*In silico* characterization of nonaugmented open-cell structures was previously conducted (Chapter 2) [Ramos-Infante and Pérez, 2017]. The obtained mean results are shown in Table 5, and the process is revised in this chapter. Prior to cement augmentation of the open-cell structures, computed tomography (CT) acquisition was performed in a Phillips Brilliance system using 64 detectors with the following parameters: slice thickness = 0.672 mm, KVP = 120, spacing between slices = 0.672 mm and pixel spacing = 0.234 mm. A 3D bicubic interpolation algorithm was applied to reduce the slice thickness to 0.16 mm (voxel size). The interpolated images were reconstructed using a semiautomatic reconstruction (MIMICS, Materialise NV; Leuven, Belgium). The specimens were digitally cut, and a representative volume element was chosen. A voxel mesh was generated using the voxel create mesh module (MIMICS, Materialise NV; Leuven, Belgium).

Therefore, the discrete particle model for cement infiltration (Section 3.2.1) was run within the voxel mesh created for each specimen. As indicated, two directions of injection and two cement viscosities were modelled. Once the cement injection was simulated, a new voxel mesh was generated (bone plus cement) to simulate the compression test. The boundary condition for the voxel mesh was based on an idealization of those in a uniaxial compression test [Keaveny et al., 1993]. A uniaxial displacement (strain of 2%) was applied to the top surface of the cubic bone samples, and the bottom surface was kept fixed [Keaveny et al., 1993] (Figure 21).

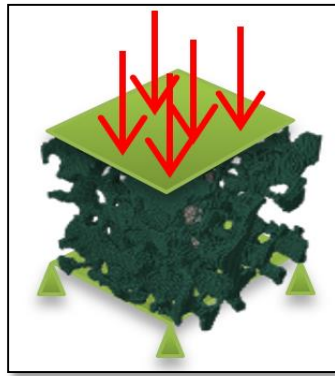


*Figure 21: Augmented FE model*

The bone and cement were assumed to be linear elastic and isotropic with Young's modulus of 3200 MPa (Sawbones; Malmö, Sweden) and 2000 MPa [Jaasma et al., 2002], respectively. Poisson's ratio was defined as 0.3.

Non-linear FE analyses were performed in ABAQUS v6.14 (Dassault Systemes Simulia Corp., Suresnes Frances) and run in a computational cluster of 224 cores with 576 GB of RAM. After FE analysis, the augmented mechanical properties (Young's modulus) were estimated to calculate the final improvement of the specimen mechanical properties. Prior to the experimental compression tests, CT acquisition of the augmented specimens was again performed (one acquisition per cement type, direction of injection and open-cell structure type). In this case, the cement clouds and filling patterns inside the open-cell structures were reconstructed [Basafa and Armand, 2013], and their sphericity was calculated using the following equation [Corey, 1963]:

$$Sphericity = \frac{c}{\sqrt{a + b}} \quad (4)$$

where a, b and c (in mm) correspond to the cement cloud dimensions (Figure 22).

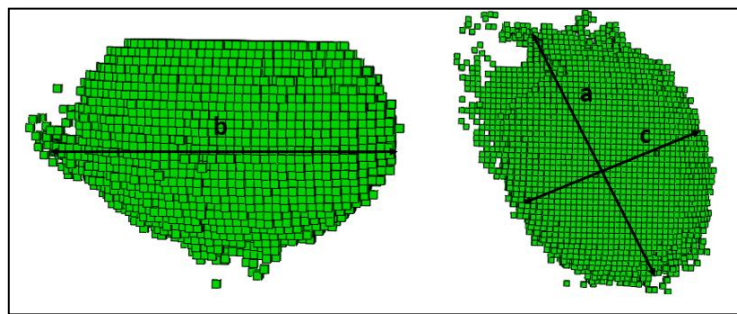


*Figure 22: Frontal (on the left) and lateral (on the right) view of the cement cloud*

### 3.2.4 Statistical analysis

Statistical analysis of the results was performed. A dependent samples t test was applied to determine whether statistically significant differences were identified. Additionally, Pearson correlation coefficients were calculated.

## 3.3 Results

In general, the augmented specimens exhibited enhanced mechanical properties regardless of the direction of injection, cement viscosity or open-cell structure type (Table 6 and Figure 23). Low-viscosity cement showed better improvements for all the specimens and directions, except for specimen #30 and the diagonal direction (see Table 6 and Figure 23B). As specimen #30 showed the lowest porosity fraction (see Table 5), both cement viscosities were difficult to inject using the commercial injection system because cement was not able to reach neighbour pores as easily as it was in specimens #15 and #20, which had high porosity fractions.

Although all the augmented specimens exhibited increased mechanical properties for all cement viscosities, the specimen with the highest porosity fraction (specimen #15), similar to osteoporotic bone, showed considerable improvements in mechanical properties (Figure 23) because the cement was able to infiltrate more fully. In addition, similar mechanical property improvements were achieved regardless of the direction of injection. However, we noted certain differences in specimen #20 (Figure 23), for which the diagonal injection showed better Young's modulus improvements.

**Table 6: Mean Young's modulus improvement (%) in all the cases tested *in vitro* and *in silico*. STD indicates standard deviation. Bold numbers in the p-value column indicate a negative (-1) Pearson correlation coefficient.**

INJECTION	SPECIMEN	IN VITRO		IN SILICO		P-VALUE
		VALUE	MEAN (STD)	VALUE	MEAN (STD)	
DIAGONAL	HIGH_15_1	87.4	91.0	86.3	101.9 (15.6)	0.53
	HIGH_15_2	94.7	(3.7)	117.5		
VERTICAL	HIGH_15_3	29.1	105.7	26.5	98.33 (71.79)	0.37
	HIGH_15_4	182.3	(76.6)	170.1		
DIAGONAL	HIGH_20_1	118.1	182.8	51.4	49.31 (2.07)	<b>0.29</b>
	HIGH_20_2	247.4	(64.7)	47.2		
VERTICAL	HIGH_20_3	54.7	68.9	47.8	47.62 (0.19)	<b>0.38</b>
	HIGH_20_4	83.2	(14.2)	47.4		
DIAGONAL	HIGH_30_1	35.5	93.9	47.9	80.46 (32.6)	0.69
	HIGH_30_2	152.4	(58.4)	113.1		
VERTICAL	HIGH_30_3	44.8	87.8	47.2	77.98 (30.74)	0.57
	HIGH_30_4	130.7	(43.0)	108.7		
DIAGONAL	LOW_15_1	93.1	123.9	80.6	130.01	0.80
	LOW_15_2	154.6	(30.7)	179.5		
VERTICAL	LOW_15_3	186.4	154.3	186.0	159.29	0.52
	LOW_15_4	122.1	(32.1)	132.6		
DIAGONAL	LOW_20_1	211.3	246.9	225.0	237.95	0.76
	LOW_20_2	282.4	(35.6)	250.9		
VERTICAL	LOW_20_3	111.7	60.1	58.3	59.74 (1.47)	<b>0.99</b>
	LOW_20_4	8.4	(51.7)	61.2		
DIAGONAL	LOW_30_1	66.3	34.1	66.7	33.38 (33.28)	0.63
	LOW_30_2	2.0	(32.1)	0.1		
VERTICAL	LOW_30_3	64.9	99.9 (35.0)	88.7	90.21 (1.47)	0.82

The computational predictions were notably close to the experimental values (see Table 6 and Figure 23). None of the results presented statistically significant differences between the computational and experimental results ( $p > 0.05$ , t-student). The computational results for specimen #20 with high-viscosity cement (vertical and diagonal) and low-viscosity cement

(only vertical) compared poorly with the experimental results (the Pearson correlation coefficient was -1, see bold numbers in Table 6).

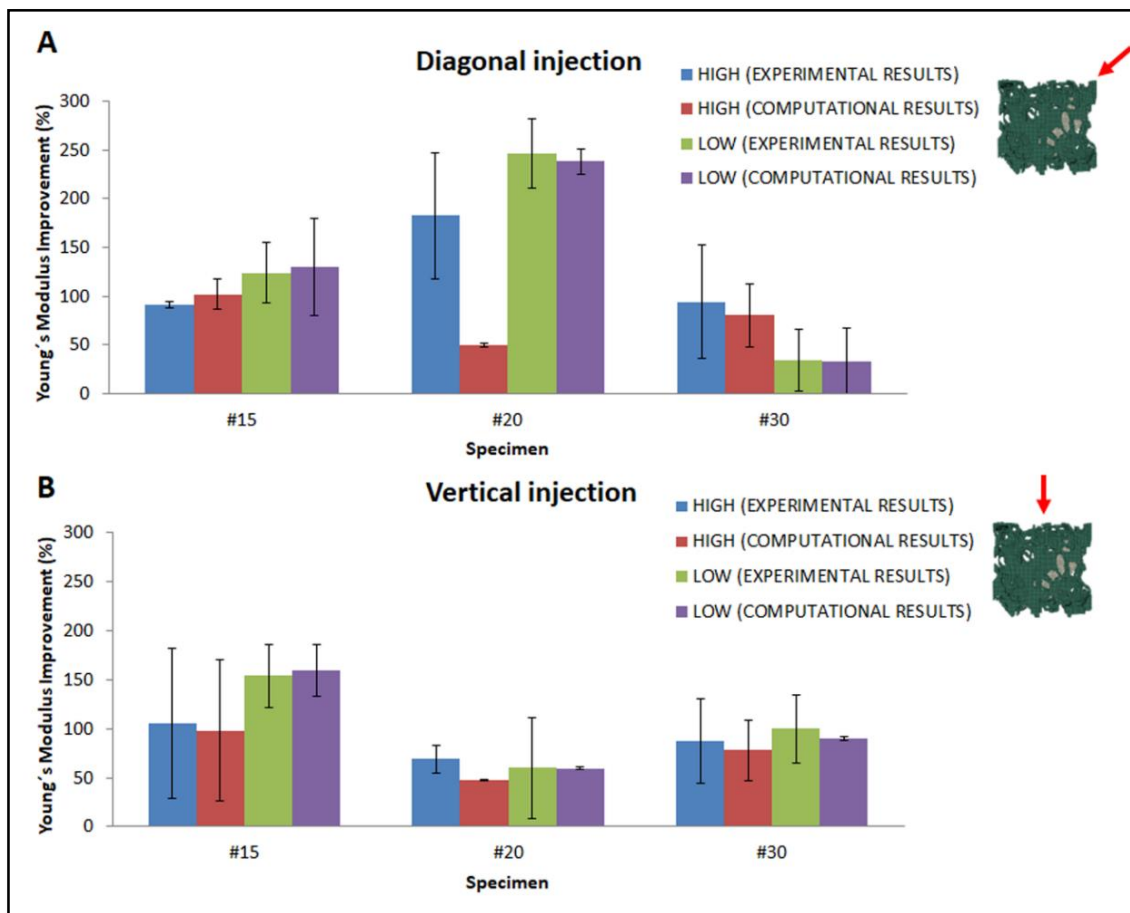


Figure 23: Mean Young's modulus improvement (%) in all the cases tested in vitro and in silico: a) vertical and b) diagonal directions of injection. Bars indicate the standard deviation values (see Table 6)

SPECIMEN	HIGH-VISCOSITY BONE CEMENT (F20)				LOW-VISCOSITY BONE CEMENT (OPACITY+)			
	DIAGONAL		VERTICAL		DIAGONAL		VERTICAL	
	EXPERIMENTAL INJECTION	COMPUTATIONAL INJECTION	EXPERIMENTAL INJECTION	COMPUTATIONAL INJECTION	EXPERIMENTAL INJECTION	COMPUTATIONAL INJECTION	EXPERIMENTAL INJECTION	COMPUTATIONAL INJECTION
#15								
#20								
#30								

Figure 24: Qualitative comparison of the cement infiltration patterns within certain open-cell structures in each case simulated

Table 7: Sphericity of the cement cloud in all cases tested *in vitro* and *in silico*. STD indicates standard deviation.

INJECTION	SPECIMEN	IN VITRO		IN SILICO		P-VALUE
		VALUE	MEAN (STD)	VALUE	MEAN (STD)	
DIAGONAL	HIGH_15_1	0.72	0.80 (0.07)	0.81	0.82 (0.02)	0.74
	HIGH_15_2	0.87		0.84		
VERTICAL	HIGH_15_3	0.71	0.74 (0.04)	0.86	0.87 (0.01)	0.15
	HIGH_15_4	0.78		0.88		
DIAGONAL	HIGH_20_1	0.93	0.86 (0.06)	0.79	0.77 (0.02)	0.30
	HIGH_20_2	0.80		0.75		
VERTICAL	HIGH_20_3	0.84	0.82 (0.01)	0.86	0.83 (0.03)	0.66
	HIGH_20_4	0.81		0.80		
DIAGONAL	HIGH_30_1	0.73	0.80 (0.07)	0.73	0.75 (0.02)	0.46
	HIGH_30_2	0.86		0.77		
VERTICAL	HIGH_30_3	0.86	0.87 (0.004)	0.80	0.73 (0.02)	0.26
	HIGH_30_4	0.87		0.85		
DIAGONAL	LOW_15_1	0.74	0.59 (0.15)	0.53	0.52 (0.005)	0.73
	LOW_15_2	0.44		0.52		
VERTICAL	LOW_15_3	0.80	0.82 (0.02)	0.55	0.56 (0.01)	0.03
	LOW_15_4	0.84		0.57		
DIAGONAL	LOW_20_1	0.79	0.71 (0.08)	0.53	0.53 (0.03)	0.22
	LOW_20_2	0.64		0.52		
VERTICAL	LOW_20_3	0.78	0.74 (0.04)	0.59	0.56 (0.03)	0.03
	LOW_20_4	0.70		0.53		
DIAGONAL	LOW_30_1	0.63	0.51 (0.12)	0.57	0.55 (0.02)	0.75
	LOW_30_2	0.39		0.53		
VERTICAL	LOW_30_3	0.68	0.74 (0.06)	0.56	0.57 (0.01)	0.18
	LOW_30_4	0.80		0.58		

To further validate the model, the filling pattern was successfully predicted based on a comparison of the computational and experimental infiltration (Figure 24). High-viscosity cement created a denser cement volume, whereas low-viscosity cement tended to spread more fully inside the trabecular bone. The sphericity (equation (4)) of the injected cement was quantified in Table 7. The sphericity was higher with high-viscosity cement than with low-

viscosity cement. Most of the results did not presented statistical significant differences between the experimental and computational results ( $p > 0.05$ , t-student). Only when low-viscosity cement was injected in the vertical direction, significant differences were observed for specimens #15 and #20 (see Table 7, last column numbers in italics). The Pearson correlation coefficient was positive ( $= 1$ ) in all cases.

### 3.4 Discussion

The results of this chapter support our original hypothesis that femoroplasty increases the mechanical properties compared with nonaugmented controls (Table 6 and Figure 23). A few recent studies have reported attempts at restoring the mechanical strength of femur specimens using a relatively small amount of infiltrated cement with limited or no success [Beckmann et al., 2011; Fliri et al., 2012; Steenhoven et al., 2012; Sutter et al., 2010b]. The procedure requires precise planning and execution. Effective planning relies on (among other factors) an accurate method for predicting the diffusion of the cement through the porous medium of osteoporotic trabecular bone. A crucial step in the planning process is to determine the optimum volumen and filling pattern of the cement such that the best outcome is achieved [Basafa and Armand, 2013]. A successful planning framework should include a module for predicting the cement infiltration inside trabecular bone. The majority of fragility fractures occur at trabecular-dominant bone sites. Indeed, the trabecular bone plays important roles in the load transmission and energy absorption in major joints.

Our goal was to develop a discrete particle model for cement infiltration based on the random-walk theory [Pérez and Prendergast, 2007]. Random-walk on a grid is similar to methods used in lattice gas and Lattice Boltzmann simulations of diffusion without convection [Zeiser et al., 2008]. The main novelty of this chapter is that the proposed model was qualitatively and quantitatively validated through *in vitro* experiments using two cement viscosities and three different open-cell structures.

We performed an experimental set of validation tests using nonaugmented specimens as surrogate trabecular bone tissue and injected 4 ml of cement in a controlled manner. This amount is far less than the amounts used in first-generation femoroplasty experiments [Beckmann et al., 2007; Heini et al., 2004; Sutter et al., 2010a], in which approximately 40-50 ml of cement was needed to obtain a 30-40% increase in the fracture load. Second-generation

femoroplasty approaches resulted in mechanical property improvements of more than 100% when 12 ml of cement was infiltrated [Basafa and Armand, 2014], even though the model was not experimentally validated. Finally, a recent study achieved an increase in mechanical properties of more than 100% by injecting approximately 10 ml of cement [Varga et al., 2017]. All previous studies agree in augmenting the upper side of the femoral neck, where the maximum traction loads are reached. In fact, augmentation of the superior and inferior position of the femoral neck close to the cortex results in the most favourable outcome [Niebur et al., 2000]. This observation supports the hypothesis that the use of subject-specific models and optimization, combined with intra-operative tools for precise cement delivery, reduces the required cement volume [Varga et al., 2017].

Two cement viscosities were used in this work, and the simulation and experimental results were compared. Strong correlations between experimental and simulation results were obtained for spreading distance and cement clouds (Figure 24). The cement pattern created inside the open-cell structures by the discrete particle model involved augmentation following the vertical and diagonal directions, similar to the directions inside the femoral neck. The material distribution was highly similar to the results obtained in the literature [Basafa and Armand, 2014; Basafa and Armand, 2013]. Our model showed that 4 ml of cement resulted in Young's modulus increases ranging from 91.04% (high-viscosity cement) to 154.29% (low-viscosity cement) in specimen #15 (Figure 23), which had a porosity fraction close to that of the osteoporotic femur. The target Young's modulus in the current work was set to nearly 20% higher than Young's modulus of a healthy trabecular femur (Ehealthy trabecular femur ~ 11.4 GPa) [Zysset et al., 1999], although the proposed model supplies sufficient versatility to set the target to any desired value depending on the direction of injection and cement viscosity.

Notably, the infiltration of the two cements showed different results depending on the direction of injection and cement viscosity. In most cases, excellent agreement between the experimental and computational results was achieved and there were no statistically significant differences between the two results (Figure 23 and Table 6). Specimen #20 showed a particular increase in mechanical properties when cement was infiltrated in the diagonal direction with respect to the other specimens (Figure 23B). In contrast, when cement was infiltrated in the vertical direction, the improvement in mechanical properties was lower (Figure 23A). However, when performing statistical analysis between both directions of injection, no statistically significant differences were estimated ( $p = 0.26$ , t-student for high-viscosity cement;  $p = 0.27$ , t-student for low-viscosity cement). In addition, for the diagonal direction, important



differences between the computational and experimental results were observed for high-viscosity cement in specimen #20 (Figure 23). There could be two reasons for these differences. First, the manufacturing process of the open-cell structures could lead to a decrease in porosity and a change in the micro-architecture of the specimen itself. Second, the position of the structure formed by the solidified cement within the open-cell structure could affect the final mechanical properties. For example, if the solidified structure happens to form at the weak-point of the open-cell structure, a more important enhancement of the mechanical properties could result. Therefore, we cannot conclude that cement diffusion is the only crucial mechanism in the improvement of mechanical properties; the direction of injection, the specimen manufacturing process and its micro-architecture and the final position of the structured-formed must also be considered. Human trabecular bone is anisotropic by nature.

Additionally, the cement viscosity affected the compactness of the cement final shape. A high-viscosity cement produces a cement cloud with high sphericity (Table 7 and Figure 24). This observation suggests that medium or low cement viscosities (low sphericity) are ideal for injections inside porous media, including osteoporotic trabecular bone, because the final shape is sufficiently compact [Basafa and Armand, 2013].

Notably, the proposed model was used in conjunction with FE analyses to predict the effect of various hypothetical augmentation scenarios on the mechanical properties of bone [Basafa and Armand, 2013]. An increase in the mechanical properties was observed regardless of the cement viscosity. In addition, low-viscosity cement showed better Young's modulus improvements. However, mechanical property improvements were highly similar in specimens #15 and #30, regardless of the direction of injection (Figure 23).

Nevertheless, the proposed methodology presents certain limitations. The validation was performed with only two specimens of each type; therefore, additional data are needed to further validate the model. The probability values assumed for the application of the random-walk theory [Pérez and Prendergast, 2007] are mainly phenomenological. Another assumption was the number of voxels considered for the jump size in the low- and high-viscosity cements, considering that more than five voxels (low) generated an unrealistic cement cloud pattern (data are not shown). No previous measurements were collected. However, we have based our hypothesis in experimental data collected from the literature [Farrar et al., 2001]. It is a fact that, considering a simple shear flow, Newton's law of viscosity relates shear stress,  $\sigma$ , to the velocity gradient or shear rate,  $\gamma$ , through the equation:  $\sigma = \mu\gamma$ , where  $\mu$  is the coefficient of

viscosity, or simply the viscosity. For Newtonian fluids, the viscosity is a constant independent of shear rate. However, many fluids, including many polymer solutions and suspensions, are said to be non-Newtonian, and the viscosity is not a coefficient but a function of the shear rate and/or the time of shearing. For example, it is common for viscosity to decrease with increase in shear rate behaviour known as “shear thinning”. Conversely, it is possible for viscosity to increase with shear rate referred to as “shear thickening”. Alternatively, it is possible that at a constant shear stress the viscosity decreases over time. In our particular model, we have hypothesized that the viscosity is a function of the jump size (or shear rate) that a particle could undergo. For a constant value of the shear stress, the viscosity decreases as the jump size increases its value. For instance, for high-viscosity cement, the jump size was assumed to be one voxel, whereas for low-viscosity cement, the jump size was equal to five voxels. This parameter considers, in a phenomenological manner, the different diffusive capacities due to cement viscosity.

With respect to the limitations of the *in silico* characterization, to avoid the long computation times that can arise for more complex analyses [Jaasma et al., 2002; Loeffel et al., 2008; Bayraktar et al., 2004; Lü et al., 2015], we have used smaller sub-regions to show the correlations between the experimental and computational results [Ramos-Infante and Pérez, 2017]. This approximation has resulted in errors as large as 9.5% in predictions of apparent stiffness [Loeffel et al., 2008]. However, we obtained similar correlations between the experimental and computational results in nonaugmented specimens [Ramos-Infante and Pérez, 2017]. Furthermore, injection and pressure rates were not controlled, even though changes in injection rate do not have significant effects on the spread of the cement [Bhan et al., 2014].

In general, small differences were detected between the *in silico* and *in vitro* results. These differences could be due to a loss of accuracy in the image acquisition methodology. The CT images were acquired at the highest in-plane resolution possible, which was limited by the size of the detectors and the field of view of the scanning device. As this CT system is actually used in clinical practice, these conclusions can be translated to obtain similar differences between simulations and real mechanical behaviour. We expect that a finer CT resolution would increase the accuracy of the simulation results, noting that the trabecular structure is very finely spaced, especially for osteoporotic specimens. Nevertheless, increasing the number of voxels also increases the number of fixed particles, which drastically slows the simulations. With the current resolution, our simulations yielded reasonable accuracy, and the added computational cost of finer resolution CT and ionizing radiation dose for patients would not be justified

[Basafa and Armand, 2013]. A change on the voxel size would imply a readjustment of the jump size parameter value. One must consider that the proposed model is intended for use in the preoperative planning of bone augmentation, and computational efficiency is of crucial importance.

In our simulations, we ignored the presence of the bone marrow. Selected pilot simulations have demonstrated that considering such a fluid has a negligible effect on the end results [Baroud et al., 2003]. As reasons for this observation, we hypothesize that the bone marrow viscosity is orders of magnitude smaller than the viscosity of the cement [Baroud et al., 2003] and that the interactions between the two fluid particles are minimal. Notably, one of the main problems of the augmentation technique is high temperatures inside the bone during the curing process. Future research must also verify the assumption that by minimizing the injection volume, we can avoid thermal necrosis caused by the exothermic curing process of the cement [Basafa et al., 2015]. Additionally, a validated model for heat generation and propagation could be incorporated into the planning module for the design of safer augmentations by keeping the heat damage away from more vulnerable sites, such as the arteries [Palumbo et al., 2014]. Mechanical improvement by means of cement augmentation as reported in the literature does not always translate to zero fracture risk. The risk of fracture also depends on a variety of factors including patient anatomy, height of fall, and floor covering [Zhong et al., 2011; Parkkari et al., 1997; Kannus et al., 1999].

### **3.5 Conclusions**

In summary, the cement injection pattern was closely predicted in all the simulated cases (Figure 24 and Table 7), and all the augmented specimens exhibited increased mechanical properties (Figure 23 and Table 6). As the cement injection volume increased, the mechanical properties also improved. In fact, the specimens with the highest porosity fraction (specimen #15) showed a considerable increase in mechanical properties. This increase was mainly due to the high capacity of the cement to diffuse within a more porous trabecular structure.

Therefore, our proposed discrete particle model of cement infiltration allows us to plan and improve cement augmentation in a patient-specific model and also identifies generalizable patterns of cement location that could be applied via simple surgical guidelines. Our model suggests a comprehensive planning strategy that considers several scenarios and can determine

the best augmentation strategy for each patient. The results of this study suggest that the chosen method of cement diffusion modelling is an appropriate candidate for our intended application of predicting cement diffusion into the porous structure of trabecular bone.

Femoroplasty significantly increases the mechanical properties when osteoporotic femora are loaded, and cement filling may play an important role in the extent to which femoroplasty affects the mechanical strength of the proximal femur. Consequently, the simplicity and superior performance of the proposed method suggest that it can be used as a tool for optimum subject-specific planning of bone augmentation.

# Chapter 4

---

*Development of a rabbit fracture model for  
evaluation of cement augmentation: an in  
vivo biomechanical study*



## 4.1 Introduction

The currently available methods of prevention include noninvasive physical protection and various pharmacological agents. Padded hip protectors and energy-absorbing mattresses have been shown to have limited effectiveness in reducing hip fractures [Kannus et al., 2000; Sawka et al., 2005]. An array of drugs, including calcium, vitamin D, bisphosphonates, and strontium ranelate, have been used to improve bone mineral density, thus decrease the risk of fractures. However, there are many issues associated with the use of these methods (e.g., cost, side effects, patient compliance, and time for onset of action) that can inhibit efficacy [Recker et al., 2005]. A logical solution is the development of a prophylactic surgical intervention to increase the strength of the proximal femur and to decrease the risk of fracture. This technique should be quick, easy, and minimally invasive and carry minimal risk to the patients. Femoroplasty, the injection of cement into the proximal femur to augment the femur and to prevent fracture, has been an option with great potential, as we have shown in Chapter 2 and 3.

Prophylactic cement augmentation of proximal femur remains at the stage of biomechanical testing. There have only been some *in vitro* studies in cadaveric bone, which showed beneficial effect of femoroplasty in reinforcing bone strength [Beckmann et al., 2007, 2011; Sutter et al., 2010a, 2010b; Heini et al., 2004; Fliri et al., 2013]. However, there has not been enough evidence to support its clinical feasibility and benefits. Moreover, its acceptance in clinical application is still hampered by possible adverse effects, which include exothermic reaction during cement hardening, the effect on blood supply of bone and adjacent soft tissues, the increase in intramedullary pressure, and the risk of fat embolism [Sutter et al., 2010a; Beckmann et al., 2007; Heini et al., 2004]. Therefore, before femoroplasty can become a viable clinical option, these potential adverse effects must be investigated with appropriate *in vivo* studies to evaluate the safety issues and therapeutic potential of femoroplasty.

The purpose of this chapter was to investigate the ability of femoroplasty to attenuate the potential for fracture when a rabbit femur is loaded under stance configuration. Specifically, the purpose of our study was to test the hypothesis that femoroplasty would increase the Young's Modulus, failure load and stiffness in a rabbit femur.

## **4.2 Materials and methods**

Under anesthesia, 2 ml polymethylmethacrylate (PMMA) cement was injected by an interventional radiologist into the right femoral head of 10 rabbits (New Zealand) under fluoroscopy guide. The femoral head region was evaluated *in vivo* using magnetic resonance imaging (MRI) before and 3 months after cementation. At 3 months postinjection, both femurs (injected and control) were excised and subjected to biomechanical tests using a servo-hydraulic material testing machine (Microtest; model EFH, Spain). Finally, the mechanical properties of the augmented femurs were analyzed, considering the contralateral nonaugmented femurs as the control reference.

### **4.2.1 Biomechanical testing**

All femora were stored in sealed plastic bags at -20 °C after postinjection until 1 day before biomechanical testing, at which time they were removed from the freezer and allowed to thaw overnight to room temperature in the same sealed plastic bags.

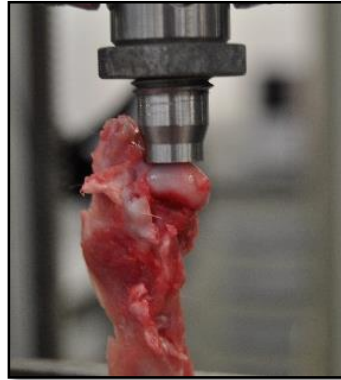


*Figure 25: Setup for mechanical testing*

Biomechanical tests were performed in a configuration that simulated the mechanical axis of the rabbit femur (Figure 25). The distal femur of the specimen was embedded into a cylindrical tray with Huntsman glue mixture (Araldite AW2104 + Hardener HW2934, Huntsman, Switzerland). The femoral shaft was oriented so that the center of femoral head and the center of the knee joint were located in the same vertical line, which represented the biomechanical axis for load testing. The whole construct was placed in a servo hydraulic grip control testing machine under a stainless steel spherical pressing shell with 10 mm diameter.



The vertical load was applied through the femoral mechanical axis until fractures occurred. The quasi-static compression load was measured with a commercial load cell (1 kN) applied at a constant velocity rate of 1 mm/min. The fracture position and fracture load were recorded.

#### 4.2.2 Statistical analysis

Significant differences, defined by  $p < 0.05$ , in the variables of interest (fracture load and Young's Modulus) between the nonaugmented group and the augmented group using paired t-tests were assessed.

### 4.3 Results

All ten specimens from the augmented groups fractured at the femoral neck, while fractures occurred at the femoral neck or other sites of proximal femur in the nonaugmented groups (Figure 26).

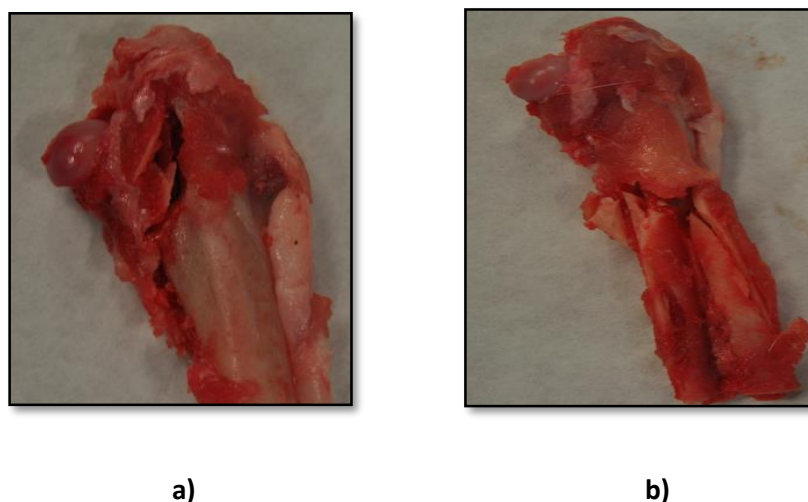


**Figure 26:** Fractures occurred a) at the femoral neck in augmented group and b) at the distal región in the nonaugmented group

For biomechanical properties, the average Young's Modulus in the augmented state was  $110.85 \pm 32.73$  MPa while  $61.36 \pm 36.43$  MPa in the nonaugmented state (Figure 27). Statistical analysis verifies this difference ( $p = 0.0037$ ). However, no relevant differences between failure loads were observed (Figure 28). Statistical analysis also verifies this observation ( $p = 0.8089$ ).

Nevertheless, important differences between force-displacement curves were observed, in which strain energies were higher in the augmented rabbit femur specimens (Figure 29).

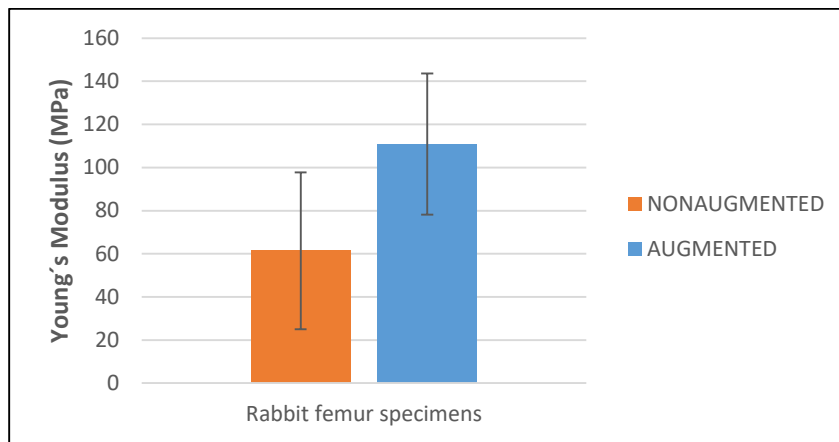


Figure 27: Young's Modulus in the nonaugmented and augmented rabbit femur specimens. Bars indicated standard deviation

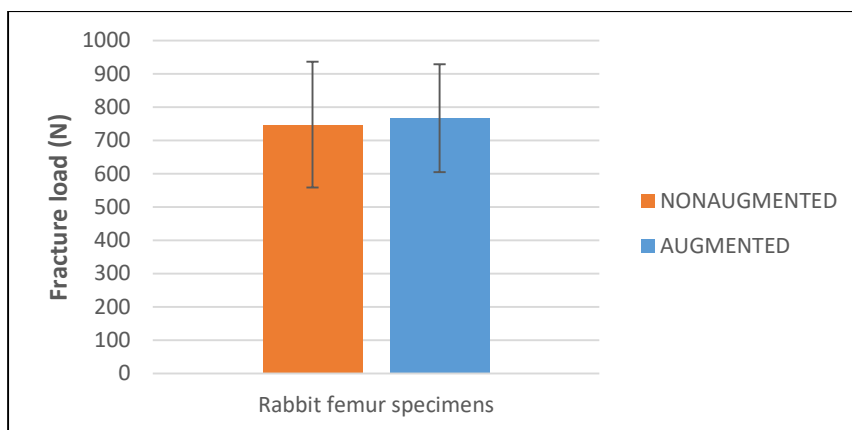


Figure 28: Fracture load in the nonaugmented and augmented rabbit femur specimens. Bars indicated standard deviation

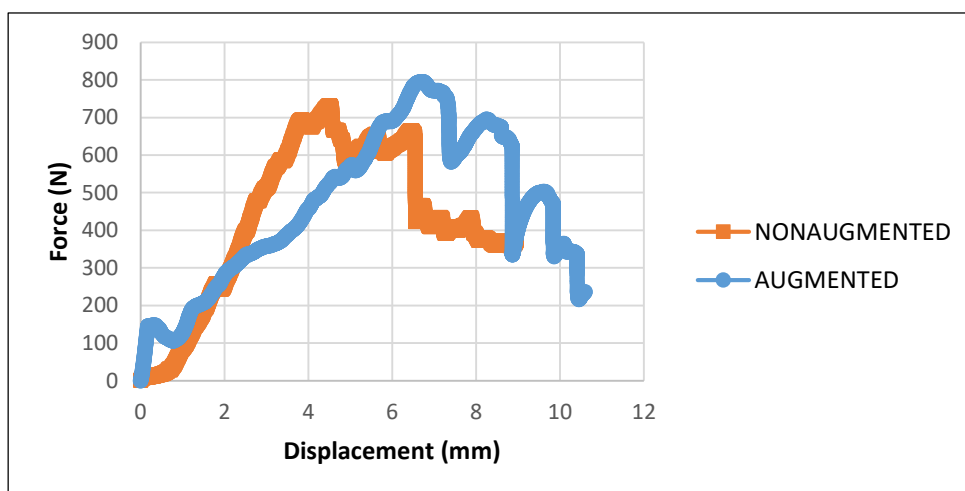


Figure 29: Force-displacement curves for the nonaugmented and augmented rabbit femur specimens

## 4.4 Discussion

Osteoporotic hip fracture is a great challenge to most orthopedic surgeons, and the complication rates after surgery are high. However, the currently available preventive methods, including noninvasive physical protection and various pharmacological agents, are far from ideal and hindered by adverse effects, patients' compliance, or onset time of action. Hence in the past few decades, doctors have attempted to develop a prophylactic surgical procedure to protect the osteoporotic hip.

There is a vast number of published studies that supports that femoroplasty can reinforce the proximal femur and potentially decrease the risk of hip fracture. The side effects related to this surgical procedure were presented and roughly addressed using cadaveric osteoporotic bone [Beckmann et al., 2007, 2011; Heini et al., 2004; Sutter et al., 2010a, 2010b; Fliri et al., 2013]. However, until now the safety and feasibility issues had not been addressed *in vivo*; a specific animal model for femoroplasty *in vivo* study did not even exist. Luo et al. [2014] carried out an *in vivo* femoroplasty study in goat femur specimens, but no cement was injected. In that case, they hypothesized that with a bone defect in the goat proximal femur, it could be enough to study femoroplasty technique.

Through injecting cement in the rabbit proximal femur, we carried out *in vitro* mechanical tests to assess the reinforcement of the specimens. The results shows that the mechanical properties improve 1.45 times over the nonaugmented rabbit femur specimens (Figure 27), but the fracture loads don't improve their values (Figure 28). Nevertheless, the augmented fracture load was reached at higher displacements of the force-displacements curves in comparison with nonaugmented rabbit femur specimens, that is, the strain energy reached in augmented specimens was higher than in the control group.

In this study, we aimed to develop an animal model to mimic human hip fracture. The results showed that the rabbit model consistently fractured at femoral necks when subjected to vertical load (Figure 26), and the fracture line was similar to osteoporotic femoral neck fracture that occurs in humans. In addition, the mechanical axis of the rabbit femur was tested biomechanically, and the newly developed configuration was practicable during this study.

There are some limitations in this study. First, human osteoporotic hip fracture can hardly be duplicated on a large four-legged animal. Most osteoporotic hip fractures happen when individuals sustain low-energy trauma falling from standing height [Luo et al., 2014].

Although rabbits offer the advantage over small rodents of larger bones to accept prosthetic fixators, the mechanical stresses differ greatly between fore and hindlimbs [Reeve and Schuetz, 2016] Additionally, rabbits have little chance of falling on the great trochanter. Second, most human hip fractures are intertrochanteric fractures. Possibly because the rabbit femur is much shorter than the human femur, this model's fracture location was at the femoral neck rather than the intertrochanteric region. Third, the configuration of falling on the greater trochanter is widely accepted as a test of the biomechanical properties of the femur [Dragomir-Daescu et al., 2011; Duchemin et al., 2008; Keyak et al., 2003]; however, when it is applied to a rabbit femur, we found that fracture location was different. So, the configuration of one leg stance was selected. In addition, because osteoporotic rabbit bone can hardly be obtained, the rabbit femora used in this study were healthy. That is the reason why fracture loads don't differ between augmented and nonaugmented specimens even though Young's Modulus and strain energy do improve. Indeed, these results were similar to those obtained in Chapter 3 (Figure 23 and Table 6), in which specimen #30, which resemble healthy trabecular bone, showed lower Young's Modulus improvement than specimen #20 and #15.

## **4.5 Conclusions**

In summary, the aim of establishing this rabbit femoral fracture model was to evaluate the safety and feasibility of femoroplasty. Results shows that cement can definitely improve the mechanical properties of nonaugmented rabbit femur specimens. The limitations of this model will not matter too much for further *in vivo* study of femoroplasty.

# Chapter 5

---

## *High- and low-viscosity cement for osteoporotic femoral augmentation: a computational subject-specific approach*

This chapter was submitted as:

Samuel Jesús Ramos-Infante and María Ángeles Pérez. High- and low-viscosity cement for osteoporotic femoral augmentation: a computational subject-specific approach. Engineering Fracture Mechanics (under review).



## 5.1 Introduction

Osteoporotic proximal femur fractures are associated with high morbidity and mortality and dramatically decrease quality of life [Freitas et al., 2017; Roth et al., 2010, Koivumäki et al., 2012]. The high rate of occurrence of these injuries, which is continually increasing, puts a substantial load on the healthcare system [Pike et al., 2010]. Thus, there is a critical need for preventive actions that can help reduce fracture risk.

Femoroplasty has been suggested to be a potential near-term preventive measure for osteoporotic hip fractures (as we have already shown in Chapter 3). The reinforcement is achieved by means of percutaneous cement injection in order to prevent progressive deformity or collapse and alleviate disabling pain (see Chapter 4) [Heini & Berlemann 2001]. Cement has been widely used in implant fixation and bone augmentation [Belkoff et al., 2007; Heini et al. 2001; Pal et al., 2013] due to its mechanical properties. The suitability of this material explains the reason why most of femoral augmentation studies use commercial cement as the reinforcing agent [Heini et al., 2004; Sutter et al., 2010a; Sutter et al., 2010b; Beckmann et al., 2011; Fliri et al., 2013; Springorum et al., 2014; Basafa et al., 2015; Raas et al., 2016; Varga et al., 2016a] (Table 1). However, cement presents certain disadvantages such as a high polymerization temperature, toxicity and insufficient osseointegration [Vaishya et al., 2013]. Therefore, there are considerable risks involved in femoral augmentation when using large amounts of cement, including bone necrosis due to high temperatures, risk of cement leakage into the blood vessels or development of regions of stress concentration. To this end, computational studies have been conducted to determine the optimum amount of cement and injection locations to minimize the aforementioned possible side effects [Basafa and Armand, 2014; Santana Artiles et al., 2017; Varga et al., 2017] (Table 1).

Computational finite element (FE) analysis is a useful method for studying the mechanical characteristics of hip fracture. FE analysis was previously recognized as a noninvasive tool to estimate fracture load [Bessho et al., 2007; Dragomir-Daescu et al., 2011; Duchemin et al., 2008; Keyak et al., 2003; Verhulp et al., 2008] or the risk for a specific fracture type [Bessho et al., 2007; Dragomir-Daescu et al., 2011; Duchemin et al., 2008; Keyak et al., 2003; Verhulp et al., 2008; Gómez-Benito et al., 2005; Thevenot et al., 2009]. CT-based nonlinear FE analysis, which incorporates three-dimensional geometry and bone density distribution, has been used to estimate fracture load of the proximal femur with reasonable accuracy for given boundary conditions [Bessho et al., 2007; Keyak et al., 2001].

Bessho et al. and Keyak [Bessho et al., 2007; Keyak et al., 2001] used a stance loading configuration, which may not adequately elucidate the failure mechanisms behind the clinical osteoporotic hip fractures that typically occur in sideways falls. Few previous FE studies have estimated the experimental fracture load in a configuration that simulates a fall to the side [Dragomir-Daescu et al., 2011; Duchemin et al., 2008; Keyak et al., 2003]. However, a limited number of femur specimens and linear FE analyses were used in these studies. The generation of an accurate FE model using nonlinear analysis and strain-based criteria with a larger simple size for a sideways fall configuration is therefore required [Nalla et al., 2003; Taylor, 2003; Bayraktar et al., 2004b; Cowin and He, 2005; Currey, 2004; Bayraktar et al., 2004a]. Thus, it seems advisable to implement strain-based criteria in FE models of bone for the prediction of fracture risk.

Given the high volume of published computational studies, it is clear that results from numerical simulations depend on a variety of factors such as the bone morphology, the degree of osteoporosis, the imposed boundary conditions and the material properties of the augmented bone [Rohlmann et al., 2010; Wijayathunga et al., 2013]. The bone geometry, the degree of osteoporosis and the respective material properties are often obtained from a CT scan [Basafa and Armand, 2014; Santana Artiles et al., 2017; Varga et al., 2017; Soyka et al., 2016]. Similarly, the most commonly used boundary conditions in experimental and computational studies of femoroplasty replicate a lateral fall on the greater trochanter [Sutter et al., 2010a; Sutter et al., 2010b; Beckmann et al., 2011; Fliri et al., 2013; Springorum et al., 2014; Basafa et al., 2015].

In chapter 3, we described our approach to computer-assisted planning of femoroplasty to optimize cement volume and placement. In summary, we showed that by introducing 4 ml of high- and low-viscosity cement (substantially less than the 10-50 ml volumes used in previous experimental studies [Beckmann et al., 2007, Heini et al., 2004; Sutter et al., 2010a; Basafa et al., 2015, Santana Artiles and Venetsanos, 2017]) into open-cell structures with different porosities resembling different trabecular bone structures, it was possible to improve the mechanical properties (Young's modulus). Thus, computational and experimental differences between high- and low-viscosity cement were shown under the same loading conditions.

The purpose of the current chapter is to computationally augment healthy and osteoporotic femur specimens according to an efficient generalized augmentation strategy by



which we will control the cement volume and its injection location. We hypothesize that the resulting cement augmentation (with high- and low-viscosity cement) will increase the mechanical strength of the femur compared to nonaugmented controls, as was observed in Chapter 3 with open-cell structures. We also hypothesize that the experimentally measured augmented parameters of interest will not be significantly different from those of model predictions; moreover, these results will be obtained using smaller cement volumes than previously reported for significant augmentation. To our knowledge, no other report has been published on the comparison between high- and low-viscosity cement for osteoporotic bone augmentation.

## **5.2 Materials and methods**

The methodology proposed in this chapter consists in two parts. First, nonlinear strain-based FE simulations were utilized to predict the ideal reinforcement zones and fracture risks of the proximal femur under loads from a sideways fall. Second, a new efficient generalized augmentation strategy was developed based on the minimum density and total volume of the failure zone and used to virtually augment thirty-five femur specimens (healthy and osteoporotic). The volume of the cement cloud varied among femur specimens according to the different failure areas achieved after FE simulations. Thus, changes in the biomechanical properties and fracture risk of the augmented bones (with high- and low-viscosity cement) were evaluated by means of nonlinear strain-based FE simulations and compared sample-wise to the nonaugmented state.

### **5.2.1 Study sample**

Eighteen healthy femurs (female/male: 7/13, age: mean  $44.5 \pm 28.5$  years, left: 18) and seventeen osteoporotic femurs (female/male: 6/11, age: mean  $70.5 \pm 14.5$  years, left: 17) were previously collected and scanned using a CT system (Brilliance 64, Philips Healthcare, Netherlands) with the following parameters: tube current = 257 mA, voltage = 120 KV, slice thickness = 0.65 mm, spacing between slices = 2 mm and pixel spacing = 0.234 mm. The healthy femurs were obtained from the Hospital Quirón (Valencia, Spain) and the osteoporotic femurs, from the Hospital Universitario y Politécnico La Fe (Valencia, Spain). Both healthy

and osteoporotic femurs were retrospectively extracted from the picture archiving and communications systems (PACS).

### **5.2.2 Model development**

The scanned images were reconstructed using a semiautomatic reconstruction (MIMICS, Materialise NV; Leuven, Belgium) to obtain a 3D solid bone model. The mesh was generated using tetrahedral elements (C3D4), comprising of  $105304 \pm 27480$  elements for the healthy femora and  $110481 \pm 32720$  elements for the osteoporotic femora.

Inhomogeneous isotropic bone properties were mapped from the CT images to the mesh (MIMICS, Materialise NV; Leuven, Belgium). Normally, CT calibration phantom is used to obtain the radiological density ( $\rho_{QCT}$ ). However, in the present paper, as no scanner calibration was available for the used files, each Hounsfield unit (HU) was converted into radiological density ( $\rho_{QCT}$ ) using information from the images and the literature [Santana Artiles and Venetsanos, 2017]. In more detail, Equation (5) was used to convert HUs into radiological density for the healthy tissue:

$$\rho_{QCT}(healthy) = 0.209 + 0.001086 \cdot HU \quad (5)$$

Equation (6) was used to convert HU into radiological density for the osteoporotic tissue:

$$\rho_{QCT}(osteoporotic) = 0.1712 + 0.0007058 \cdot HU \quad (6)$$

The bone mineral density (BMD) of an osteoporotic femur is approximately 65% of the BMD of a healthy femur [Looker et al., 2012]. This relation was considered to obtain Equation (6) from Equation (5).

For material heterogeneity, an average grey value of all of the voxels inside an element was calculated in Mimics (MIMICS, Materialise NV; Leuven, Belgium). The bone equivalent density (ash density,  $\rho_{ash}$ ) was then defined by assuming a linear relationship by which the density is proportional to the attenuation ( $\rho_{ash} = \rho_{QCT}$ ) (Koivumäki et al., 2012).

Finally, elastic modulus for each element (in MPa) was calculated using the following equations (Morgan et al., 2003; Keller, 1994) for femoral neck specimens (Schileo et al., 2008):

$$E_{cortical} = 10500 \cdot \rho_{ash}^{2.29}; \quad \nu = 0.32 \quad (7)$$

$$E_{trabecular} = 6850 \cdot \rho_{ash}^{1.49}; \nu = 0.2 \quad (8)$$

### 5.2.3 Boundary and loading conditions

The examined load case was that of a lateral fall onto the greater trochanter. To this end, the femur was distally and fully constrained, while the lateral side of the greater trochanter was restricted to move only in one plane [Bessho et al., 2004]. The total applied force was uniformly distributed over the medial nodes of the femoral head, while the force direction was tilted  $15^\circ$  in the frontal plane, as seen in Figure 30.

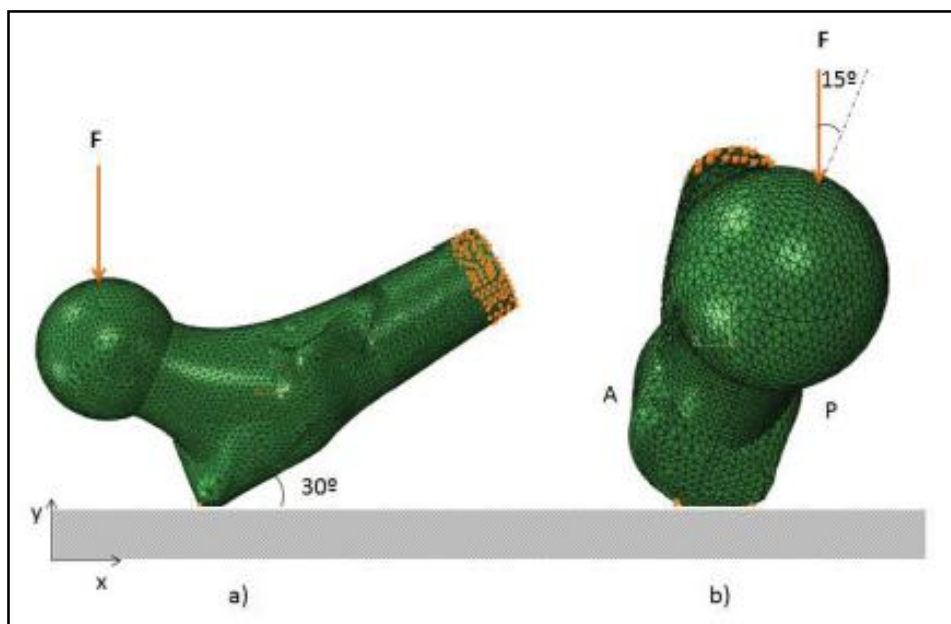


**Figure 30:** Boundary and loading conditions of the fall configuration: vertical load on the femoral head toward the floor with the femoral shaft slanted by  $30^\circ$  and internally rotated  $15^\circ$  relative to the floor

### 5.2.4 Fracture load prediction of nonaugmented subject-specific models

Non-linear strain-based FE simulations were utilized to predict the ideal reinforcement zones and fracture risks of the proximal femur under loads from a sideways fall. To compute the fracture load under the fall configuration, a maximum principal strain criterion, including asymmetry in the tensile/compressive limit values, was selected. This criterion incorporates many of the fundamental bone elastic limit characteristics reported in the literature and can be

easily implemented [Schileo et al., 2008]. In each element of the FE mesh,  $e_{min}$  and  $e_{max}$  were assigned as follows:

$$\text{If } \varepsilon_1 > 0 \text{ then } e_{max} = \frac{\varepsilon_1}{\varepsilon_{limT}} \text{ if not } e_{max} = \frac{\varepsilon_1}{\varepsilon_{limC}} \quad (9)$$

$$\text{If } \varepsilon_3 > 0 \text{ then } e_{min} = \frac{\varepsilon_3}{\varepsilon_{limT}} \text{ if not } e_{min} = \frac{\varepsilon_3}{\varepsilon_{limC}} \quad (10)$$

where  $\varepsilon_{limT} = 0.0073$  and  $\varepsilon_{limC} = 0.0104$  [Bayraktar et al., 2004b]. Thus, the fracture risk (RF) was evaluated as  $RF = \max(|e_{max}|, |e_{min}|)$ . If the element RF exceeded 1, its volume was added to the volume of the failed elements. We increased the load until the total volume of the failed elements reached 2% of the total volume of the specimen [Pistoia et al., 2002; Niebur et al., 2000] (Figure 31).

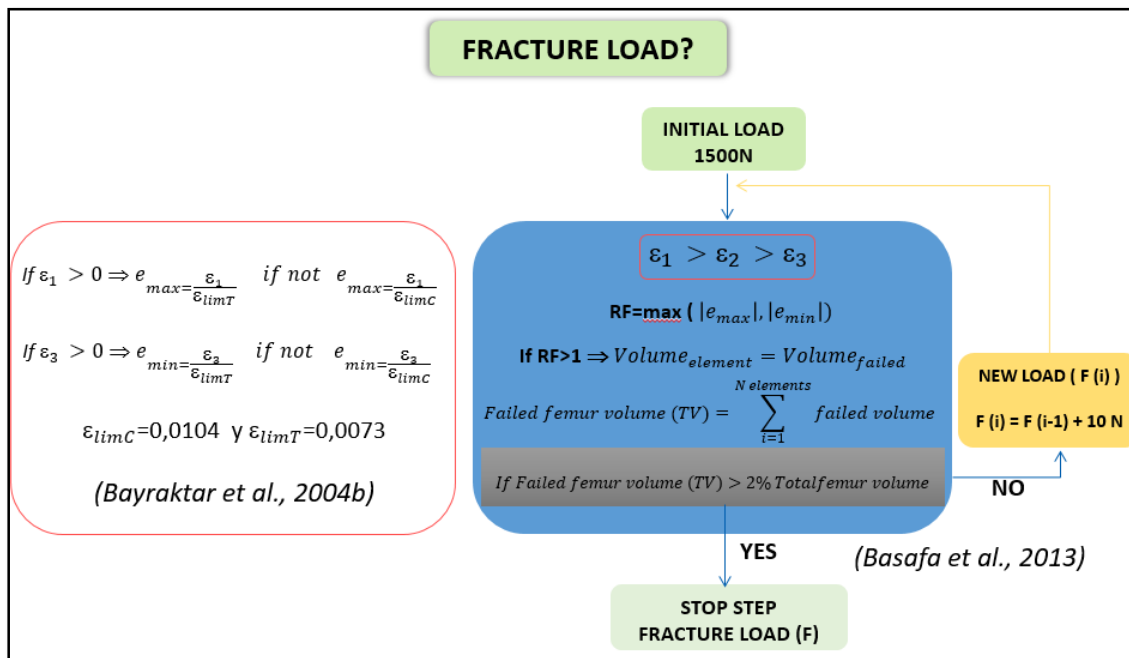


Figure 31: Workflow for the non-linear strain-based FE simulations for the prediction of the fracture risk [Schileo et al. 2008]

The value of 2% was selected somewhat arbitrarily according to the literature because it is not known what percentage of bone tissue actually exceeds the yield strain when bone fractures occur [Pistoia et al., 2002]. To determine whether another value would yield a better estimation of the bone failure load, the fracture load was also calculated under the assumptions that fracture occurs when 1%, 2% or 3% of the bone tissue exceeds the yield strain. Therefore, the instant of fracture was defined by assessing the volume of the failed elements, in line with previous studies [Bessho et al., 2004; Koivumaki et al., 2012] (Figure 31). No degradation of

the material properties of the failed elements was considered. The algorithm was implemented as a user defined material (UMAT) subroutine in Abaqus v6.14 (Dassault Systèmes Simulia Corp., Suresnes Frances) and run in a computational cluster of 224 cores with 576 GB of RAM.

### 5.2.5 Local bone augmentation strategy

The optimum volume of cement and its distribution within the femur was computed for each model following the next approach.

In chapter 3, a discrete particle model for cement infiltration within open cell structures resembling trabecular bone was developed. Briefly, this particle model allowed us to predict the improvement in the mechanical properties depending on the bone density, cement viscosity and injected cement volume. The computational approach was experimentally validated. Data generated in Ramos-Infante et al. [2018] consisted in cement volumen injected, average density of the open-cell structures, and improvement of the mechanical properties between augmented and nonaugmented open-cell structures using two cement types (high- and low-viscosity cements). Thus, using previous data and the Curve Fitting Toolbox of Matlab (Matlab r2017a, The Mathworks Inc., Natick, USA), a powerful law to predict femur strength improvement was proposed (Equation (8) and Table 8).

$$IF (\%) = P00 + (P10 \cdot TV) + (P01 \cdot MD) + (P20 \cdot TV^2) + (P11 \cdot TV \cdot MD) + (P30 \cdot TV^3) + (P21 \cdot MD \cdot TV^2) \quad (11)$$

where IF is the improvement factor (in %), TV is the total accumulated volume of the failed elements or total volumen of cement injected (in cm<sup>3</sup>), MD is the minimum density associated with this femur area or the average density of the open-cell structures resembling trabecular bone [Ramos-Infante et al., 2018] (in g/cm<sup>3</sup>) and P00, P10, P01, P20, P11, P30 and P21 are the coefficients associated with the cement viscosity (Table 8).

Once the fracture load for each nonaugmented femur specimen was obtained, we were able to determine the minimum density (MD) associated with this failed area and the total accumulated volumen (TV) of the failed elements, which will be considered as equivalent to the cement volume injected. Then, the local IF of the mechanical properties was obtained using Equation (11).

Table 8: Calculated coefficients for each element

High viscosity cement		Low viscosity cement	
<b>P00</b>	-2.474	<b>P00</b>	6.571
<b>P10</b>	4.784	<b>P10</b>	69.77
<b>P01</b>	13.68	<b>P01</b>	77.8
<b>P20</b>	3.609	<b>P20</b>	18.52
<b>P11</b>	-8.348	<b>P11</b>	-268.6
<b>P30</b>	-0.1458	<b>P30</b>	-4.224
<b>P21</b>	-4.49	<b>P21</b>	24.49
<b>R-square</b>	0.9921	<b>R-square</b>	0.9978

Later, once we obtain the local IF, the Young's modulus (in MPa) of the failed elements was changed to that of augmented trabecular elements using the following equation:

$$E_{trabecular}^{IF} = \left( 1 + \left( \frac{IF}{100} \right) \right) \cdot 6850 \cdot \rho_{ash}^{1.49}; \nu = 0.3 \quad (12)$$

Finally, the fracture load was calculated using the maximum principal strain criterion (Figure 30 and Figure 31) and compared with nonaugmented cases.

## 5.3 Results

### 5.3.1 Local bone augmentation

Table 9 shows the TV, MD and the corresponding improvement factor (IF) related to the type of cement that was injected (high- and low-viscosity cement).

Table 9: Calculated TV, MD and IF for the healthy and osteoporotic bone models (mean  $\pm$  SD)

Parameter	Healthy bone model	Osteoporotic bone model
	(Mean $\pm$ SD)	(Mean $\pm$ SD)
<b>TV (cm<sup>3</sup>)</b>	3.36 $\pm$ 0.75	3.03 $\pm$ 0.62
<b>MD (g/cm<sup>3</sup>)</b>	0.14 $\pm$ 0.06	0.08 $\pm$ 0.03
<b>IF high viscosity (%)</b>	40.66 $\pm$ 14.61	37.48 $\pm$ 11.25
<b>IF low viscosity (%)</b>	202.13 $\pm$ 46.28	224.08 $\pm$ 30.03

Important differences between cement viscosities can be easily observed for similar total volumes of the healthy and osteoporotic femur specimens.

### 5.3.2 Subject-specific fracture load prediction

All augmented femur specimens exhibited increased fracture-relevant properties of the femora compared with the nonaugmented state. As commented in Section 5.2.1, 35 femur specimens were assessed (18 healthy femur specimens and 17 osteoporotic femur specimens). Figure 32 shows the mean fracture loads for all simulations from this study. For the nonaugmented state, the mean fracture load was  $5078.33 \pm 1356.59$  N for the healthy subjects and  $2437.65 \pm 758.91$  N for the osteoporotic bone model. For a given cement volume (TV), the relative increase depended on the nonaugmented properties MD and cement viscosity (high and low) (Table 9). Augmentation with approximately 3 ml of high-viscosity cement resulted in a  $9.41 \pm 3.66\%$  increase in fracture load in healthy specimens ( $5622.78 \pm 1557.45$  N) and  $10.32 \pm 3.22\%$  increase in osteoporotic specimens ( $2728.24 \pm 863.98$  N). Similarly, augmentation with approximately 3 ml of low-viscosity cement resulted in a  $25.19 \pm 6.00\%$  increase in fracture load in healthy specimens ( $6800.00 \pm 1827.92$  N) and a  $28.93 \pm 7.04\%$  increase in osteoporotic specimens ( $3478.00 \pm 1189.43$  N). Regarding the fracture load improvements for the different ratios considered (the volume of failed elements with respect to the local volume of the specimen), Table 10 shows that the difference between RATIO 1 and RATIO 2 is considerably greater than the difference between RATIO 2 and RATIO 3. These differences could also be observed in Figure 33, in which the cement injection cloud is similar in Figure 33b and Figure 33c.

**Table 10: Results of the sensitivity analysis: fracture load improvement (%) (mean  $\pm$  SD)**

Parameter	RATIO 1	RATIO 2	RATIO 3
Augmented (healthy/high viscosity)	$3.09 \pm 1.46$	$9.41 \pm 3.66$	$16.16 \pm 5.42$
Augmented (healthy/low viscosity)	$16.45 \pm 3.24$	$25.19 \pm 6.00$	$23.70 \pm 10.61$
Augmented osteoporotic/high viscosity)	$3.14 \pm 1.33$	$10.32 \pm 3.22$	$18.26 \pm 4.69$
Augmented (osteoporotic/low viscosity)	$17.10 \pm 4.81$	$28.93 \pm 7.04$	$32.65 \pm 10.19$

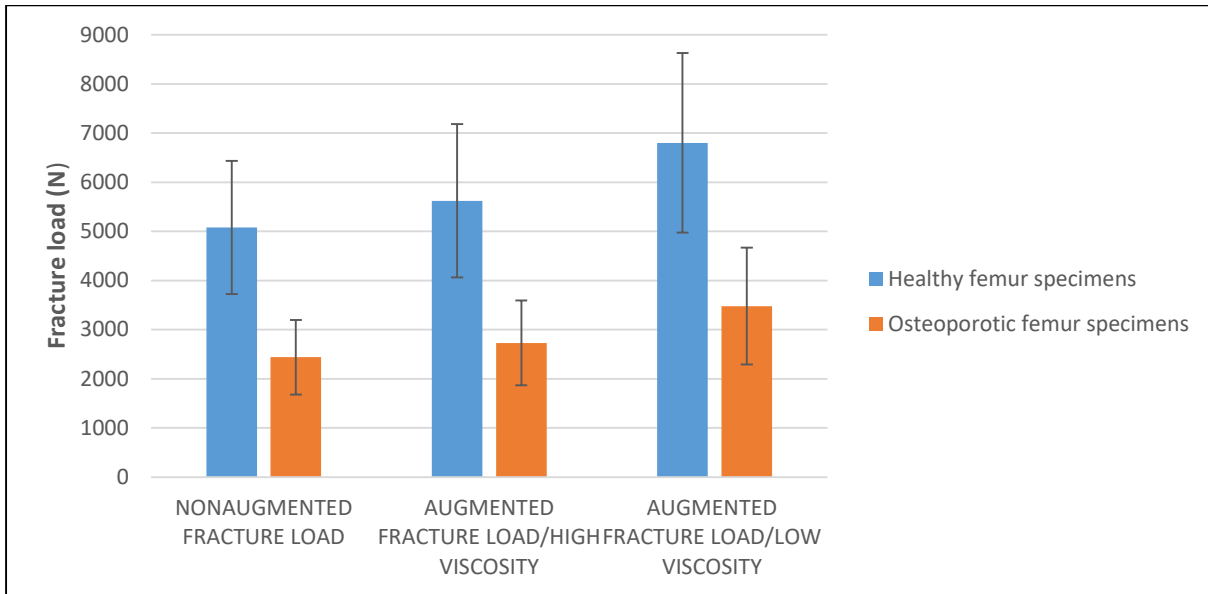


**Figure 32:** Calculated fracture loads for the healthy and osteoporotic bone model for the nonaugmented and augmented states (high- and low-viscosity cement). Bars indicated standard deviation.

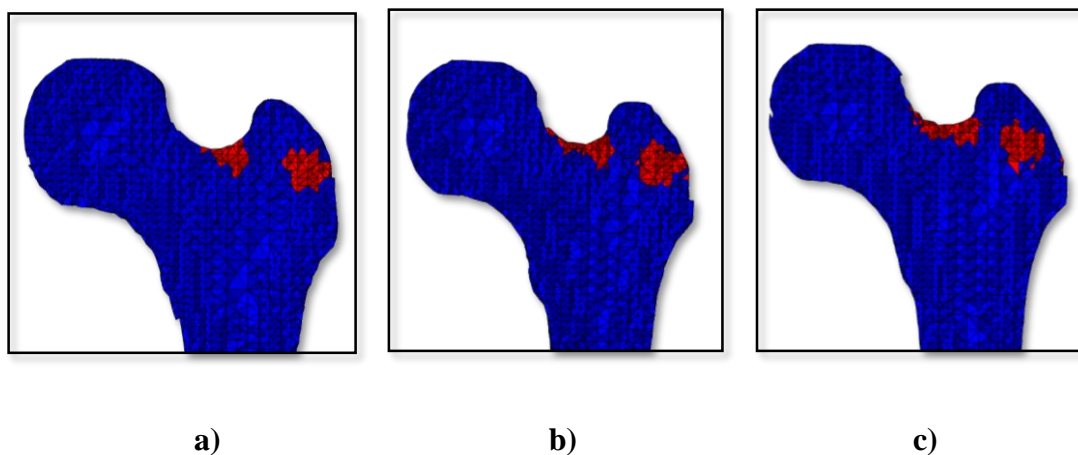


**Figure 33:** Cement injection cloud (red area) for an augmented osteoporotic femur specimen for a) RATIO 1, b) RATIO 2 and c) RATIO 3 (transversal section)

## 5.4 Discussion

Augmentation of an osteoporotic femur using cement to prevent or reduce the risk of fracture has been suggested as an alternative preventive treatment [Basafa and Armand, 2013]. The results of the current study support our original hypothesis that femoroplasty improves the mechanical properties of the femur compared with nonaugmented controls (Figure 32). A few



recent studies have reported attempts to restore the mechanical strength of femur specimens using a relatively small amount of infiltrated cement with limited or no success [Beckmann et al., 2011; Fliri et al., 2012; Steenhoven et al., 2012; Sutter et al., 2010b]. A successful planning framework should include a module for predicting the cement infiltration inside trabecular bone. The majority of fragility fractures occur at trabecular-dominant bone sites. Indeed, the trabecular bone plays important roles in load transmission and energy absorption in major joints. Indeed, most proximal femur fractures initiate at the femoral neck superior cortex under compression, followed by damage of the inferior cortex under tension [de Bakker et al., 2009; Nawathe et al., 2014].

Reinforcing this region may help to delay the superior cortex collapse and increase the overall strength of the proximal femur to protect against injury during sideways falls.

In chapter 3, a discrete particle model for cement infiltration within open cell structures was developed. As discussed in Section 5.2.5, this particle model allowed us to build a generalized local bone augmentation strategy to control cement volume and its injection placement in healthy and osteoporotic femur specimens.

The goal of the present chapter was to quantify and compare the differences between high- and low-viscosity cement for osteoporotic bone augmentation at the macroscopic level. Indeed, the main novelty of the current work was that our hypothesis to build the model was based on previous results (Chapter 2 and Chapter 3) in which the computational approaches were experimentally validated. Thus, as a multiscale problem, thirty-five femur specimens were augmented based on the developed model to computationally quantify the fracture load improvement when high- and low-viscosity cement was injected.

We performed a control set of validation tests using nonaugmented healthy and osteoporotic femur specimens. Thus, fracture loads were 53.41% lower in the osteoporotic femur specimens, similar to the values reported in the literature [Van der Zijden et al., 2015]. Some significant differences can be observed in comparing the method presented in the aforementioned articles with the method presented in this study. First, as the generation of an accurate FE model using nonlinear analysis and strain-based criteria with a larger sample size for a sideways fall configuration was required [Nalla et al., 2003; Taylor, 2003; Bayraktar et al., 2004b; Cowin and He, 2005; Currey, 2004; Bayraktar et al., 2004a], the method presented uses principal strain values as the optimization criterion.

Although the goal of this chapter was not to set any optimization volume for bone augmentation, the results suggest that by injecting approximately 3 ml of high- and low-viscosity cement, the inherent mechanical properties of healthy and osteoporotic femora are improved. Additionally, a mechanical improvement factor based on the total volume generated by the failed elements of nonaugmented controls and the minimum local density, allowed us to predict the improvement in mechanical properties that could be achieved in the failed area, such as, the femoral neck. Basafa and Armand (2014) applied a constant load and scaled the strains assuming linearity. In fact, their BESO methodology terminated when there was a 100% increase in the predicted yield load of the osteoporotic femur model. Santana Artiles and Venetsanos (2017) established a target load 15% higher than the yield load of the healthy femur. Varga et al. (2017) used different sizes of cement cylinders within the trabecular bone domain and quantified the mechanical improvement. In our particular case, the target loads and hypotheses established in the literature were integrated to develop a powerful model.

Two cement viscosities were used in this thesis. The results of our FE analyses suggested that low-viscosity cement led to a better improvement in the mechanical properties and fracture loads of the proximal femora in sideways falls than the high-viscosity cement (Figure 32). This fact was experimentally observed in our previous work [Ramos-Infante et al., 2018]. The material distribution was highly similar to the results obtained in the literature [Basafa and Armand, 2014; Basafa et al., 2015; Santana Artiles and Venetsanos, 2017; Varga et al., 2017] (Figure 33). Our model showed that approximately 3 ml of high-viscosity cement resulted in fracture loads increases ranging from 9.41% (healthy femur specimens) to 10.32% (osteoporotic femur specimens). Similarly, approximately 3 ml of low-viscosity cement resulted in fracture loads increases ranging from 25.19% (healthy femur specimens) to 28.93% (osteoporotic femur specimens). These observations were also confirmed by the sensitivity analysis (Table 10), in which regardless of the amount of cement injected, both cement types increases the fracture loads of nonaugmented states. As shown in Table 9, the minimum density values were similar in healthy and osteoporotic femur specimens. The main reason for this similarity is that any calibration phantom was obtained. The density calibration phantom provides a basis for HU conversion to density values [Michalski et al., 2016; Bessho et al., 2007; Kaneko et al., 2015]. As discussed in the literature, one inherent problem in bone augmentation research is the fact that osteoporotic femora, on which researchers base the development of their computational models have different morphologies. Therefore, the ideal case would involve a set of different bones and the material properties for different T-score

levels for each bone [Santana Artiles and Venetsanos, 2018]. In this particular case, we assessed thirty-five femur specimens with their material properties defined by HUs.

Human trabecular bone is anisotropic by nature. Additionally, the cement viscosity affected the compactness of the final shape of the cement. A high-viscosity cement produces a cement cloud with high sphericity [Ramos-Infante et al., 2018]. This observation suggested that mid- or low-viscosity cements (low sphericity) were ideal for injections into porous media, including osteoporotic trabecular bone, because the final shape was sufficiently compact [Basafa and Armand, 2013; Baroud et al., 2006].

The results presented are quite promising. Nevertheless, the proposed methodology presents certain limitations. Validation through experimental tests was not performed. However, our fracture load predictions were in the same range as those obtained in other similar works in the literature [Van der Zijden et al., 2015; Santana Artiles and Venetsanos, 2017, 2018; Varga et al., 2017]. In addition, the particle model for cement modelling used here included simplified assumptions that were likely a source of differences between the modelled behaviour and actual cement behaviour [Ramos-Infante et al., 2018]. These assumptions included the unmodeled viscoelastic behaviour of the cement, especially at large viscosities, and the interaction of the cement with the surrounding soft tissue (bone marrow, blood, etc.). However, regarding the latter assumption, similar experiments [Heini et al., 2004; Beckmann et al., 2007; Sutter et al., 2010a, 2010b] and our previous tests [Basafa et al., 2013c] have shown that displacing the bone marrow does not pose a practical issue, especially in the case of osteoporotic femora, in which a major portion of bone density is lost due to osteoporosis. Moreover, the time-dependent cement injection process and the solidification of the injected cement were not simulated. Another simplification of this study is that cement may be injected independently and separately at any location. In theory, this technique might be achieved through minimally invasive surgical techniques and miniaturization, although this technique has not yet been applied in femoroplasty [Santana Artiles and Venetsanos, 2017; Beckmann et al., 2011]. Another limitation is that when failed elements were predicted, no degradation of material properties was simulated [Basafa et al., 2013; Santana Artiles and Venetsanos, 2017]. In future work, other numerical techniques could be implemented, such as: eXtended Finite Element Method (XFEM), material property degradation at the element level, element deletion and other variants with incremental crack growth [Marco et al., 2018]. Additionally, other fall configurations could be assessed in order to further validate the model.

## **5.5 Conclusions**

The main purpose and contribution of this chapter were to introduce patient-specific planning of femoroplasty for injection of high- and low-viscosity cement. Low-viscosity cement notably increased the fracture load of nonaugmented femur specimens in comparison with high-viscosity cement. These encouraging numerical results suggest an enhanced potential of low-viscosity cements for augmentation, but require experimental confirmation. Healthy and osteoporotic femur specimens were computationally augmented according to our generalized augmentation strategy to control the volume and placement of cement injection. Thus, this methodology could be used as a preoperative planning tool for bone augmentation surgery.

# Chapter 6

---

*Conclusions and future work and  
contributions*



## 6.1 General conclusions

In this thesis, we have designed and developed a multiscale model for the osteoporotic fracture prevention. Here, we summarize the main conclusions of each chapter and, finally, we provide a general conclusion about our modeling proposal.

### 6.1.1 *In vitro* and *in silico* characterization of open-cell structures for trabecular bone

At tissue level, we obtained experimental and computational results throughout compression tests and FEA, respectively. Therefore, the model was validated with experimental results performed on fifty-three specimens and with computational results performed on eighteen specimens. Initially, the open-cell structures were scanned using  $\mu$ CT, whose data was used to non-destructively predict the specimen elastic moduli developing voxel-based and tetrahedral FE models. A 3D reconstruction was performed using MIMICs and 3-MATIC (Materialise NV, Leuven, Belgium) and FE analyses were run in ABAQUS (Dassault Systèmes Simulia Corp., Suresnes France). A comparison among different element types (linear and quadratic tetrahedrons and voxel-base meshes), experimental and computational results and computational results with data provided by Sawbones (Sawbones, Malmö, Sweden) were carried out. As a result, important differences in the elastic modulus and porosities were obtained. Linear tetrahedral elements showed better correlations in specimens with higher volume fractions. In contrast, specimens with low volume fractions showed better correlations with quadratic tetrahedral elements.

### 6.1.2 Discrete particle model for cement infiltration within open-cell structures: prevention of osteoporotic fracture

The development of a cement diffusion model based on the random-walk theory for simulating cement infiltration within open-cell structures resembling trabecular allowed us to increase the mechanical properties. Model parameters considered the cement viscosity (high and low) and the desired direction of injection (vertical and diagonal). *In vitro* and *in silico* characterizations of augmented open-cell structures validated the computational model and quantified the improved mechanical properties (Young's Modulus) of the augmented specimens. Indeed, the cement injection pattern was successfully predicted in all the simulated

cases and the augmented specimens exhibited enhanced mechanical properties computationally and experimentally. As a result, the open-cell structures with high porosity fraction showed a considerable increase in mechanical properties. Cement augmentation in low porosity fraction specimens resulted in a lesser increase in mechanical properties. The results suggested that the proposed discrete particle model was adequate for use as a femoroplasty planning framework.

### **6.1.3 Development of a rabbit fracture model for evaluation of cement augmentation: an *in vivo* biomechanical study**

In order to further validate our femoroplasty approach experimentally, we developed an *in vivo* rabbit fracture model for the evaluation of cement augmentation. Under anesthesia, cement was injected into the right femoral head of 10 rabbits (New Zealand). The femoral head region was evaluated *in vivo* using MRI before and three months after cementation. At three months postinjection, both femurs (nonaugmented and augmented) were excised and subjected to biomechanical tests using a servo-hydraulic material testing machine (Microtest; model EFH, Spain). Finally, the mechanical properties of the cemented femurs were analyzed, considering the contralateral nonaugmented femurs as the control reference.

As it could be observed with augmented open-cell structures, all augmented rabbit femora showed enhanced mechanical properties. Thus, the safety and feasibility of the technique were assessed successfully.

### **6.1.4 High- and low-viscosity cement for osteoporotic femoral augmentation: a computational subject-specific approach**

At a macroscopic level and considering the results presented in previous chapters, 35 femur specimens (18 healthy femora and 17 osteoporotic femora) were computationally augmented following a novel efficient generalized augmentation strategy based on a strain-based criterion. The proposed methodology incorporated cements (high- or low-viscosity) that were assessed to augment healthy and osteoporotic femora controlling cement volume and its injection placement.

All the augmented specimens exhibited enhanced fracture loads regardless of the cement viscosity used. Low viscosity cement showed a higher fracture load improvement than high-



viscosity cement. Additionally, augmentation of osteoporotic femurs estimated a larger improvement in the fracture load with respect to healthy femurs. Thus, osteoporotic femur specimens showed a greater improvement in mechanical properties when low-viscosity cement was injected. The results suggest that low-viscosity cement can be a powerful candidate for use in femoroplasty.

Additionally, the proposed methodology can be efficiently used for preoperative planning of bone augmentation surgery.

## 6.2 Future work

As commented in previous sections, femoroplasty improves the mechanical properties of bone in comparison with the nonaugmented state. In particular, low-viscosity cement has shown its potential for its use in augmentation framework. Indeed, the findings achieved in this thesis add significant insights into the future of such a technique as preventive intervention in patients with severe osteoporosis and bone loss, since this would minimize fracture risk and consequently the socio-economic impact.

In general, as future work, it is needed that computational and animal models were validated in humans in order to clarify the femoroplasty feasibility. Additionally, it could be interesting the development of a multiscale methodology based on neural networks in order to perform faster simulations with a reduction of the computational cost.

In particular, if we focus on the methodology proposed in this thesis, it could be interesting to present the future lines proposed for each chapter:

- **Chapter 2.** Trabecular bone plays an important role in load transmission and energy absorption. Because bone is anisotropic, a large number of experiments are necessary to adequately describe the behavior of trabecular bone in general and within each anatomical location. Thus, computational models are considered as a powerful tool to elucidate these fracture mechanisms. Although linear, quadratic tetrahedral and voxel meshes allowed us to accurately predict the mechanical properties of open-cell structures, it could be interesting the use of other meshes, such as (skeletonization) that help us to know more about the microstructure damage and a better trabecular bone characterization. Additionally, the incorporation of

inhomogeneous material properties based on mineralization of different anatomical locations could allow to accurately characterize the trabecular bone.

- **Chapter 3.** One of the main problems of the augmentation technique is high temperature inside the bone during the curing process. Future research must also verify the assumption that by minimizing the injection volume, we can avoid thermal necrosis caused by the exothermic curing process of the cement [Basafa et al., 2015]. Additionally, a validated model for heat generation and propagation could be incorporated into the planning module for the design of safer augmentations by keeping the heat damage away from more vulnerable sites, such as the arteries [Palumbo et al., 2014].
- **Chapter 4.** The use of animal models as previous step to human models is one of the best approaches to determine the feasibility of femoroplasty. However, as future work, *in vivo* models must be used in conjunction with computational models. Also, other animal models and different cement volumes could be considered in order to clarify the risk of high-cement volumes injected.
- **Chapter 5.** As regards the cement, the time-dependent cement injection process, the solidification of the cement and the material property degradation could be simulated. Also, other fall configurations could be assessed in augmented femora to elucidate fracture risks and cement placement. The final goal would be to obtain a generalized cement augmentation strategy regardless of the fall configuration. However, as in chapter 4, computational models should be validated with experimental data.

## **6.3 Contributions**

### **6.3.1 Articles in peer-review journals**

Published work:

- Samuel Jesús Ramos-Infante and María Ángeles Pérez. *In vitro* and *in silico* characterization of open-cell structures for trabecular bone. *Computer Methods in Biomechanics and Biomedical Engineering*, Vol. 20(14), 1562–1570. October (2017).

- Samuel Jesús Ramos-Infante, Amadeo Ten-Esteve, Ángel Alberich-Bayarri and María Ángeles Pérez. Discrete particle model for cement infiltration within open-cell structures: Prevention of osteoporotic fracture. *PloS ONE*, Vol. 13(6), e0199035. June (2018).

Submitted work under review:

- Samuel Jesús Ramos-Infante and María Ángeles Pérez. High- and low-viscosity cement for osteoporotic femoral augmentation: a computational subject-specific approach. *Engineering Fracture Mechanics*.

### 6.3.2 Presentations in conferences

The work shown in this thesis has been presented in the national and international conferences listed below.

- Oral presentations
  - In vitro and in silico characterization of open-cell structures for trabecular bone.* 22nd Congress of the European Society of Biomechanics. Lyon 2016 (France) (EMEA Second Prize Winner of the Mimics Innovation Awards 2016).
  - A particle model for prediction of cement infiltration in osteoporotic femoral augmentation.* Particles 2017. Hannover 2017 (Germany).
  - Multiscale simulation in bone tissue engineering: from micro to organ level.* COST Action MP1301 - NEWGEN - New Generation Biomimetic and Customized Implants for Bone Engineering. Vienna 2017 (Austria).
  - In vitro and in silico characterization of cement infiltration in osteoporotic bones.* VPH-Virtual Physiological Human Conference 2018. Zaragoza 2018 (Spain).
  - Patient-specific planning of proximal femoral augmentation: in vitro and in silico approaches.* EORS-European Orthopaedic Research Congress. Galway 2018 (Ireland).
- Poster presentations
  - Personalized cement augmentation of the proximal femur using a discrete cement diffusion model.* Termis 2017. Davos 2017 (Switzerland).



# Chapter 7

---

*Conclusiones, trabajo futuro y  
contribuciones*



## 7.1 Conclusiones generales

Esta tesis doctoral se fundamenta en el diseño y desarrollo de una plataforma multiescala para la prevención de la fractura osteoporótica. Para ello, a continuación, se resumirán las conclusiones alcanzadas en cada uno de los capítulos que conforman el presente documento.

### 7.1.1 Caracterización *in vitro* e *in silico* de estructuras open-cell para hueso trabecular

A nivel tisular, se han obtenido resultados experimentales y computacionales a través de ensayos de compresión pura y simulaciones por medio del método de los elementos finitos, respectivamente. El modelo fue validado a través de la ejecución conjunta de ensayos de compresión sobre 35 estructuras open-cell, de las cuales 18 fueron previamente escaneadas usando un  $\mu$ CT, a fin de predecir de manera no destructiva el módulo elástico de la estructura en cuestión, mediante la generación de mallas basadas en tetraedros y voxels. La reconstrucción de los modelos 3D fue llevada a cabo usando los softwares MIMICS y 3-MATIC (Materialise NV, Lovaina, Bélgica); el análisis por elementos finitos fue realizado mediante el software ABAQUS (Dassault Systèmes Simulia Corp., Suresnes Frances). De esta manera, se realizó un estudio comparativo entre los diferentes tipos de elementos empleados (tetraedros lineales y cuadráticos y voxels), entre los resultados experimentales y computacionales, y entre los resultados computacionales y los proporcionados por Sawbones (Sawbones, Malmö, Suecia). Así, se apreciaron grandes diferencias en términos de módulo elástico y porosidad. Las mallas basadas en tetraedros lineales presentaban mayores correlaciones con las estructuras con menores porosidades, mientras que las mallas basadas en tetraedros cuadráticos presentaban mayores correlaciones con las estructuras con mayor porosidad.

### 7.1.2 Modelo discreto de partículas para infiltración de cemento a través de estructuras open-cell: prevención de la fractura osteoporótica

Las estructuras open-cell presentan una microestructura y morfología similar al hueso trabecular. El desarrollo de un modelo de difusión de cemento basado en la teoría del movimiento aleatorio a través de este tipo de estructuras permitió obtener un incremento notable de las propiedades mecánicas. Los parámetros del modelo incluían la viscosidad del cemento

(alta y baja), así como la dirección de inyección preferencial (vertical y diagonal). Las caracterizaciones *in vitro* e *in silico* de estructuras open-cell cementadas validaron el modelo computacional y cuantificaron la mejora de propiedades (módulo de Young). Además, el patrón de inyección de cemento fue predicho satisfactoriamente en todas las simulaciones, así como que las estructuras cementadas en cuestión mejoraron notablemente sus rigideces tanto desde un punto de vista computacional como experimental. Así, las estructuras open-cell con mayor porosidad mostraron un aumento considerable en las propiedades mecánicas, al contrario que las estructuras con menor porosidad, las cuales presentaban menores incrementos. Dichos resultados sugerían que el modelo discreto de partículas era adecuado para su uso en la planificación de la femoroplastia.

### **7.1.3 Desarrollo de un modelo de fractura en conejo para la evaluación de la cementación femoral: un estudio biomecánico *in vivo***

A fin de validar el modelo de femoroplastia a nivel experimental, se desarrolló un modelo de fractura en conejo para la evaluación de la cementación femoral. Bajo anestesia, se inyectó cemento (PMMA) en el fémur derecho de 10 conejos (Nueva Zelanda). Tras 3 meses de cementación, se llevó a cabo un escaneo *in vivo* de la región del fémur proximal por resonancia magnética, seguido de la extirpación y ensayo experimental del conjunto de fémures (cementados y no cementados) mediante máquina universal servohidráulica (Microtest; modelo EFH, España). Así, se analizaron las propiedades mecánicas de los fémures cementados tomando como referencia los no cementados.

Tal y como ocurría con las estructuras open-cell cementadas, todos los fémures de conejo cementados mostraron un aumento de propiedades mecánicas. Por tanto, la seguridad y la factibilidad de la técnica fueron evaluadas exitosamente.

### **7.1.4 Cemento de alta y baja viscosidad para la cementación del fémur osteoporótico: un acercamiento computacional al paciente específico**

A nivel macroscópico y considerando los resultados presentados en capítulos anteriores, 35 fémures (18 sanos y 17 osteoporóticos) fueron cementados computacionalmente siguiendo una estrategia eficiente de cementación basada en el criterio de deformación. La metodología



propuesta incorporó cementos (alta y baja viscosidad) que fueron evaluados para cementar fémures sanos y osteoporóticos controlando el volumen de cemento y su localización.

Como ya ocurría con las estructuras open-cell y los fémures de conejo, todos los fémures presentaban mejoras en las cargas de fractura independientemente de la viscosidad de cemento empleada. Los cementos de baja viscosidad mostraron una mejora de propiedades mayor que los cementos de alta viscosidad. Además, la cementación de fémures osteoporóticos presentaron unas mejoras en lo que a carga de fractura se refiere mayores que los fémures sanos. Por tanto, los fémures osteoporóticos aumentaron notablemente sus rigideces cuando se inyectaban cementos de baja viscosidad. Así, los resultados sugerían que los cementos de baja viscosidad pueden ser idóneos para su uso en femoroplastia dado que presentan una esfericidad suficientemente compacta.

En definitiva, la metodología propuesta puede ser usada eficientemente para la planificación preoperatoria en la cirugía de cementación ósea.

## 7.2 Trabajo futuro

Como se ha comentado anteriormente, la femoroplastia mejora las propiedades mecánicas del hueso en comparación con el caso no cementado. En particular, los cementos de baja viscosidad han mostrado su gran potencial para su uso en dicha técnica. En efecto, los estudios contemplados en esta tesis doctoral reflejan las bondades de la femoroplastia para su aplicación como técnica preventiva en pacientes con osteoporosis y pérdida de masa ósea, ya que la misma minimizaría el riesgo de fractura y, por tanto, el impacto socio-económico.

En general, como trabajo futuro, es necesario que los modelos computacionales y animales sean validados en humanos a fin de clarificar la factibilidad de la femoroplastia. Además, podría ser interesante el desarrollo de una metodología basada en redes neuronales a fin de llevar a cabo simulaciones más rápidas y disminuir el coste computacional.

En particular, si se focaliza en la metodología propuesta en esta tesis doctoral, podría ser interesante la proposición de líneas futuras por capítulo:

- **Capítulo 2.** El hueso trabecular juega un papel fundamental en la transmisión de carga y en la absorción de energía. Como el hueso es anisótropo, se necesitan un gran número de ensayos mecánicos para describir de una manera más precisa el

comportamiento del hueso trabecular en general y, en particular, a través de cada localización anatómica. Por tanto, los modelos computacionales son considerados como una herramienta idónea para poner de manifiesto los mecanismos asociados a la fractura. Aunque las mallas basadas en tetraedros lineales, cuadráticos y voxels permitieron predecir de una manera precisa las propiedades mecánicas de las estructuras open-cell, podría ser interesante el uso de otras mallas, como las basadas en la esqueletonización (elementos barra), que nos ayuden a saber más sobre el daño microestructural. Además, la incorporación de propiedades de material heterogéneas, basadas en la mineralización de diferentes regiones anatómicas, podría permitir una caracterización más precisa.

- **Capítulo 3.** Uno de los principales problemas de la técnica de cementación es las altas temperaturas alcanzadas en el interior del hueso durante la polimerización del cemento. La investigación futura debe verificar la hipótesis que minimizar el volumen de inyección puede evitar, en gran medida, la necrosis térmica causada por el proceso exotérmico durante el curado [Basafa et al., 2015]. Además, se podría incorporar un modelo de generación de calor y propagación con el fin de diseñar cementaciones más seguras haciendo que el daño debido a la polimerización sea el menor posible [Palumbo et al., 2014].
- **Capítulo 4.** El uso de modelos animales como paso previo al desarrollo de modelos humanos es uno de las mejores metodologías para determinar la factibilidad de la femoroplastia. Sin embargo, como trabajo futuro, se deben usar modelos experimentales y diferentes volúmenes de cemento a fin de clarificar el riesgo de grandes volúmenes de cemento inyectado.
- **Capítulo 5.** Con respecto al cemento, se podrían simular tanto la dependencia del tiempo en el proceso de inyección, como la solidificación y la degradación de las propiedades. También, se deberían contemplar otras configuraciones de caída en los fémures cementados para clarificar riesgos de fractura y nuevas localizaciones de cemento. De esta manera, el objetivo final sería obtener una estrategia generalizada del proceso de cementación con independencia de la configuración de caída adoptada. Sin embargo, como en el capítulo 4, los modelos computacionales deberían ser validados con datos experimentales.

## 7.3 Contribuciones

### 7.3.1 Artículos en revistas

Artículos publicados:

- Samuel Jesús Ramos-Infante and María Ángeles Pérez. *In vitro* and *in silico* characterization of open-cell structures for trabecular bone. *Computer Methods in Biomechanics and Biomedical Engineering*, Vol. 20(14), 1562–1570. October (2017).
- Samuel Jesús Ramos-Infante, Amadeo Ten-Esteve, Ángel Alberich-Bayarri and María Ángeles Pérez. Discrete particle model for cement infiltration within open-cell structures: Prevention of osteoporotic fracture. *PloS one*, Vol. 13(6), e0199035. June (2018).

Artículos en revisión:

- Samuel Jesús Ramos-Infante and María Ángeles Pérez. High- and low-viscosity cement for osteoporotic femoral augmentation: a computational subject-specific approach. *Engineering Fracture Mechanics*.

### 7.3.2 Presentaciones en congresos

El trabajo presentado en esta tesis doctoral ha sido presentado en congresos nacionales e internacionales como se muestra a continuación:

- Presentaciones orales
  - a. *In vitro* and *in silico* characterization of open-cell structures for trabecular bone. 22nd Congress of the European Society of Biomechanics. Lyon 2016 (Francia) (EMEA Second Prize Winner of the Mimics Innovation Awards 2016).
  - b. *A particle model for prediction of cement infiltration in osteoporotic femoral augmentation*. Particles 2017. Hanover 2017 (Alemania)
  - c. *Multiscale simulation in bone tissue engineering: from micro to organ level*. COST Action MP1301 - NEWGEN - New Generation Biomimetic and Customized Implants for Bone Engineering. Viena 2017 (Austria).

- d. *In vitro and in silico characterization of cement infiltration in osteoporotic bones.* VPH-Virtual Physiological Human Conference 2018. Zaragoza 2018 (España).
- e. *Patient-specific planning of proximal femoral augmentation: in vitro and in silico approaches.* EORS-European Orthopaedic Research Congress. Galway 2018 (Irlanda).
- Poster presentations
  - a. *Personalized cement augmentation of the proximal femur using a discrete cement diffusion model.* Termis 2017. Davos 2017 (Suiza).

## References

---

- [1] Bayarri AA. In vivo morphometric and mechanical characterization of trabecular bone from high resolution magnetic resonance imaging. 2010. (Doctoral dissertation).
- [2] Anderson AE, Ellis BJ, Weiss JA. Verification, validation and sensitivity studies in computational biomechanics. *Comput Methods Biomech Biomed Eng.* 2007. 10(3):171–184.
- [3] Aquarius R, Homminga J, Hosman AJF, Verdonschot N, Tanck E. Prophylactic vertebroplasty can decrease the fracture risk of adjacent vertebrae: an in vitro cadaveric study. *Med Eng Phys.* 2014; 36:944–948.
- [4] Baron R. Anatomy and ultrastructure of bone. In: Favus MJ (ed) *Primer on the metabolic bone diseases and disorders of mineral metabolism.* New York, NY: Raven, 2003.
- [5] Baroud G, Crookshank M, Böhner M. High-viscosity cement significantly enhances uniformity of cement filling in vertebroplasty: an experimental model and study on cement leakage. *Spine.* 2006; 31:2562–8.
- [6] Baroud G, Wu JZ, Böhner M, Sponagel S, Steffen T. How to determine the permeability for cement infiltration of osteoporotic cancellous bone. *Med Eng Phys.* 2003; 25:283–288.
- [7] Basafa E, Armand M. Cement placement optimization in femoral augmentation using an evolutionary algorithm. *Proceedings of the ASME Design Engineering Technical Conference.* Vol. 4. Portland (OG): American Society of Mechanical Engineers, 2013.
- [8] Basafa E, Armand M. Subject-specific planning of femoroplasty: a combined evolutionary optimization and particle diffusion model approach. *J Biomech.* 2014; 47:2237–2243.
- [9] Basafa E, Murphy RJ, Otake Y, Kutzer MD, Belkoff SM, Mears SC. Subject-specific planning of femoroplasty: An experimental verification study. *J Biomech.* 2015; 48(1):59–64.

- [10] Bayraktar HH, Keaveny TM. Mechanisms of uniformity of yield strains for trabecular bone. *J Biomech.* 2004; 37:1671–1678.
- [11] Bayraktar HH, Morgan EF, Niebur GL, Morris GE, Wong EK, Keaveny TM. Comparison of the elastic and yield properties of human femoral trabecular and cortical bone tissue. *J Biomech.* 2004; 37:27–35.
- [12] Bayraktar HH, Gupta A, Kwon RY, Papadopoulos P, Keaveny TM. The modified super-ellipsoid yield criterion for human trabecular bone. *J Biomech Eng.* 2004a; 126, 677–684.
- [13] Bayraktar HH, Morgan EF, Niebur GL, Morris GE, Wong EK, Keaveny TM. Comparison of the elastic and yield properties of human femoral trabecular and cortical bone tissue. *J Biomech.* 2004b; 37, 27–35.
- [14] Beckmann J, Ferguson SJ, Gebauer M, Luering C, Gasser B, Heini P. Femoroplasty - augmentation of the proximal femur with a composite bone cement - feasibility, biomechanical properties and osteosynthesis potential. *Med Eng Phys.* 2007; 29:755–764.
- [15] Beckmann J, Springorum R, Vettorazzi E, Bachmeier S, Luering C, Tingart M. Fracture prevention by femoroplasty-cement augmentation of the proximal femur. *J Orthopaed Res.* 2011; 29:1753–1758.
- [16] Belkoff SM, Mathis JM, Jasper LE, Deramond H. The biomechanics of vertebroplasty: The effect of cement volume on mechanical behavior. *Spine.* 2001; 26: 1537-1541.
- [17] Bessho M, Ohnishi I, Matsuyama J, Matsumoto T, Imai K, Nakamura K. Prediction of strength and strain of the proximal femur by a CT-based finite element method. *J Biomech.* 2007; 40:1745–53.
- [18] Bessho M, Ohnishi I, Okazaki H, Sato W, Kominami H, Matsunaga S. Prediction of the strength and fracture location of the femoral neck by CT-based finite-element method: a preliminary study on patients with hip fracture. *J Orthop Sci.* 2004; 9(6):545–50.
- [19] Bevill G, Farhamand F, Keaveny TM. 2009. Heterogeneity of yield strain in low-density versus high-density human trabecular bone. *J Biomech.* 2009; 42(13):2165–2170.
- [20] Bhan S, Levine IC, Laing AC. Energy absorption during impact on the proximal femur is affected by body mass index and flooring surface. *J Biomech.* 2014; 47(10):2391–2397.

- [21] Borau C, Polacheck WJ, Kamm RD, García-Aznar JM. Probabilistic Voxel-Fe model for single cell motility in 3D. *In silico cell and tissue Sci* 2014; 1(1):1–17.
- [22] Bourne BC, van der Meulen MC. Finite element models predict cancellous apparent modulus when tissue modulus is scaled from specimen CT-attenuation. *J Biomech.* 2004; 37(5):613–621.
- [23] Buehler MJ. Nanomechanics of collagen fibrils under varying cross-link densities: atomistic and continuum studies. *J Mech Behav Biomed Mater.* 2007; 1, 59–67.
- [24] Burr DB. The use of finite element analysis to estimate the changing strength of bone following treatment for osteoporosis. *Osteoporos Int.* 2016; 27(9):2651–2654.
- [25] Carter DR, Hayes WC. The compressive behavior of bone as a two-phase porous structure. *J Bone & Joint Surg.* 1977; 59(7), 954-962.
- [26] Chen JH, Liu C, You L, Simmons CA. Boning up on Wolff's Law: mechanical regulation of the cells that make and maintain bone. *J Biomech.* 2010; 43(1), 108-118.
- [27] Chevalier Y, Pahr D, Allmer H, Charlebois M, Zysset P. Validation of a voxel-based FE method for prediction of the uniaxial apparent modulus of human trabecular bone using macroscopic mechanical tests and nanoindentation. *J Biomech.* 2007; 40(15):3333–3340.
- [28] Chevalley T, Guilley E, Herrmann FR, Hoffmeyer P, Rapin CH, Rizzoli R. Incidence of hip fracture over a 10-year period (1991-2000): reversal of a secular trend. *Bone.* 2007;40(5):1284-9.
- [29] Cianferotti L, Fossi C, Brandi ML. Hip protectors: are they worth it? *Calcif Tissue Int.* 2015; 97:1–11.
- [30] Clavet S, Beaudoin P, Poulin P. Particle-based viscoelastic fluid simulation. In *Proc ACM SIGGRAPH/Eurographics Symp Comput Anim.* 2005; 219–228.
- [31] Cook RB, Zioupos P. The fracture toughness of cancellous bone. *J Biomech.* 2009; 42(13), 2054-2060.
- [32] Corey AT. Influence of shape on the fall velocity of sand grains. Audio Visual Service, Colorado State University, 1963.
- [33] Cowin SC. The mechanical properties of cortical bone tissue. Boca Raton (FL): CRC Press. 1989.

- [34] Cowin SC, He QC. Tensile and compressive stress yield criteria for cancellous bone. *J Biomech.* 2005; 38, 141–144.
- [35] Crawford RP, Cann CE, Keaveny TM. Finite element models predict in vitro vertebral body compressive strength better than quantitative computed tomography. *Bone.* 2003; 33(4):744–750.
- [36] Cristofolini L, Taddei F, Baleani M., Baruffaldi F, Stea S, Viceconti M. Multiscale investigation of the functional properties of the human femur. *Philos Trans R Soc London Ser A.* 2008; 366(1879), 3319-3341.
- [37] Cummings SR, Melton LJ III. Epidemiology and outcomes of osteoporotic fractures. *Lancet.* 2002; 359:1761-7.
- [38] Currey JD. Tensile yield in compact bone is determined by strain, post-yield behaviour by mineral content. *J Biomech.* 2004; 37, 549–556.
- [39] Dall’Ara E, Luisier B, Schmidt R, Kainberger F, Zysset P, Pahr D. A nonlinear QCT-based finite element model validation study for the human femur tested in two configurations in vitro. *Bone.* 2013; 52(1):27–38.
- [40] Daszkiewicz K, Maquer G, Zysset PK. The effective elastic properties of human trabecular bone may be approximated using micro-finite element analyses of embedded volumen elements. *Biomech Model Mechanobiol.* 2017; 16(3):731–742.
- [41] de Bakker PM, Manske SL, Ebacher V, Oxland TR, Cripton PA, Guy P. During sideways falls proximal femur fractures initiate in the superolateral cortex: evidence from high-speed video of simulated fractures. *J. Biomech.* 2009; 42, 1917–1925.
- [42] De Laet CEDH, Van Hout BA, Burger H, Hofman A, Weel AEAM, Pols HAP. Hip fracture prediction in elderly men and women: validation in the Rotterdam Study. *J Bone Miner Res.* 1998; 13: 1587–93.
- [43] Dendorfer S, Maier HJ, Taylor D, Hammer J. Anisotropy of the fatigue behaviour of cancellous bone. *J Biomech.* 2008; 41(3):636–641.
- [44] Dobson CA, Sistas G, Phillips R, Fagan MJ, Langton CM. Three dimensional stereolithography models of cancellous bone structures from  $\mu$ CT data: testing and validation of finite element results. *Proc Inst Mech Eng Part H. J Eng Med.* 2006; 220(3): 481–484.
- [45] Dragomir-Daescu D, Op Den Buijs J, McEligot S, Dai Y, Entwistle RC, Salas C, Melton 3rd LJ, Bennet KE, Khosla S, Amin S. Robust QCT/FEA models of



- proximal femur stiffness and fracture load during a sideways fall on the hip. *Ann Biomed Eng.* 2011;39: 742–55.
- [46] Duchemin L, Mitton D, Jolivet E, Bousson V, Laredo JD, Skalli W. An anatomical subject—specific FE-model for hip fracture load prediction. *Comput Methods Biomech Biomed Engin.* 2008; 11:105–11.
- [47] Elffors L. Are osteoporotic fractures due to osteoporosis?. *Aging Clin Exp Res.* 1998; 10(3), 191-204.
- [48] Eswaran SK, Gupta A, Adams MF, Keaveny TM. Cortical and trabecular load sharing in the human vertebral body. *J Bone Miner Res.* 2006; 21(2):307–314.
- [49] Farrar DF, Rose J. Rheological properties of PMMA bone cements during curing. *Biomaterials.* 2001; 22: 3005–3013.
- [50] Faulkner KG, Cann CE, Hasegawa BH. Effect of bone distribution on vertebral strength: assessment with patientspecific nonlinear finite element analysis. *Radiology.* 1991; 179(3):669–674.
- [51] Feng H, Feng J, Li Z, Feng Q, Zhang Q, Qin D. Percutaneous femoroplasty for the treatment of proximal femoral metastases. *Eur J Surg Oncol.* 2014; 40:402–405.
- [52] Ferrari S, Reginster JY, Brandi ML, Kanis JA, Devogelaer JP, Kaufman JM. Unmet needs and current and future approaches for osteoporotic patients at high risk of hip fracture. *Arch Osteoporos.* 2016; 11(1):37.
- [53] Fields AJ, Eswaran SK, Jekir MG, Keaveny TM. Role of trabecular microarchitecture in whole-vertebral body biomechanical behavior. *J Bone Miner Res.* 2009; 24(9):1523– 1530.
- [54] Fliri L, Sermon A, Wähnert D, Schmoelz W, Blauth M, Windolf M. Limited V-shaped cement augmentation of the proximal femur to prevent secondary hip fractures. *J Biomater App.* 2013; 28: 136-143.
- [55] Fliri L, Sermon A, Whnert D, Schmoelz W, Blauth M, Windolf M. Limited v-shaped cement augmentation of the proximal femur to prevent secondary hip fractures. *J Biomater App.* 2012; 28:136–143.
- [56] Follet H, Peyrin F, Vidal-Salle E, Bonnassie A, Rumelhart C, Meunier PJ. Intrinsic mechanical properties of trabecular calcaneus determined by finite-element models using 3D synchrotron microtomography. *J Biomech.* 2007; 40(10):2174–2183.

- [57] Freitas A, Neri G, de Macedo Neto SL, Borges JLC, de Paula AP. Can be the cement augmentation an improvement method of preventing hip fractures in osteoporotic patients? *Geriatr Gerontol Aging*. 2017; 11(1), 42-47.
- [58] Baroud G, Falk R, Crookshank M, Sponagel S, Steffen T. Experimental and theoretical investigation of directional permeability of human vertebral cancellous bone for cement infiltration, *J. Biomech*. 2004; 37, 189–196.
- [59] Gibson L. The mechanical behaviour of cancellous bone. *J Biomech*. 1985; 18(5):317–328.
- [60] Gibson LJ, Ashby MF, Harley BA. *Cellular materials in nature and medicine*. Cambridge: Cambridge University Press. 2010.
- [61] Gibson LJ, Ashby MF, Schajer GS, Robertson CI. The mechanics of two-dimensional cellular materials. *Proc Math Phys Eng Sci R Soc*. 1982; 382(1782):25–42.
- [62] Gibson LJ, Ashby MF. *Cellular solids: structure and properties*. Cambridge: Cambridge University Press. 1999.
- [63] Gibson LJ, Ashby MF. The mechanics of three-dimensional cellular materials. *Proc Math Phys Eng Sci R Soc*. 1982; 382(1782):43–59.
- [64] Gomberg BR, Saha PK, Wehrli FW. Topology-based orientation analysis of trabecular bone networks. *Med Phys*. 2003; 30(2):158–168.
- [65] Gómez-Benito MJ, García-Aznar JM, Doblaré M. Finite element prediction of proximal femoral fracture patterns under different loads. *J Biomech Eng*. 2005; 127:9–14.
- [66] Gupta HS, Zioupos P. Fracture of bone tissue: The hows and the whys. *Med Eng Phys*. 2008; 30(10):1209–1226.
- [67] Hambli R. Micro-CT finite element model and experimental validation of trabecular bone damage and fracture. *Bone*. 2013; 56(2):363–374.
- [68] Hamed E, Jasiuk I, Yoo A, Lee Y, Liszka T. Multi-scale modelling of elastic moduli of trabecular bone. *J R Soc Interface*. 2012.
- [69] Hara T, Tanck E, Homminga J, Huiskes R. The influence of microcomputed tomography threshold variations on the assessment of structural and mechanical trabecular bone properties. *Bone*. 2002; 31(1):107–109.
- [70] Harrison NM, McDonnell PF, O’Mahoney DC, Kennedy OD, O’Brien FJ, McHugh PE. Heterogeneous linear elastic trabecular bone modelling using

- micro-CT attenuation data and experimentally measured heterogeneous tissue properties. *J Biomech.* 2008; 41(11):2589–2596.
- [71] Heini P, Berlemann U. Bone substitutes in vertebroplasty. *Eur Spine J* 2001; 10(SUPPL. 2): S205– S213.
- [72] Heini PF, Franz T, Fankhauser C, Gasser B, Ganz R. Femoroplasty-augmentation of mechanical properties in the osteoporotic proximal femur: a biomechanical investigation of pmma reinforcement in cadaver bones. *Clin Biomech.* 2004; 19:506–512.
- [73] Hernlund E, Svedbom A, Ivergård M, Compston J, Cooper C, Stenmark J. Osteoporosis in the European Union: medical management, epidemiology and economic burden. *Arch Osteoporos.* 2013; 8:136.
- [74] Hildebrand T, Rüegsegger P. Quantification of bone microarchitecture with the structure model index. *Comput Methods Biomech Biomed Eng.* 1997; 1(1):15–23.
- [75] Homminga J, Van-Rietbergen B, Lochmuller EM, Weinans H, Eckstein F, Huiskes R. The osteoporotic vertebral structure is well adapted to the loads of daily life, but not to infrequent Berror loads. *Bone.* 2004; 34(3):510–516.
- [76] Hopley C, Stengel D, Ekkernkamp A, Wich M. Primary total hip arthroplasty versus hemiarthroplasty for displaced intracapsular hip fractures in older patients: systematic review. *BMJ Brit Med J.* 2010: 340, c2332.
- [77] Hou FJ, Lang SM, Hoshaw SJ, Reimann DA, Fyhrie DP. Human vertebral body apparent and hard tissue stiffness. *J Biomech.* 1998; 31(11):1009–1015.
- [78] Imai K, Ohnishi I, Bessho M, Nakamura K. Nonlinear finite element model predicts vertebral bone strength and fracture site. *J Spine.* 2006; 31:1789–1794.
- [79] Ito Y, Shum PC, Shih AM, Soni BK, Nakahashi K. Robust generation of high-quality unstructured meshes on realistic biomedical geometry. *Int J Numer Methods Eng.* 2006; 65(6):943–973
- [80] Webb JCJ, Spencer RF. The role of polymethylmethacrylate bone cement in modern orthopaedic surgery. *J Bone Joint Surg.* 2007; 89, 851–857.
- [81] Teo JC, Teoh SH. Permeability study of vertebral cancellous bone using micro-computational fluid dynamics, *Comput Methods Biomech Biomed Engin.* 2012; 15, 417–423.

- [82] Jaasma MJ, Bayraktar HH, Niebur GL, Keaveny TM. Biomechanical effects of intraspecimen variations in tissue modulus for trabecular bone. *J Biomech.* 2002; 35:237–246.
- [83] Jakob F, Ebert R, Ignatius A, Matsushita T, Watanabe Y, Groll J, Walles H. Bone tissue engineering in osteoporosis. *Maturitas.* 2013; 75(2), 118-124.
- [84] Jensen ME, Evans AJ, Mathis JM, Kallmes DF, Cloft HJ, Dion JE. Percutaneous polymethylmethacrylate vertebroplasty in the treatment of osteoporotic vertebral body compression fractures: technical aspects. *Amer J Neuroradiol.* 1997; 18:1897–1904.
- [85] Jinnai H, Watashiba H, Kajihara T, Nishikawa Y, Takahashi M, Ito M. Surface curvatures of trabecular bone microarchitecture. *Bone.* 2002; 30(1):191–194.
- [86] Jones AC, Wilcox RK. Assessment of factors influencing finite element vertebral model predictions. *J Biomech Eng.* 2007; 129(6):898–903.
- [87] Kabel J, van Rietbergen B, Odgaard A, Huiskes R. Constitutive relationships of fabric, density, and elastic properties in cancellous bone architecture. *Bone.* 1999; 25(4):481–486.
- [88] Kaneko M, Ohnishi I, Matsumoto T, Ohashi S, Bessho M, Hayashi N, Tanaka S. Prediction of proximal femur strength by a quantitative computed tomography-based finite element method—Creation of predicted strength data of the proximal femur according to age range in a normal population. *Modern Rheumatology.* 2016; 26(1), 151-155.
- [89] Kanis JA, Glüer CC, for the Committee of Scientific Advisors, International Osteoporosis Foundation. An update on the diagnosis and assessment of osteoporosis with densitometry. *Osteoporos Int.* 2000; 11: 192–202.
- [90] Kanis JA, Johnell O, Oden A, De Laet C, Mellstrom D. Diagnosis of osteoporosis and fracture threshold in men. *Calcif Tissue Int.* 2001; 69: 218–21.
- [91] Kanis JA, Johnell O, Oden A. Long-term risk of osteoporotic fracture in Malmo. *Osteoporos Int.* 2000; 11: 669–74.
- [92] Kanis JA, McCloskey EV, Johansson H, Cooper C, Rizzoli R, Reginster JY. European guidance for the diagnosis and management of osteoporosis in postmenopausal women. *Osteoporos Int.* 2013; 24 (1):23–57.
- [93] Kanis JA, Melton LJ, Christiansen C, Johnston CC, Khaltsev N. The diagnosis of osteoporosis. *J Bone Miner Res.* 1994; 9: 1137–41.

- [94] Kanis JA. Diagnosis of osteoporosis and assessment of fracture risk. *The Lancet*. 2002; 359(9321), 1929-1936.
- [95] Kannus P, Parkkari J, Poutala J. Comparison of force attenuation properties of four different hip protectors under simulated falling conditions in the elderly: an in vitro biomechanical study. *Bone*. 1999; 25:229–23 PMID: 10456390
- [96] Keaveny TM, Borchers RE, Gibson LJ, Hayes WC. Trabecular bone modulus and strength can depend on specimen geometry. *J Biomech*. 1993; 26(8): 427–991–1000.
- [97] Keaveny TM, Pinilla TP, Crawford RP, Kopperdahl DL, Lou A. Systematic and random errors in compression testing of trabecular bone. *J Orthop Res*. 1997; 15(1):101–110.
- [98] Keller TS. Predicting the compressive mechanical behavior of bone. *J Biomech*. 1994; 22(9),1159–1168.
- [99] Keyak JH, Falkinstein Y. Comparison of in situ and in vitro CT scan-based finite element model predictions of proximal femoral fracture load. *Med Eng Phys*. 2003; 25:781–7.
- [100] Keyak JH, Rossi SA, Jones KA, Skinner HB. Prediction of femoral fracture load using automated finite element modeling. *J Biomech*. 1997; 31(2):125–133.
- [101] Keyak JH. Improved prediction of proximal femoral fracture load using nonlinear finite element models. *Med Eng Phys*. 2001; 23:165–73.
- [102] Koivumäki JE, Thevenot J, Pulkkinen P, Kuhn V, Link TM, Eckstein F, Jämsä T. Ct-based finite element models can be used to estimate experimentally measured failure loads in the proximal femur. *Bone*. 2012; 50(4), 824-829.
- [103] Ladd AJC, Kinney JH. Numerical errors and uncertainties in finite-element modeling of trabecular bone. *J Biomech*. 1998; 31:941–945.
- [104] Landgraf R, Ihlemann J, Kolmeder S, Lion A, Lebsack H, Kober C. Modelling and simulation of acrylic bone cement injection and curing within the framework of vertebroplasty. *ZAMM-Z Angew Math Me*. 2015; 95(12): 1530–1547.
- [105] Lane J, Russell L, Khan S. Osteoporosis. *Clin. Orthop. Relat. Res*. 2000; 372, 139–150.
- [106] Lawrence TM, Wenn R, Boulton CT, Moran CG. Age-specific incidence of first and second fractures of the hip. *J Bone Joint Surg Br*. 2010; 92(2):258-61.

- [107] Liu M, Chang J, Li H. Numerical modeling of injection flow of drug agents for controlled drug delivery. In Proc IEEE EMBS. 2007; 1152–1155.
- [108] Loeffel M, Ferguson SJ, Nolte LP, Kowal JH. Experimental characterization of Polymethylmethacrylate bone cement spreading as a function of viscosity, bone porosity, and flow rate. *Spine*. 2008; 33:1352–1359.
- [109] Looker AC, Borrud LG, Hughes JP, Fan B, Shepherd JA 3rd LJM, Melton LJ 3rd. 2012. Lumbar spine and proximal femur bone mineral density, bone mineral content, and bone area: United States, 2005–2008. Vital and health statistics Series 11. Data from the national health survey. 251:1–132.
- [110] Lü L, Meng G, Gong H, Zhu D, Gao J, Fan Y. Tissue level microstructure and mechanical properties of the femoral head in the proximal femur of fracture patients. *Acta Mech Sinica*. 2015; 31(2):259–267.
- [111] Luisier B, Dall’Ara E, Pahr DH. Orthotropic HR-pQCTbased FE models improve strength predictions for stance but not for sideways fall loading compared to isotropic QCTbased FE models of human femurs. *J Mech Behav Biomed Mater*. 2014; 32:287–299.
- [112] MacLean C, Newberry S, Maglione M, McMahon M, Ranganath V, Suttorp M. Systematic review: comparative effectiveness of treatments to prevent fractures in men and women with low bone density or osteoporosis. *Ann Intern Med*. 2008;148(3):197-213.
- [113] Magnan B, Bondi M, Maluta T, Samaila E, Schirru L, Dall’Oca C. Acrylic bone cement: current concept review. *Musculoskeletal surgery*. 2013; 97(2), 93-100.
- [114] Marco M, Giner E, Larraínzar-Garijo R, Caeiro JR, Miguélez MH. Modeling of femur fracture using finite element procedures. *Eng Fract Mech*. 2018, 196: 157-167.
- [115] Marks SC, Hermey DC. The structure and development of bone. In: Principles of bone biology. Bilezikian JB, Raize LG, Rodan GA (eds). New York, NY: Academic Press, 1996.
- [116] Martin H, Werner J, Andresen R, Schober HC, Schmitz KP. Noninvasive assessment of stiffness and failure load of human vertebrae from CT-data. *Biomed Tech*. 1998; 43(4):82–88.

- [117] Michalski AS, Edwards BW, Boyd SK. QCT Reconstruction Kernel has Important Quantitative Effects on Finite Element Estimated Bone Strength. *CMBES Proceedings*. 2016; 39(1).
- [118] Morgan EF, Bayraktar HH, Keaveny TM. Trabecular bone modulus- density relationships depend on anatomic site. *J Biomech*. 2003; 36,897–904.
- [119] Müller R, Rügsegger P. Three-dimensional finite element modelling of non-invasively assessed trabecular bone structures. *Med Eng Phys*. 1995; 17(2):126–133.
- [120] Nalla RK, Kinney JH, Ritchie RO. Mechanistic fracture criteria for the failure of human cortical bone. *Nature Materials*. 2003; 2, 164–168.
- [121] Nawathe S, Akhlaghpour H, Bouxsein ML, Keaveny TM. Microstructural failure mechanisms in the human proximal femur for sideways fall loading. *J Bone Miner Res*. 2013; 29:507–515.
- [122] Niebur GL, Feldstein MJ, Yuen JC, Chen TJ, Keaveny TM. High-resolution finite element models with tissue strength asymmetry accurately predict failure of trabecular bone. *J Biomech*. 2000; 33:1575–1583.
- [123] O’Brien FJ, Taylor D, Lee TC. An improved labelling technique for monitoring microcrack growth in compact bone. *J Biomech*. 2002; 35(4):523–526
- [124] Odén A, McCloskey EV, Johansson H, Kanis JA. Assessing the impact of osteoporosis on the burden of hip fractures. *Cal Tis Int*. 2013; 92(1), 42-49.
- [125] Odgaard A. Three-dimensional methods for quantification of cancellous bone architecture. *Bone*. 1997;20(4):315–28.
- [126] Olszta MJ, Cheng XG, Jee SS, Kumar R, Kim YY, Kaufman MJ, Douglas E. P, Gower LB. Bone structure and formation: a new perspective. *Mater Sci Eng R*. 2007; 58, 77–116.
- [127] Pahr DH, Dall’Ara E, Varga P, Zysset PK. HR-pQCT-based homogenised finite element models provide quantitative predictions of experimental vertebral body stiffness and strength with the same accuracy as  $\mu$ FE models. *Comput Methods Biomech Biomed Eng*. 2012; 15(7):711–720.
- [128] Pahr DH, Zysset PK. A comparison of enhanced continuum FE with micro FE models of human vertebral bodies. *J Biomech*. 2009; 42:455–462.
- [129] Pahr DH, Zysset PK. Finite element-based mechanical assessment of bone quality on the basis of in vivo images. *Curr Osteoporos Rep*. 2016; 14(6):374–385.

- [130] Pahr DH, Zysset PK. Influence of boundary conditions on computed apparent elastic properties of cancellous bone. *Biomech Model Mechanobiol.* 2008; 7(6):463–476.
- [131] Pal B, Puthumanapully PK, Amis AA. (ii) Biomechanics of implant fixation. *Orthop and Trauma.* 2013; 27: 76-84.
- [132] Palumbo BT, Nalley C, Gaskins RB, Gutierrez S, Alexander GE, Anijar L. Biomechanical analysis of impending femoral neck fractures: the role of percutaneous cement augmentation for osteolytic lesions. *Clin Biomech.* 2014; 29(3):289–295.
- [133] Parkinson IH, Badiei A, Stauber M, Codrington J, Müller R, Fazzalari NL. Vertebral body bone strength: the contribution of individual trabecular element morphology. *Osteoporos Int.* 2012; 23(7):1957–1965.
- [134] Parkkari J, Kannus P, Heikkilä J, Poutala J, Heinonen A, Sievänen H. Impact experiments of an external hip protector in young volunteers. *Calc tissue Int.* 1997; 60(4):354–357.
- [135] Pérez MA, Prendergast PJ. Random-walk models of cell dispersal included in mechanobiological simulations of tissue differentiation. *J Biomech.* 2007; 40(10):2244–2253.
- [136] Perilli E, Baleani M, Öhman C, Fognani R, Baruffaldi F, Viceconti M. 2008. Dependence of mechanical compressive strength on local variations in microarchitecture in cancellous bone of proximal human femur. *J Biomech.* 2008; 41(2):438–446.
- [137] Pike C, Birnbaum HG, Schiller M, Sharma H, Burge R, Edgell ET. Direct and indirect costs of non-vertebral fracture patients with osteoporosis in the US. *Pharmaco Economics.* 2010; 28:395–409.
- [138] Pioletti DP. Biomechanics in bone tissue engineering. *Comput Methods Biomech Biomed Engin.* 2010; 13(6):837–846.
- [139] Pistoia W, van Rietbergen B, Laib A, Ruegsegger P. Highresolution three-dimensional-pQCT images can be an adequate basis for in-vivo  $\mu$ FE analysis of bone. *J Biomech Eng.* 2001; 123(2):176–183.
- [140] Pistoia W, Van Rietbergen B, Lochmüller EM, Lill CA, Eckstein F, Rügsegger P. Estimation of distal radius failure load with micro-finite element analysis models based on three-dimensional peripheral quantitative computed tomography images. *Bone.* 2002; 30(6), 842-848.



- [141] Querin OM, Steven GP, Xie YM. Evolutionary structural optimisation using an additive algorithm. *Finite Elem Anal Des.* 2000; 34:291–308.
- [142] Widmer RP and Ferguson SJ. On the interrelationship of permeability and structural parameters of vertebral trabecular bone: a parametric computational study, *Comput Methods Biomech Biomed Eng.* 2013; 16, 908–922.
- [143] Raas C, Hofmann-Fliri L, Hörmann R, Schmoelz W. Prophylactic augmentation of the proximal femur: an investigation of two techniques. *Arch Orthop Trauma Surg.* 2016; 136: 345-351.
- [144] Rajan K. Linear elastic properties of trabecular bone: a cellular solid approach. *J Mater Sci Lett.* 1985; 4(5):609–611.
- [145] Ramos-Infante SJ, Pérez MA. In vitro and in silico characterization of open-cell structures for trabecular bone. *Comput Methods Biomech Biomed Eng.* 2017; 20(14): 1562–1570.
- [146] Ramos-Infante SJ, Ten-Esteve A, Alberich-Bayarri A, Pérez MA. Discrete particle model for cement infiltration within open-cell structures: Prevention of osteoporotic fracture. *PloS ONE.* 2018; 13(6), e0199035.
- [147] Recker RR, Barger-Lux J. Risedronate for prevention and treatment of osteoporosis in postmenopausal women. *Expert Opin Pharmacother.* 2005; 6:465–477.
- [148] Reeve-Johnson L, Schuetz MA. Review of Major Animal Models Relevant to Contemporary Orthopaedic Repair of the Appendicular Skeleton in Humans. *EC Orthop.* 2016; 4, 483-510.
- [149] Rohlmann A, Boustani HN, Bergmann G, Zander T. A probabilistic finite element analysis of the stresses in the augmented vertebral body after vertebroplasty. *Eur Spine J.* 2010; 19: 1585-1595.
- [150] Roth T, Kammerlander C, Gosch M, Luger TJ, Blauth M. Outcome in geriatric fracture patients and how it can be improved. *Ost Int.* 2010; 21(4), 615-619.
- [151] Ryg J, Rejnmark L, Overgaard S, Brixen K, Vestergaard P. Hip fracture patients at risk of second hip fracture: a nationwide population-based cohort study of 169,145 cases during 1977-2001. *J Bone Miner Res.* 2009;24(7):1299-307.
- [152] Santana Artiles ME, Venetsanos DT. A new evolutionary optimization method for osteoporotic bone augmentation. *Comput Methods Biomech Biomed Eng.* 2017; 20(7):691–700.

- [153] Santana Artiles ME, Venetsanos DT. Numerical investigation of the effect of bone cement porosity on osteoporotic femoral augmentation. *Int J Numer Methods Biomed Eng.* 2018; e2989.
- [154] Santesso N, Carrasco-Labra A, Brignardello-Petersen R. Hip protectors for preventing hip fractures in older people. *Cochrane Database Syst Rev.* 2014; CD001255.
- [155] Schileo E, Taddei F, Malandrino A, Cristofolini L, Viceconti M. Subject-specific finite element models can accurately predict strain levels in long bones. *J Biomech.* 2007; 40(13):2982–2989.
- [156] Soyka RPW, Helgason B, Marangalou JH, Van Den Bergh JP, Van Rietbergen B, Ferguson SJ. The effectiveness of percutaneous vertebroplasty is determined by the patient-specific bone condition and the treatment strategy. *PLoS ONE.* 2016; 11.
- [157] Springorum HR, Gebauer M, Mehrl A, Stark O, Craiovan B, Puschel K, Amling M, Grifka J, Beckmann J. Fracture prevention by prophylactic femoroplasty of the proximal femur—metallic compared with cemented augmentation. *J Orthop Trauma.* 2014; 28:403–409.
- [158] Stauber M, Nazarian A, Müller R. Limitations of global morphometry in predicting trabecular bone failure. *J Bone Miner Res.* 2014; 29(1):134–141.
- [159] Steele K, Cline D, Egbert PK, Dinerstein J. Modeling and rendering viscous liquids. *Comp Anim Virtual Worlds.* 2004; 15:183–192.
- [160] Steenhoven TJ, Schaasberg W, Vries AC, Valstar ER, Nelissen RGHH. Cyclic loading of fractured cadaveric femurs after elastomer femoroplasty: an in vitro biomechanical study. *Clin Biomech.* 2012; 27:819–823.
- [161] Strauss EJ, Pahk B, Kummer FJ, Egol K. Calcium phosphate cement augmentation of the femoral neck defect created after dynamic hip screw removal. *J Ortho Trauma.* 2007; 21(5), 295-300.
- [162] Ström O, Borgström F, Kanis JA, Compston J, Cooper C, McCloskey EV. Osteoporosis: burden, health care provision and opportunities in the EU. A report prepared in collaboration with the International Osteoporosis Foundation (IOF) and the European Federation of Pharmaceutical Industry Associations (EFPIA). *Arch Osteoporos.* 2011; 6:59–155.

- [163] Sutter EG, Mears SC, Belkoff SM. A biomechanical evaluation of femoroplasty under simulated fall conditions. *J Orthopaed Trauma*. 2010a; 24:95–99.
- [164] Sutter EG, Wall SJ, Mears SC, Belkoff SM. The effect of cement placement on augmentation of the osteoporotic proximal femur. *Geriatr Orthopaed Surg Rehabil*. 2010b; 1:22–26.
- [165] Zeiser T, Bashoor-Zadeh M, Darabi A, Baroud G. Pore-scale analysis of Newtonian flow in the explicit geometry of vertebral trabecular bones using lattice Boltzmann simulation, *Proc Inst Mech Eng, Part H: J. Eng Med* 2008; 222 185–194.
- [166] Taddei F, Schileo E, Helgason B, Cristofolini L, Viceconti M. The material mapping strategy influences the accuracy of CTbased finite element models of bones: an evaluation against experimental measurements. *Med Eng Phys*. 2007; 29(9): 973–979.
- [167] Taylor D. Fracture mechanics: How does bone break? *Nature Materials*. 2003; 2, 133–134.
- [168] Thevenot J, Pulkkinen P, Koivumäki JEM, Kuhn V, Eckstein F, Jämsä T. Discrimination of cervical and trochanteric hip fractures using radiography-based twodimensional finite element models. *Open Bone J*. 2009; 1:16–22
- [169] Thompson MS, McCarthy ID, Lidgren L, Ryd L. Compressive and shear properties of commercially available polyurethane foams. *J Biomech Eng*. 2003; 125(5), 732-734.
- [170] Tohmeh AG, Mathis JM, Fenton DC, Levine AM, Belkoff SM. Biomechanical efficacy of unipedicular versus bipedicular vertebroplasty for the management of osteoporotic compression fractures. *Spine*. 1999; 24:1772–1776.
- [171] Treece GM, Prager RW, Gee AH. Regularised marching tetrahedra: improved iso-surface extraction. *Comput Graph*. 1999; 23(4):583–598.
- [172] Turner CH, Cowin SC, Rho JY, Ashman RB, Rice JC. The fabric dependence of the orthotropic elastic constants of cancellous bone. *J Biomech*. 1990; 23(6):549–561.
- [173] Ulrich D, van Rietbergen B, Weinans H, Rügsegger P. Finite element analysis of trabecular bone structure: a comparison of image-based meshing techniques. *J Biomech*. 1998; 31(12):1187–1192.

- [174] Vaishya R, Chauhan M, Vaish A. Bone cement. *J Clin Orthop and Trauma*. 2013; 4: 157-163.
- [175] Van der Zijden AM, Janssen D, Verdonshot N, Groen BE, Nienhuis B, Weerdesteyn V, Tanck E. Incorporating in vivo fall assessments in the simulation of femoral fractures with finite element models. *Med Eng Phys*. 2015; 37(6), 593-598.
- [176] van Lenthe GH, Stauber M, Müller R. Specimen-specific beam models for fast and accurate prediction of human trabecular bone mechanical properties. *Bone*. 2006; 39(6):1182– 1189.
- [177] van Rietbergen B, Weinans H, Huiskes R, Odgaard A. A new method to determine trabecular bone elastic properties and loading using micromechanical finite-element models. *J Biomech*. 1195; 28(1), 69-81.
- [178] Varga P, Inzana JA, Schwiedrzik J, Zysset PK, Gueorguiev B, Blauth M. New approaches for cement-based prophylactic augmentation of the osteoporotic proximal femur provide enhanced reinforcement as predicted by non-linear finite element simulations. *Clin Biomech*. 2017; 44: 7–13.
- [179] Verhulp E, van Rietbergen B, Huiskes R. Comparison of microlevel and continuum-level voxel models of the proximal femur. *J Biomech*. 2006; 39(16):2951–2957.
- [180] Verhulp E, Van Rietbergen B, Huiskes R. Load distribution in the healthy and osteoporotic human proximal femur during a fall to the side. *Bone*. 2008; 42:30-5.
- [181] Verhulp E, Van Rietbergen B, Müller R, Huiskes R. Micro-finite element simulation of trabecular-bone postyield behaviour—effects of material model, element size and type. *Comput Methods Biomech Biomed Eng*. 2008; 11(4):389–395.
- [182] Viceconti M, Bellingeri L, Cristofolini L, Toni A. A comparative study on different methods of automatic mesh generation of human femurs. *Med Eng Phys*. 1998; 20(1):1–10.
- [183] Viceconti M, Hunter P, Hose R. Big data, big knowledge: big data for personalized healthcare. *IEEE J Biomed Health*. 2015; 19(4):1209–1215.
- [184] Wachtel EF, Keaveny TM. Dependence of trabecular damage on mechanical strain. *J Orthop Res*. 1997; 15(5):781–787.

- [185] Wall A, Board T. The compressive behavior of bone as a two-phase porous structure. In *Classic Papers in Orthopaedics*. 2014; (pp. 457-460). Springer, London.
- [186] Wang J, Zhou B, Liu XS, Fields AJ, Sanyal A, Shi X, Adams M. Trabecular plates and rods determine elastic modulus and yield strength of human trabecular bone. *Bone* 2015; 72:71–80.
- [187] Who. Prevention and management of osteoporosis. World Health Organization technical report series. 2003:9211–164, back cover.
- [188] Widmer RP, Ferguson SJ. A mixed boundary representation to simulate the displacement of a biofluid by a biomaterial in porous media. *J Biomech Eng* 2011; 133(5):051007.
- [189] Wijayathunga VN, Oakland RJ, Jones AC, Hall RM, Wilcox RK. Vertebroplasty: Patient and treatment variations studied through parametric computational models. *Clin Biomech*. 2013; 28: 860-865.
- [190] Yang J, Zhang K, Zhang S, Fan J, Guo X, Dong W, Yu B. Preparation of calcium phosphate cement and polymethyl methacrylate for biological composite bone cements. *Med Sci Monit: Int Med J Exp Clin Research*. 2015; 21, 1162.
- [191] Yeh OC, Keaveny TM. Relative roles of microdamage and microfracture in the mechanical behavior of trabecular bone. *J Orthop Res*. 2001; 19(6):1001–1007.
- [192] Yosibash Z, Tal D, Trabelsi N. Predicting the yield of the proximal femur using high-order finite-element analysis with inhomogeneous orthotropic material properties. *Philos Trans A Math Phys Eng Sci*. 2010; 368(1920):2707–2723.
- [193] Zeiser T, Bashoor-Zadeh M, Darabi A, Baroud G. Pore-scale analysis of Newtonian flow in the explicit geometry of vertebral trabecular bones using lattice Boltzmann simulations. *Proc Inst Mech Eng Part H: J Eng Med*. 2008; 222(2): 185–194.
- [194] Zhong Z, Akkus O. Effects of age and shear rate on the rheological properties of human yellow bone marrow. *J Biorheol*. 2011; 48:89–97.
- [195] Zhu Y, Brdison R. Animating sand as a fluid. *ACM Trans Graph*. 2005; 24:965–972.
- [196] Zimmerman S, Magaziner J, Birge SJ, Barton BA, Kronsberg SS, Kiel DP. Adherence to hip protectors and implications for U.S. long-term care settings. *J Am Med Dir Assoc*. 2010; 11:106–115.

- [197] Zoarski GH, Snow P, Olan WJ, Stallmeyer MJB, Dick BW, Hebel JR. Percutaneous vertebroplasty for osteoporotic compression fractures: quantitative prospective evaluation of long-term outcomes. *J Vasc Int Radiol*. 2002; 13:139–148.
- [198] Zysset P, Pahr D, Engelke K, Genant HK, McClung MR, Kendler DL, Recknor C. Comparison of proximal femur and vertebral body strength improvements in the FREEDOM trial using an alternative finite element methodology. *Bone*. 2015; 81:122–130.
- [199] Zysset PK, Dall'Ara E, Varga P, Pahr DH. Finite element analysis for prediction of bone strength. *Bone*. 2013. Key reports, 2.
- [200] Zysset PK, Guo XE, Hoffler CE, Moore KE, Goldstein SA. Elastic modulus and hardness of cortical and trabecular bone lamellae measured by nanoindentation in the human femur. *J Biomech*. 1999; 32(10):1005–1012.
- [201] Zysset PK. A review of morphology-elasticity relationships in human trabecular bone: theories and experiments. *J Biomech*. 2003; 36(10):1469–1485.